The Islamic University of Gaza
Deanery of Graduate Studies
Faculty of Engineering
Electrical Engineering Department

MODELING AND PARAMETERS IDENTIFICATION OF A MAGNETIC LEVITATION MODEL

By

Khaled A. M. ALI

Supervisor

Prof. Dr. Muhammed Abdelati

"A Thesis Submitted in Partial Fulfillment of the Requirements for the Degree of Master of Science in Electrical Engineering."

1430 - 2009

Abstract

In this thesis modelling and identification of a laboratory magnetic levitation with the final aim to design a control system is presented. The CE152 made by Humusoft is a laboratory magnetic levitation designed for studying system dynamics and control engineering principles. First, the magnetic levitation set-up is depicted, then the whole system is disassembled into simpler subsystems, then theoretical modeling is systematically described. Identification of the necessary parameters is tackled using direct and indirect measurement methods and their results are presented. As the system is nonlinear and unstable, it should be linearized at operating point and a modified PID digital controller with a fine tuned parameters is designed to track a small varying input signal. Finally our modelling (mathematical model) is validated with the real system, the results show that the simulation's model is adequately represents the real magnetic levitation model. A laboratory Magnetic Levitation System Apparatus has been built, and analog PD controller has been designed to stabilize the system. This apparatus could be used as visual demonstrations of control principles and electronic design.

عنوان البحث بالعربية:

"عمل نموذج لجهاز التعليق المغناطيسي وإيجاد قيم الثوابت الخاصة به"

ملخص البحث بالعربية:

يهدف هذا البحث إلى عمل نموذج لجهاز التعليق المغناطيسي وإيجاد قيم الثوابت الخاصة به، ومن ثم عرض نظام للتحكم. هذا الجهاز يحمل تصنيف موديل CE152 من شركة هموسوفت مصمم لأغراض تعليمية مثل دراسة ديناميكية النظام ومبادئ هندسة التحكم. بداية تم شرح مبسط عن آلية عمل النظام وبعد ذلك تم تقسيم الجهاز إلي مكونات فرعية، تلاها وصفاً نظرياً وبنائياً بطريقة نظامية. وبعد ذلك تم إيجاد وعرض جميع قيم الثوابت الخاصة بالنموذج وذلك باستخدام طرق مختلفة منها القياسات المباشرة والغير مباشرة. وحيث أن النظام غير خطي وغير مستقر فتم تقريب النظام إلي خطي عند نقطة التشغيل (العمل) وتصميم متحكم رقمي نوع (بي أي دي) المعدل للقيام بالمقدرة علي تتبع أشارة ذات تغير صغير. وأخيرا تمت مصادقة النموذج المقترح (المحاكاة) مع النموذج الحقيقي, حيث أشارت النتائج بأن نموذج المحاكاة يماثل بدرجة كافية النموذج الحقيقي. كذلك تم بناء جهاز تعليق مغناطيسي، وتم تصميم متحكم تناظري لعمل اتزان واستقرار للنظام. هذا الجهاز يمكن أن يستخدم لغرض التطبيقات العملية لمفاهيم تصميم أنظمة التحكم باستخدام الإلكترونيات.

Dedication

To all my family members who have been a constant source of motivation, inspiration, and support.

Acknowledgements

I would like to thank my thesis supervisor, Prof. Dr. Muhammed Abdelati, for his support, encouragement and professional assistance.

Special thanks to all other Islamic University staff members that I may have called upon for assistance especially Assoc. Dr. Mohammed Hussein and Asst. Dr. Hattim Elaydi, as their suggestions have helped with the development of this thesis. I would also like to extend my gratitude to my family for the support they have given me.

And I would like to thank the best university for this precious opportunity it has granted me to study in. Also I would like to thank my students in Gaza Training Center for their assistance in building a Laboratory Magnetic Levitation apparatus.

Contents

List of Tables

List of Figures

Chapter 1

Introduction and Literature Review

1.1 Research Motivation and Goal

Magnetic levitation system which can suspend objects without any contact attract increasingly attention as means of eliminating Coulomb friction due to mechanical contact [1]. This technology has been widely utilized for various industrial purpose, such as suspension vehicles, suspension bearing, flywheels, magnetic vibration isolation, magnetically suspended wind tunnel, etc. Furthermore, in recent years, the need for high performance, accurate magnetic levitation systems is becoming more and more important [2]. For magnetic levitation systems, modelling and feedback control is indispensable since they are nonlinear and essentially unstable [3]. In this thesis an accurate Simulink model will be implemented and validation experiment will be set up. After that, PI-D controller will be designed and tuned to improve the system's performance.

1.2 Literature Review

Magnetic levitation systems are widely used in industry, e.g. levitated vehicles, magnetic bearing, etc. In a DC magnetic levitation system, it is necessary to construct an accurate model and a high performance feedback controller to stabilize and control the suspended object since it is an open-loop nonlinear and unstable system.

The modeling methods is sometime quit complicated if we want an exact and detailed model. This has received many researches in recent years, e.g. the Euler-Lagrange's force balance, lookup table, segmented linear approximation and black box identification.

In 1992, C.E.line, H.L. Jou and Y.R. Sheu presented an improved model identification method for magnetic suspension system to establish reliable and exact parameters to describe the dynamic motion characteristic. The parameter for each

test sample can be calculated under the specific operation conditions after some magnetic field measurements. The results lead effectively to controller design for magnetic suspension system [4].

In 1997, Toru Namerikawat and Masayuki Fujitaj proposed the set of plant models of magnetic suspension systems considered various types uncertainties, they transformed the obtained model to the LFT represented interconnection structure with the structured mixed uncertainty [5].

In 1999, Lianming Sun, Hiromitsu Ohmori and Akira Sano proposed direct closed-loop identification method only using the plant input/output data acquired through an output inter-sampling scheme. By taking the faster sampling of the system output than the control interval, the inter-sampled plant model could also be described by a SIMO model structure, which provided the identifiably of the closed loop [6].

In 2001, M. Velasco Villa, R. Castro Linares, L.Corona-Ramirez described a detailed model of the magnetic suspension system which takes into account the nonlinear characteristic of sensor, that measures the position of the sphere, and the electromagnetic inductor [7].

In 2002, H. Yu, T.C. Yang, D. Rigas and B.V. Jayawant developed the dynamic of suspension system by using the Eular−Lagranges formulation [8].

In 2003, Roberto Kawakami, Takashi Yoneyama, Fabio Meneghetti and Rodolfo Galati proposed a new procedure for obtaining a nominal linear model for a single axis, attractive magnetic levitation system, the procedure was based on a frequency domain identification technique [9].

In 2003 , the work of John M. Watkins and George E. piper was a design of an undergraduate course in Active Magnetic levitation which focused on a project where the students modeled, analyzed, simulated, designed and implemented, an active magnetic levitation control system [10] .

In 2005, Winfreed K.N. Anakwa, Namik K. Akyil, and Jose A. Lopez presented the feedback Inc. model $33-210$ laboratory scale one DOF magnetic suspension system as an example of a mechatronic sensing and control plant in a DSP control application. The nonlinear mathematical model of the magnetic suspension system was linearized about a desired equilibrium position of $20.395e-3$ meters, and the resulting linear mathematical model was used to design classical and optimal state feedback digital controllers for stabilization and tracking [11].

In 2007 , the work of Ji Hyuck Yang, Tae Shin Kim, Su Yong Shim, Young Sam Lee and Oh Kyu Kwon considered the modeling of the sensor and actuator characteristics of a magnetic levitation system, using two methods: look up table and segmented linear approximation [12].

In this thesis, different identification methods were used in order to get exact parameters of model CE152, for example, to identify the parameters of the ball and coil subsystem, we have used two interpolation techniques, and we have chosen the technique which give less error. Our thesis mostly like the paper published in 2005 by Winfreed K.N. Anakwa, Namik K. Akyil, and Jose A. Lopez, but they used state feedback control.

1.3 Modeling, Identification and Control

Modeling is used for analysis, prediction, control and supervision of a system, models are classified into two types, linear and nonlinear, most of physical systems are nonlinear as the magnetic levitation model.

System identification is identified as building a mathematical models based on observed data from the dynamical response of a system. The identification process also could be classified into parametric and nonparametric methods:

Parametric: the system equation is described by ordinary differential equation (ODE) and difference equation along with a set of parameters.

Nonparametric: the system doesn't employ a parameter vector in search for a best description, like frequency analysis and a step response.

Moreover, identification means the determination of the model of a dynamic system from input/output measurements. The knowledge of the model is necessary for the design and implementation of a high performance control system.

System identification is an experimental approach for determining the dynamic model of a system. It includes four steps:

- Input/output data acquisition under an experimental setup.
- Finding a suitable model.
- Estimating of the model parameters by comparing the experimental with the simulated data.
- Validation of the identified model.

Linear control is a process of closed loop feedback using a linear controller like P, PI, PD or PID. However, by linear control, we can only control the magnetic levitation in a small range and it may be difficult to design a controller which gives satisfactory, anti-disturbing and robustness. Using PID controller, to get good performance is not easy since PID parameters are hard to be determined, root locus technique is used to determine the PID parameters, then a modified PID controller is used to enhance the system's performance response.

1.4 Research Results and Contributions

In this thesis, we made a mathematical model for a DC electromagnetic levitation system CE152 and identified all its parameters, then validated them by comparing its response with the real model. Since the system is nonlinear and unstable, it must be linearized at a specific operating point, then a PID controller is designed to stabilize it, then the PID controller parameters should be fine tuned to have a good system's performance. We also have built a labratory magnetic levitation apparatus that could be used as a visual demonstration of control system principles.

1.5 Thesis Structure

There are seven chapters in this thesis. Chapter 1 provides introduction and Literature review. Chapter 2 concerns about maglev principles. Chapter 3 presents the theory of continuous control system. Chapter 4 presents the theory of computer control system and explains the stability of digital system. Chapter 5 presents CE152 model setup and the experiments of identification and validation of the system. Chapter 6 presents a modified PID controller for CE152 model. Chapter 7 describe building a laboratory levitation system model. Finally, in chapter 8 the conclusions and suggestions are given.

Chapter 2

Magnetic Levitation Principles

2.1 Magnetic Levitation Background

Magnetic fields are used to describe forces at a distance from electric currents. These currents are of two types:

1. free, currents as drawn from a battery pack, power supply, or an electrical outlet.

2. bound currents as in permanent magnet materials.

The forces come in three variations:

1. An electrical current feels a force from another current.

2. a current feels a force from a permanent magnet.

3. a permanent magnet feels a force from another permanent magnet. This action at a distance is described by saying a magnetic field exists created by one of the bodies at the location of the other body. The magnetic field is the medium by which the force is transferred [13].

In this chapter, a brief discussion concerning the magnetic fields caused by magnetized materials (i.e., permanent magnets) is presented. By demonstrating that magnetic materials can be reduced to effective current distributions, this discussion forms the basis for calculating the forces on permanent magnets. The magnetic fields due to free current distributions are calculated next. These fields are used to calculate the forces felt by current-carrying conductors. Time-varying currents cause time-varying magnetic fields. These changing magnetic fields induce electric currents that, in turn, experience a force.

Maglev systems utilize the fundamental physics of electric currents experiencing forces-at-a-distance. These systems are most often described in terms of the interaction of electrical current with magnetic fields. Because the masses of the vehicles are large, large forces are required for magnetic suspension [14]. These large forces are provided by the high magnetic fields of either large superconducting currents or small air gaps in normal ferromagnetic circuits.

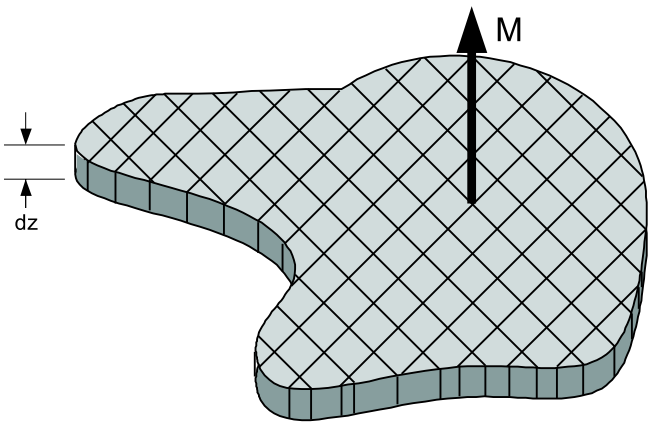

Figure 2.1: A volume of magnetized material contains a very large number of aligned electron spins.

2.2 Magnetic Fields and Forces

2.2.1 Magnetic Fields Caused by Magnetized Materials

Electron spin is a quantum mechanical phenomenon. Its significance here is the fact that there is associated with the electron spin a magnetic moment of fixed magnitude. To determine the forces on magnetic materials, we use the fact that the magnetic moment of the electron spin acts as if it is a current loop.

A volume of magnetized material contains a very large number of aligned electron spins. This is illustrated schematically in Figure 2.1. A grid pattern was superposed onto the material to indicate small volumes of materials which can be analyzed discretely.

Figure 2.2 isolates two small volumes. The one on the left generates a magnetic field due to its magnetic moment, m. The one on the right generates a magnetic field by virtue of the current wrapping the volume (this is commonly referred to as a *current sheet.*), and otherwise ignores the presence of the magnetic material. ***The two magnetic fields are entirely equivalent*** (external to the material). The material property M describes the strength of the magnetic material and the amount of current required per unit distance of height. The parameter K describes the current per unit height within the current sheet. For modern high performance neodymium-iron-boron permanent magnets, $K \approx 900,000$ $amps/meter$ [15].

Assembling many small volumes in juxtaposition, one can see in Figure 2.3 below the result of substituting the current loop for the magnetic material; the internal currents cancel while the surface currents do not cancel. Hence, no matter the shape of the material, the external magnetic field can be exactly reproduced by a current stripe along the material perimeter. (This is true if the magnetization is uniform. If the magnetization is uniform then the currents are equal and cancel. If the magnetization is not uniform, then the equivalent current distribution can be calculated by $J = curl M$, where J is the volume current density.)

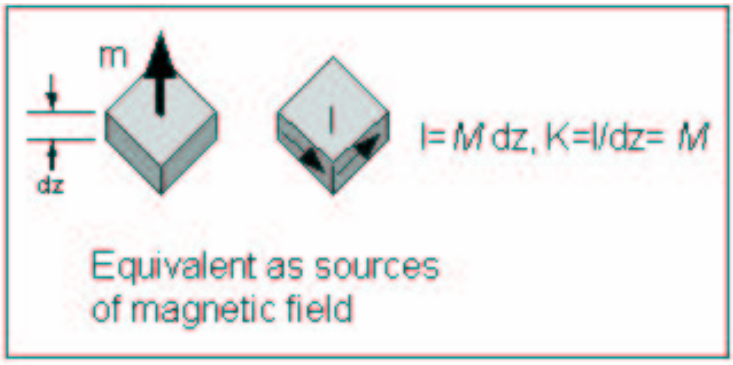

Figure 2.2: Two small volumes of magnetized material.

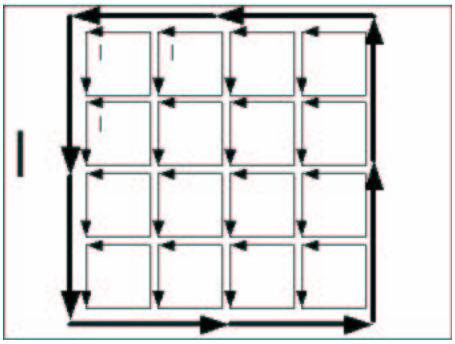

Figure 2.3: Assembling many small volumes in juxtaposition, and the resultant current loop.

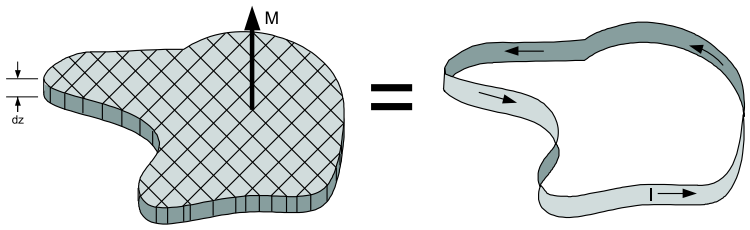

Figure 2.4: The equivalence of magnetic fields associated with a volume of magnetized material.

In summary, the magnetic field of a uniformly magnetized permanent magnet can be exactly reproduced by a current sheet along the perimeter. This equality is indicated graphically in Figure 2.4. The magnitude of the current is proportional to the material thickness with the constant of proportionality dependent upon the material itself. This equivalence of magnetic fields is commonly exploited to calculate the forces on permanent magnet materials [16].

2.2.2 Calculating Magnetic Fields

The Biot-Savart Law Equation 2.1 is the fundamental relationship between current and magnetic field [17]:

$$d\vec{B} = \frac{\mu}{4\pi}\frac{Id\vec{l}\times\vec{r}}{\vec{r}^2} \tag{2.1}$$

where,
dB= differential magnetic field, tesla,
μ= permeability, Henry/m,
I= current, amps,
dI= differential length of current-carrying element, m,
r= vector distance from current element to field point, m.

Two simple geometries for calculating the magnetic field are an infinitely long, straight conductor and a circular loop of conductor.

Straight Conductor

For the straight conductor carrying current upwards along the y-direction in Figure 2.5, the magnetic field can be calculated at any point due to a differential current element as in Equation 2.2:

$$dB = \frac{\mu}{4\pi}\frac{Idlsin\theta}{r^2} \tag{2.2}$$

By integrating along y from +/- infinity, the result is Equation 2.3:

$$B = \frac{\mu I}{2\pi R} \tag{2.3}$$

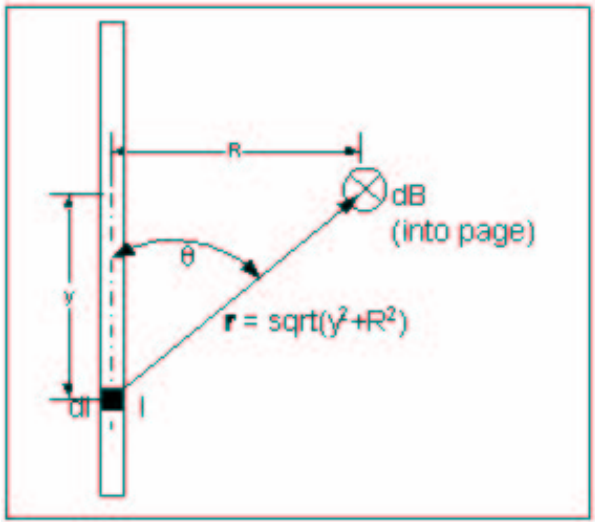

Figure 2.5: The magnetic field of an infinite straight conductor carrying current upwards a long y- axis.

Where the direction of the magnetic field is determined by the right hand rule (point the thumb of the right hand along the direction of current and the fingers curl in the direction of the magnetic field).

Circular Loop at Center

The magnetic field at the center of a circular loop of wire in Figure 2.6 can also be calculated from the Biot-Savart Law. In this case, the angle between the current element and field point is a constant (90^o) so the vector cross product always yields unity. Then the magnetic field Equation 2.4 is:

$$dB = \frac{\mu}{4\pi}\frac{I2\pi R}{R^2} = \frac{\mu I}{2R} \tag{2.4}$$

Circular Loop Anywhere Along Axis

The magnetic field along the axis of a circular loop of wire in Figure 2.7 can also be calculated from the Biot-Savart Law. In this case, the angle between the current element and field point is still a constant (90^o) so the vector cross product always yields unity. The net magnetic field from any current element has vertical and horizontal components. However, as the current element follows the conductor path, the horizontal components of the field cancel while the vertical components add. Then the axial magnetic field Equation 2.5 is:

$$B_z = \frac{\mu}{4\pi}\frac{I2\pi R}{z^2+R^2}cos\alpha = \frac{\mu IR}{2(z^2+R^2)}\frac{R}{\sqrt{z^2+R^2}} = \frac{\mu IR^2}{2(z^2+R^2)^{3/2}} \tag{2.5}$$

Due to the common occurrence of circular coils, this relationship is very important. Along the axis the magnetic field is purely vertical. For values of height, z, above the plane of the coil, which are small compared to the radius, R, (z << R) the vertical magnetic field is insensitive to z. This is due to the finite radius of the coil.

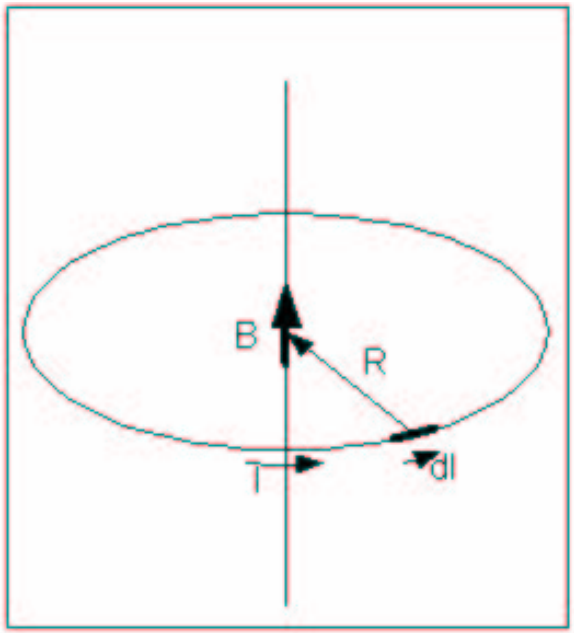

Figure 2.6: The magnetic field at the center of a circular loop of wire.

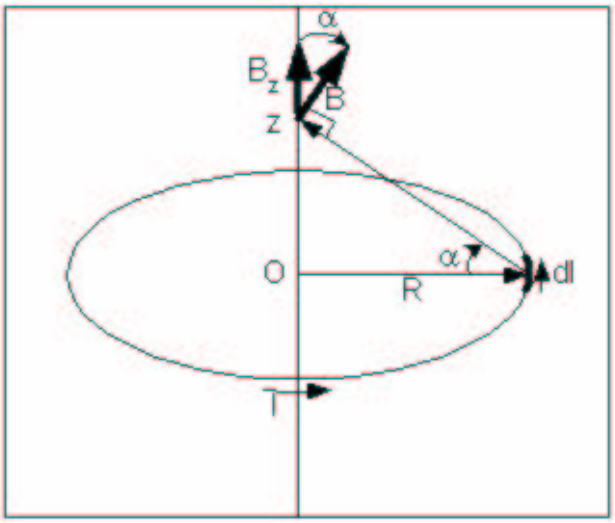

Figure 2.7: The magnetic field at anywhere a long axis a circular loop of wire.

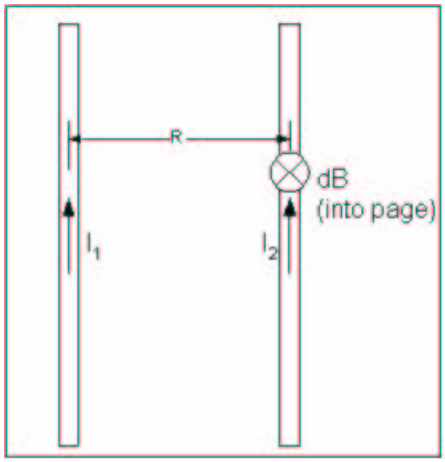

Figure 2.8: Magnetic force of a two conductors carrying current.

For heights z much larger than R (z >> R) the axial field decreases as the reciprocal third power of height. Off-axis, the radial magnetic field decreases as the reciprocal fourth power of height.

2.2.3 Calculating Magnetic Forces

The force between conductors carrying current is given by the Lorentz Law in Equation 2.6 :

$$d\vec{F} = Id\vec{l} \times \vec{B} \tag{2.6}$$

where,

dF= differential force, Newtons. One simple geometry for calculating the magnetic force per unit length is two infinitely long, straight conductors parallel to each other in Equation 2.7 and as shown in Figure 2.8.

$$\frac{F}{l} = -\frac{\mu I_1 I_2}{2\pi R} \tag{2.7}$$

The negative sign means the two parallel currents attract one another. If the direction of one of the currents were to be reversed (anti-parallel currents), the force would also reverse, and the currents would repel. Reversing both currents, of course, once again produces an attractive force.

To evaluate the magnetic field at off-axis points, the same of Equation 2.1 can be used. The mathematics quickly becomes intractable and the solution is usually implemented numerically. Alternatively, specialized computer aided design software can be used to calculate the magnetic field at arbitrary points in space. The two methods approach the calculation differently (the former is the idealized magnetic field numerically approximated while the other is the high fidelity numerical model of the detailed system). Either method will, of course, yield the same result.

The force due to a current-field interaction off-axis can be calculated according to Equation 2.5. Thus, in the case of a Neodymium Iron Boron permanent magnet

positioned above a coil, the magnet can be modeled as a current sheet of thickness equal to that of the magnet. This "current" creates a magnet field at the location of the coil conductors. The force on the coil and, by Newton's third law, the force on the magnet is simply the product of the magnetic field, current and conductor path length.

Since the equivalent current of the permanent magnet is in the theta direction (circumferential around the magnet), the vector cross product in the force equation suggests that to get an axial force, F_z we must have a radial magnetic field, $B_r(-\hat{z} = \hat{\theta} \times \hat{r})$. In developing the control system, it is convenient to express the radial magnetic field in Equation 2.8:

$$B_r = \frac{C1}{(z + C2)^N} \tag{2.8}$$

Where, $C1$ and $C2$ are constants depending upon the geometry of the permanent magnets and N is a parameter describing the decrease in magnetic field with increasing axial distance. For the case of the axial magnetic field, we saw above $C1$ is the surface current density multiplied by the magnet thickness, $C2$ is related to the square of the magnet radius, and N is three or less, depending upon the relative axial distance. The radial magnetic field decreases more rapidly with distance than the axial magnetic field by approximately one more power of the denominator: $3 < N < 4$.

In order to suit the control law, the following form of the force as Equation 2.9 for a magnet-coil interaction is sought:

$$F = \frac{K}{(z + D)^N} \frac{I}{I_{max}} \tag{2.9}$$

The various magnet-coil interactions have been analyzed and the appropriate constants have been determined. Because of the inherent non-linearity of magnetic fields, these constants can vary when the excursion from the calculated system is large, i.e., the equations have been approximated by constant parameters in the region of interest. That is, at very large axial heights or very low heights the constants will differ from those calculated.

The form of the force is the same for interactions between permanent magnets due to the equivalent current concept discussed above. In this case, however, the current is not a free parameter for control but is determined by the geometry.

2.2.4 Calculating Induced Currents

A time-varying magnetic field induces voltages in a closed loop according to Faraday's Law as in Equation 2.10 :

$$V = -N_t \frac{\partial \phi}{\partial t} \tag{2.10}$$

where,

V is the induced voltage around a closed loop,

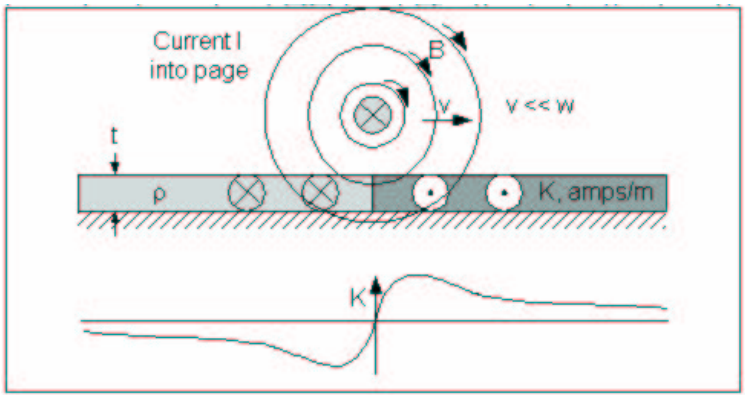

Figure 2.9: A single current-carrying conductor moving relative to a conductive sheet.

N_t is the number of turns of conductor around the loop, and,
$\partial\phi/\partial t$ is the flux rate of change through that loop.

The negative sign in Faraday's Law is the manifestation of Lenz's Law. Lenz's Law states that when currents are induced in bodies due to a changing magnetic field, the currents are in such a direction as to cancel the change in magnetic field experienced by the body. For instance, if no field is present and suddenly a field is applied, the induced currents tend to circulate to cancel the magnetic field. If, however, the magnetic field has previously existed, removal of the magnetic field causes currents to flow in an attempt to maintain the field.

Consider a single current-carrying conductor moving relative to a conductive sheet. It can be shown [16] that there is a characteristic velocity of the motion, $w = \frac{2\rho}{\mu_0 t}$, where, ρ is the sheet material resistivity, t is the thickness of the sheet and μ_0 is the permeability of free space. At standstill, the magnetic field of the current will fully permeate the sheet conductor. The magnetic field lines will be perfect circles about the current center. At very low speeds, ($v << w$) the field still permeates the sheet and the field lines will still be very nearly circular. This situation in shown in Figure 2.9, the induced current in the sheet is K amps/meter.

As the conductor speed is increased to approximately the characteristic velocity ($v \sim w$), the movement of the magnetic field through the sheet causes induced currents to flow. According to Lenz's Law, these currents flow in such a manner so as to cancel the effect of the approaching field. Nevertheless, due to finite resistance, the magnetic field will still penetrate the conductive sheet to an extent and as the conductor leaves the region of magnetic field additional currents are induced to maintain the presence of the field. This situation is shown in Figure 2.10 below. Notice the shear effect of the motion on the magnetic field.

When the speed is increased to substantially above the characteristics velocity, the conductivity of the sheet prevents the magnetic field from any significant penetration. The conductor is moving sufficiently fast that significant resistive dissipation does not occur. Each section of sheet generates the exact required current to perfectly shield the interior of the conductive sheet from the magnetic field. This

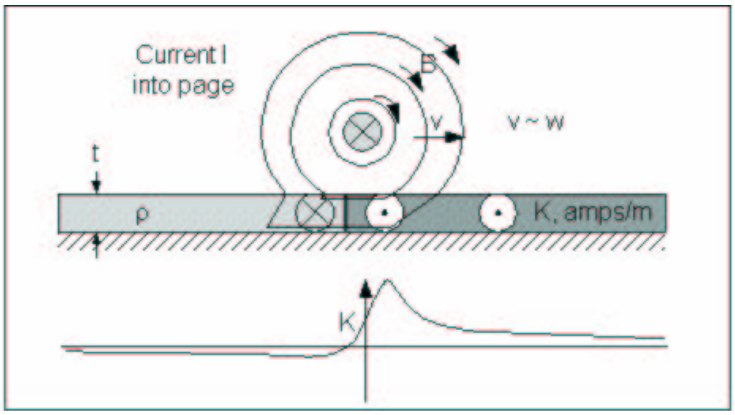

Figure 2.10: A situation when the conductor speed is increased to approximately the characteristic velocity (v $\sim$ w).

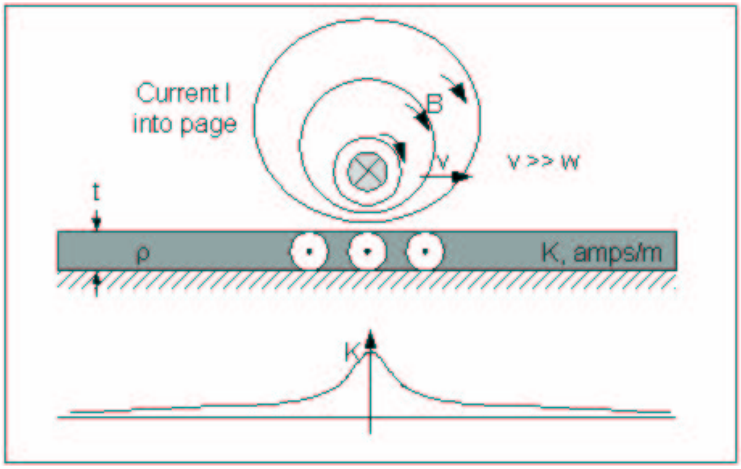

Figure 2.11: A situation when the conductor speed is increased above the characteristic velocity ($v >> w$).

situation is shown in Figure 2.11. Notice that the magnetic field lines do not enter the sheet.

2.3 Maglev Applications

Figure 2.12 shows six arrangements used in magnetic levitation of moving vehicles. Five of the arrangements rely on repulsive forces. The lower elements are fixed (say, with respect to the earth) and the upper elements levitate. The first arrangement (permanent magnet like poles) is the common one for demonstrating like magnetic poles repel. The second and fourth arrangements (permanent magnet and/or superconducting magnet flying over a normal copper lower coil) are similar to that used for the Japanese superconducting Maglev system. The third and fifth systems are similar to the Magneplane system where permanent magnets or superconducting coils fly over normal sheet conductor. Notably, this has been variously proposed as an inexpensive method to attain levitation [18, 19].

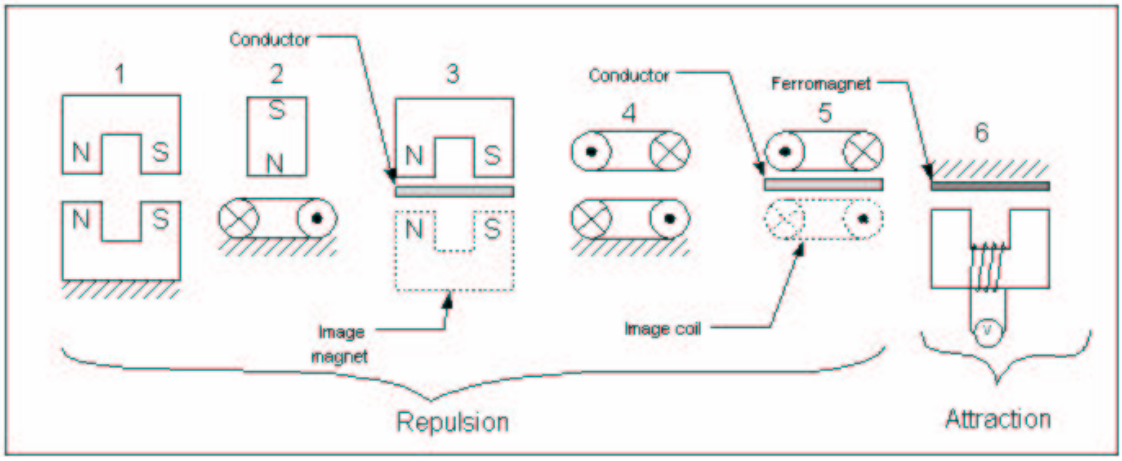

Figure 2.12: Six arrangements used in magnetic levitation of moving vehicles.

The sixth arrangement (electromagnet under a ferromagnet) is quite different and is the basis for the German Transrapid Maglev system. The fixed element is the upper ferromagnetic material and the lower electromagnet is actively controlled. If the current in the electromagnet is too large, the electromagnet feels a net upward force until it contacts the ferromagnetic material. If the current is too small, then insufficient force is available and the electromagnet falls. Hence, the current in the electromagnet must be continuously adjusted to enable levitation without contact.

For applications involving moving vehicles, all maglev designs share a common trait: while generating magnetic lift (in the direction perpendicular to travel) there is also generated magnetic drag (opposing the direction of travel). The details of the lift and drag forces, of course, depend upon the configuration, but the following Figure 2.13 (calculated for the conductor moving over the sheet, configuration 5 above) gives an idea of the variation in magnetic lift and drag with speed. Figure 2.13 shows the drag peak and the reduction in drag as speed increases-in marked contrast to aerodynamic drag. Figure 2.13 also shows the monotonic increase in lift force with increasing relative speed. Note that the lift force equals the drag force when the relative speed is equal to the characteristic velocity, w. Note also that this lift force is equal to 50% of the maximum lift force.

2.4 Current Status of Maglev Internationally

Superconducting Maglev technology was initiated in the late 1960's and early 1970's in the United States in 1969 when Drs. James Powell and Gordan Danby of New

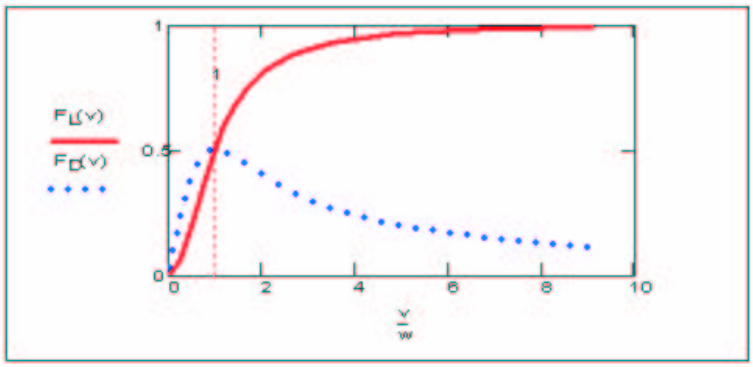

Figure 2.13: The lift and drag forces calculated for the conductor moving over the sheet.

York's Brookhaven National Laboratory invented the concept of a repulsive magnetic suspension levitation using superconducting magnets. In the mid-1970's the US stopped Maglev development due to funding problems. Other countries, however, continued to develop Maglev and today have viable systems. In the early 1990's Maglev research was rekindled at a Federal government level. At various times, the Department of Transportation's Federal Railroad Administration and Federal Transit Administration, NASA, Department of the Air Force, and Department of the Navy have joined resources for the purpose of developing Maglev and Linear Motor technology. Although each agency had its own specific application in mind, a loose consortium seemed to provide the best bang for the buck. The situation has progressed where today there are several high speed ($\approx$ 300 mph) and low speed ($\approx$ 100 mph) regions in this country where Maglev is thought to be a viable alternative means of rapid public transportation, yet it is still unproven in the United States [20, 22].

Germany's Transrapid vehicle has been extensively tested and has been proposed for use on several projects in this country. The Germans are presently constructing a Transrapid route from Hamburg to Berlin.

Japan is developing a system that uses superconducting magnets and is currently constructing a major test route that will ultimately be incorporated into a revenue-producing route. Approximately 80% of this system will be in tunnels cut into mountains. This has greatly increased the construction cost but has decreased the cost of land acquisition for the Maglev right-of-way.

Chapter 3

Continuous Control Systems

3.1 Continuous-time Models

3.1.1 Time Domain

Equation 3.1 gives an example of a differential equation describing a simple dynamic system:

$$\frac{dy}{dt} = -\frac{1}{T}y(t) + \frac{G}{T}u(t) \tag{3.1}$$

In Equation 3.1 u represents the input (or the control) of the system and y the output. This equation may be simulated by continuous means as illustrated in Figure 3.1.

The step response illustrated in Figure 3.1 reveals the speed of the output variations, characterized by the time constant T, and the final value, characterized by the static gain G.

Using the differential operator, Equation 3.1 is written as

$$(p + \frac{1}{T})y(t) = \frac{G}{T}u(t); \qquad p = \frac{d}{dt} \tag{3.2}$$

For systems described by differential equations as in Equation 3.1 we distinguish three types of time response:

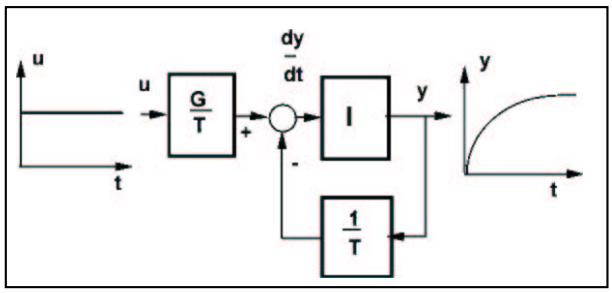

Figure 3.1: Simulation and time responses of the dynamic system described by Equation 3.1 (I- integrator).

1. The "free" response: it corresponds to the system response starting with an initial condition $y(0) = y_0$ and for an identically zero input for all $t(u = 0, \forall t)$.

2. The "forced" response: it corresponds to the system response starting with an identically zero initial condition $y(0) = 0$ and for a non-zero input $u(t)$ for all $t \geq 0$ $(u(t) = 0, t < 0; u(t) \neq 0, t \geq 0)$ and $y(t) = 0$ for $t \leq 0)$.

3. The "total" response: it represents the sum of the "free" and "forced" responses (the system being linear, the superposition principle applies) [23].

3.1.2 Frequency Domain

The characteristics of the models in the form of Equation 3.1 can also be studied in the frequency domain. The idea is then to study the system behavior when the input is a sinusoidal or a cosinusoidal input that varies over a given range of frequencies.

Remember that

$$e^{j\omega t} = cos(\omega t) + jsin(\omega t) \tag{3.3}$$

And, consequently, it can be considered that the study of the dynamic system described by an equation of the type 3.1, in the frequency domain, corresponds to the study of the system output for the inputs of the type $u(t) = e^{j\omega t}$.

Since the system is linear, the output will be a signal containing only the frequency ω, the input being amplified or attenuated (and possibly a phase Lag will appear) according to ω; i.e. the output will be of the form

$$y(t) = H(j\omega)e^{j\omega t} \tag{3.4}$$

However there is nothing to stop us from considering that the input is formed by damped or undamped sinusoids and cosinusoids, which in this case are written as

$$u(t) = e^{\sigma t}e^{j\omega t} = e^{(\sigma + j\omega)t} = e^{st}; \qquad s = \sigma + \omega \tag{3.5}$$

where s is interpreted as a complex frequency. As a result of the linearity of the system, the output will reproduce the input signal, amplified (or attenuated), with a phase lag or not, depending on the values of s; i.e. the output will have the form

$$y(t) = H(s)e^{st} \tag{3.6}$$

And it must satisfy Equation 3.1 for $u(t) = e^{st}$.

From Equation 3.6 one gets

$$\frac{dy(t)}{dt} = sH(s)e^{st} \tag{3.7}$$

And by substituting Equation 3.7 in Equation 3.1, while bearing in mind that $u(t) = e^{st}$, one obtains

$$(s + \frac{1}{T})H(s)e^{st} = \frac{G}{T}e^{st} \tag{3.8}$$

$H(s)$, which gives the gain and phase deviation introduced by the system of Equation 3.1 at different complex frequencies, is known as the transfer function. The

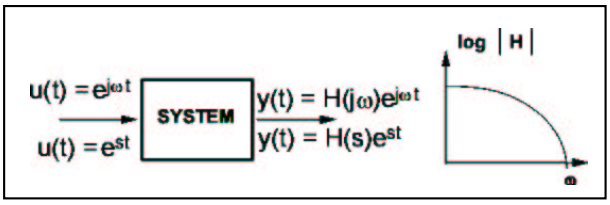

Figure 3.2: Response of a dynamic system to periodic inputs.

transfer function $H(s)$ is a function of only the complex variable s. It represents the ratio between the system output and input when the input is e^{st}. From Equation 3.8, it turns out that, for the system described by Equation 3.1, the transfer function is

$$H(s) = \frac{G}{1 + sT} \tag{3.9}$$

The transfer function $H(s)$ generally appears as a ratio of two polynomials in s ($H(s) = B(s)/A(s)$). The roots of the numerator polynomial $B(s)$ define the "zeros" of the transfer function and the roots of the denominator polynomial ($A(s)$) define the "poles" of the transfer function. The "zeros" correspond to those complex frequencies for which the system gain is null and the "poles" correspond to those complex frequencies for which the system gain is infinite.

Note that the transfer function $H(s)$ can also be obtained by two other techniques:

- Replacing p by s in Equation 3.2 and algebraic computation of the y/u ratio.
- Using the Laplace transform [24].

The use of the representation of dynamic models in the form of transfer functions presents a certain number of advantages for the analysis and synthesis of closed-loop control systems. In particular the concatenation of dynamic models described by transfer functions is extremely easy.

3.1.3 Stability

The stability of a dynamic system is related to the asymptotic behavior of the system (when $t \to \infty$), starting from an initial condition and for an identically zero input.

For example, consider the first-order system described by the differential Equation 3.1 or by the transfer function given in Equation 3.9.

Consider the free response of the system given in Equation 3.1 for $u \equiv 0$ and from an initial condition $y(0) = y_0$:

$$\frac{dy}{dt} + \frac{1}{T}y(t) = 0; \qquad y(0) = y_0 \tag{3.10}$$

A solution for y will be in the form

$$y(t) = Ke^{st} \tag{3.11}$$

in which K and s are to be determined. From Equation 3.11 one finds

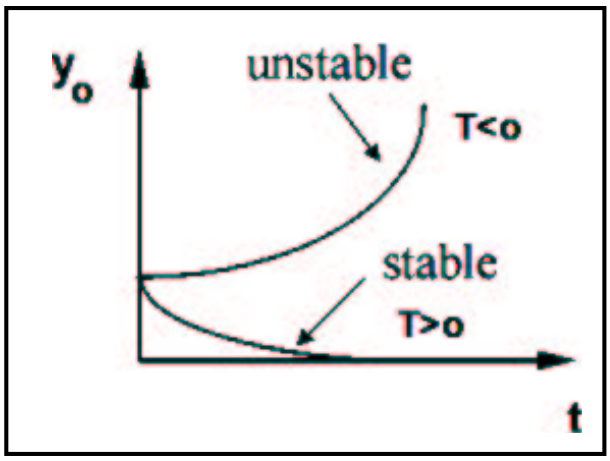

Figure 3.3: Free response of the first-order system.

$$\frac{dy}{dt} = sKe^{st} \tag{3.12}$$

And Equation 3.10 becomes

$$Ke^{st}\left(s + \frac{1}{T}\right) = 0 \tag{3.13}$$

from which one obtains

$$s = -\frac{1}{T}; \qquad K = y_0 \tag{3.14}$$

And respectively

$$y(t) = y_0 e^{-\frac{t}{T}} \tag{3.15}$$

The response for $T > 0$ and $T < 0$ is illustrated in Figure 3.3.

For $T > 0$, we have $s < 0$ and, when $t \to \infty$ the output will tend toward zero (asymptotic stability). For $T < 0$, we have $s > 0$ and, when $t \to \infty$, the output will diverge (instability). Note that $s = -\frac{1}{T}$ corresponds to the pole of the first-order transfer function of Equation 3.9.

We can generalize this result: it is the sign of the real part of the roots of the transfer function denominator that determines the stability or instability of the system. In order that a system be asymptotically stable, all the roots of the transfer function denominator must be characterized by Re $s < 0$. If one or several roots of the transfer function denominator are characterized by Re $s > 0$, then the system is unstable.

For Re $s = 0$ we have a limit case of stability because the amplitude of $y(t)$ remains equal to the initial condition (e.g. pure integrator, $(dy/dt = u(t)$; in this case $y(t)$ remains equal to the initial condition).

Figure 3.4 gives the stability and instability domains in the plane of the complex variable s.

Note that stability criteria have been developed, which allow determining the existence of unstable roots of a polynomial without explicitly computing its roots, (e.g. Routh-Hurwitz' criterion) [24].

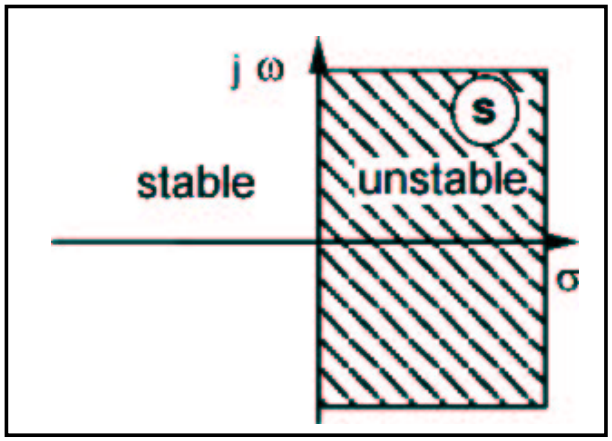

Figure 3.4: Stability and instability domains in the s-plane.

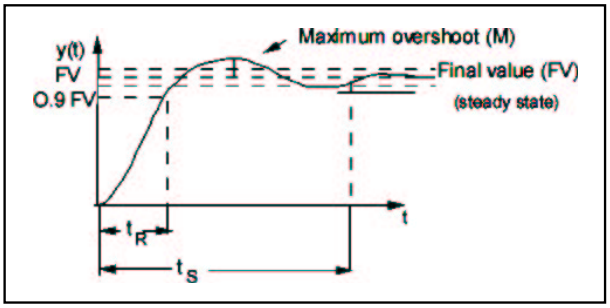

Figure 3.5: Step response.

3.1.4 Time Response

The response of a dynamic system is studied and characterized for a step input. The response of a stable system is generally of the form shown in Figure 3.5.

The step response is characterized by a certain number of parameters:

- t_R(rise time):generally defined as the time needed to reach 90% of the final value (or as the time needed for the output to pass from 10 to 90% of the final value). For systems that present an overshoot of the final value, or that have an oscillating behavior, we often define the rise time as the time needed to reach for the first time the final value. Subsequently we shall generally use the first definition of t_R.
- t_S(settling time): defined as the time needed for the output to reach and remain within a tolerance zone around the final value ($\pm 10\%$, $\pm 5\%$, $\pm 2\%$).
- FV (final value): a fixed output value obtained for $t \to \infty$.
- M (maximum overshoot): expressed as a percentage of the final value.

For example, consider the first-order system

$$H(s) = \frac{G}{1 + sT}$$

The step response for a first-order system is given by

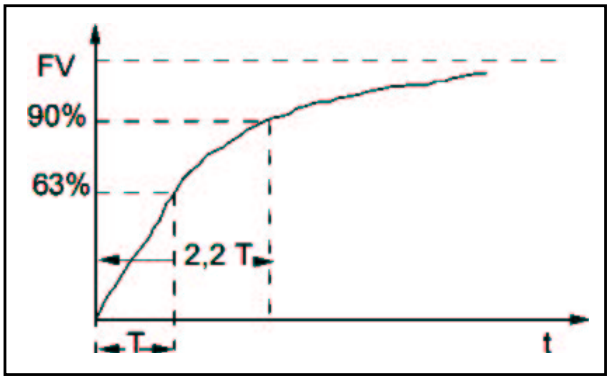

Figure 3.6: Step response for a first-order system.

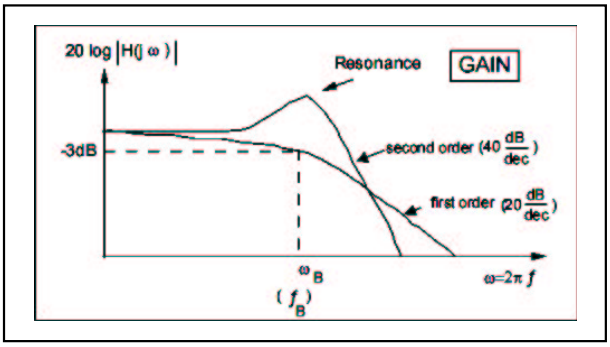

Figure 3.7: Frequency responses.

$$y(t) = G(1 - e^{-t/T})$$

Since the input is a unitary step one has

$FV = G$ (static gain); $t_R = 2.2T$; $t_S = 2.2T$(for $\pm 10\% FV$) ; $t_S = 3T$ (for $\pm 5\% FV$); $M = 0$

and the response of such a system is represented in Figure 3.6. Note that for $t = T$, the output reaches 63% of the final value.

3.1.5 Frequency Response

The frequency response of a dynamic system is studied and characterized for periodic inputs of variable frequency but of constant magnitude. For continuous-time systems, the gain-frequency characteristic is represented on a double logarithmic scale and the phase frequency characteristic is represented on a logarithmic scale only for the frequency axis.

The gain $G(\omega) = |H(j\omega)|$ is expressed in dB ($|H(j\omega)|dB = 20log|H(j\omega)|$) on the vertical axis and the frequency ω, expressed in rad/s ($\omega = 2\pi f$ where f represents the frequency in Hz) is represented on the horizontal axis. Figure 3.7 gives some typical frequency response curves.

The characteristic elements of the frequency response are:

- $f_B(\omega_B)$(bandwidth): the frequency (radian frequency) from which the zero frequency (steady-state) gain $G(0)$ is attenuated more than 3 dB; $G(\omega_B) =$

$G(0) - 3dB$; $(G(\omega_B) = 0.707G(0))$.

- $f_C(\omega_C)$(cut-off frequency): the frequency (rad/s) from which the attenuation introduced with respect to the zero frequency is greater than N dB; $G(j\omega_c) = G(0) - NdB$.
- Q (resonance factor): the ratio between the gain corresponding to the maximum of the frequency response curve and the value $G(0)$.
- Slope: it concerns the tangent to the gain frequency characteristic in a certain region. It depends on the number of poles and zeros and on their frequency distribution.

Consider, as an example, the first-order system characterized by the transfer function given by Equation 3.9. For $s = j\omega$ the transfer function of Equation 3.9 is rewritten as

$$H(j\omega) = \frac{G}{1 + j\omega T} = |H(j\omega)|e^{j\phi(\omega)} = |H(j\omega)|\angle\phi(\omega) \tag{3.16}$$

where $|H(j\omega)|$ represents the modulus (gain) of the transfer function and $\angle\phi(\omega)$ the phase deviation introduced by the transfer function. We then have

$$G(\omega) = H(j\omega) = \frac{G}{\sqrt{(1 + \omega^2 T^2)}} \tag{3.17}$$

$$\angle\phi(\omega) = tan^{-1}\left[\frac{ImG(j\omega)}{ReG(j\omega)}\right] = tan^{-1}[-\omega T] \tag{3.18}$$

From Equation 3.17 and from the definition of the bandwidth ω_B, we obtain:

$$\omega_B = \frac{1}{T}$$

Using Equation 3.18, we deduce that for $\omega = \omega_B$ the system introduces a phase deviation $\angle\phi(\omega_B) = -45^0$. Also note that for $\omega = 0$, $G(0) = G$, $\angle\phi(0) = 0^0$ and for $\omega \to \infty$, $G(\infty) = 0$, $\angle\phi(\infty) = -90°$.

Figure 3.8 gives the exact and asymptotic frequency characteristics for a first order system (gain and phase).

As a general rule, each stable pole introduces an asymptotic slope of -20 dB/dec (or 6 dB/octave) and an asymptotic phase lag of $-90°$. On the other hand, each stable zero introduces an asymptotic slope of +20 dB/dec and an asymptotic phase shift of $+90°$.

It follows that the asymptotic slope of the gain-frequency characteristic in dB, for high frequencies, is given by

$$\frac{\Delta G}{\Delta \omega} = -(n - m) \times 20dB/dec \tag{3.19}$$

where n is the number of poles and m is the number of zeros.

The relation

$$\angle\phi(\infty) = -(n - m) \times 90° \tag{3.20}$$

gives the asymptotic phase deviation.

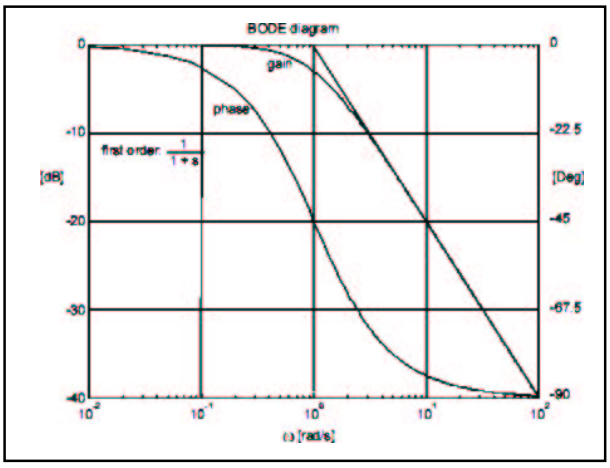

Figure 3.8: Frequency characteristic of a first-order system.

3.1.6 Study of the Second-order System

The normalized differential equation for a second-order system is given by:

$$\frac{d^2y(t)}{dt^2} + 2\zeta\omega_0\frac{dy(t)}{dt} + \omega_0^2 y(t) = \omega_0^2 u(t) \tag{3.21}$$

Using the operator $p = d/dt$, Equation 3.21 is rewritten as

$$(p^2 + 2\zeta\omega_0 p + \omega_0^2)y(t) = \omega_0^2 u(t) \tag{3.22}$$

Letting $u(t) = e^{st}$ in Equation 3.21, or $p = s$ in Equation 3.22, the normalized transfer function of a second-order system is obtained:

$$H(s) = \frac{\omega_0^2}{s^2 + 2\zeta\omega_0 s + \omega_0^2} \tag{3.23}$$

in which

- ω_0: natural frequency in rad/s($\omega_0 = 2\pi f_0$)
- ζ: damping factor

The roots of the transfer function denominator (poles) are

1. $|\zeta| < 1$, complex poles (oscillatory response):

$$s_{1,2} = -\zeta\omega_0 \pm j\omega_0\sqrt{1-\zeta^2} \tag{3.24}$$

   ($\omega_0\sqrt{1-\zeta^2}$ is called "damped resonance frequency").

2. $|\zeta| \geq 1$, real poles (aperiodic response):

$$s_{1,2} = -\zeta\omega_0 \pm \omega_0\sqrt{\zeta^2-1} \tag{3.25}$$

The following situations are thus obtained depending on the value of the damping factor ζ:

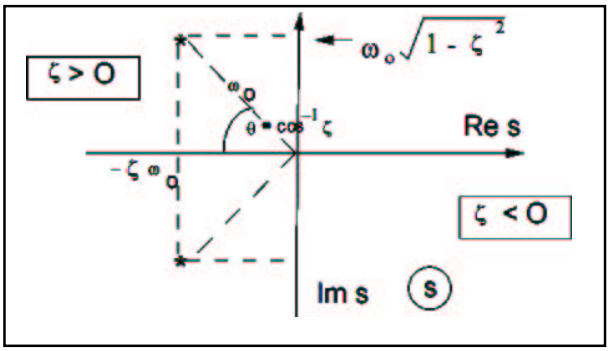

Figure 3.9: The roots of the second-order system as a function of ζ (for$|\zeta| \leq 1$).

- $\zeta > 0$ asymptotically stable system
- $\zeta < 0$ unstable system

These different cases are summarized in Figure 3.9.

The step response for the second-order system described by Equation 3.21 is given by the formula (for $|\zeta| \leq 1$)

$$y(t) = 1 - \frac{1}{\sqrt{1-\zeta^2}} e^{-\zeta\omega_0 t} \left(sin\omega_0 \sqrt{1-\zeta^2} t + \theta \right) \tag{3.26}$$

in which

$$\theta = cos^{-1}\zeta \tag{3.27}$$

Figure 3.10 gives the normalized step responses for the second-order system, This diagram makes it possible to determine both the response of a given second-order system and the values of ω_0 and ζ, in order to obtain a system having a given rise (or settling) time and overshoot.
To illustrate this, consider the problem of determining ω_0 and ζ so that the rise time (0 to 90% of The final value) is $2.75s$ with a maximum overshoot $\approx 5\%$. From Figure 3.10, it is seen that in order to ensure an overshoot $\approx 5\%$ we must choose $\zeta = 0.7$. The corresponding normalized rise time is: $\omega_0 t_M \approx 2.75$. It can be concluded that to obtain a rise time of $2.75s$, $\omega_0 = 1rad/sec$ must be taken.

In order to make easier the determination of ω_0 and ζ for a given rise time t_R and a given maximum overshoot M, the graph of M as a function of ζ and the graph of $\omega_0 t_R$ as a function of ζ have been represented in Figure 3.11 a, b.

The curve given in Figure 3.11 a allows choosing the damping factor ζ for a given maximum overshoot M. Once the value of ζ chosen, the Figure 3.11 b gives the corresponding value of $\omega_0 t_R$. This allows one to determine ω_0 for a given rise time t_R.

The settling time t_S, for different values of ζ and of the tolerance zone around the final value, can be determined from the normalized responses given in Figure 3.12 gives the normalized frequency responses for a second-order system [25].

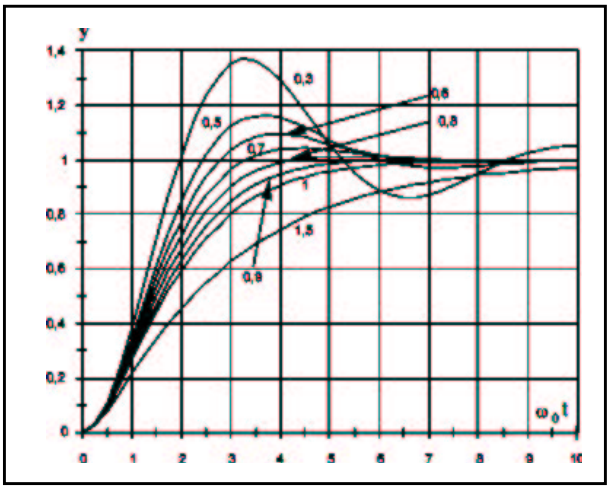

Figure 3.10: Normalized frequency responses of a second-order system to a step input.

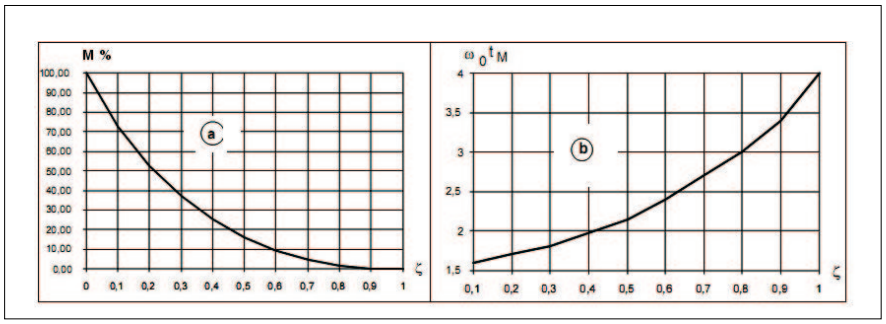

Figure 3.11: Second-order system: a) maximum overshoot M as a function of the damping factor ζ; b) normalized rise time as a function of ζ.

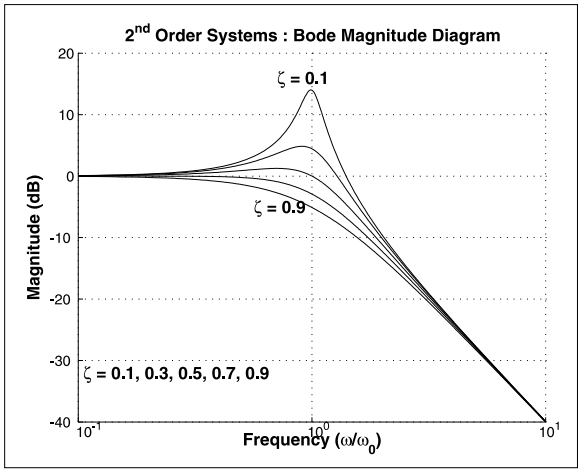

Figure 3.12: Normalized frequency responses of a second-order system (gain).

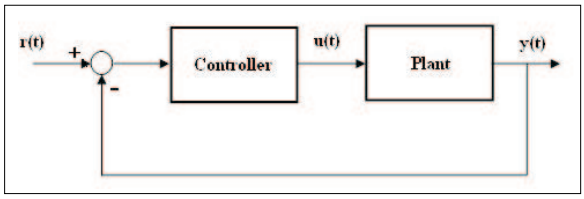

Figure 3.13: Control system.

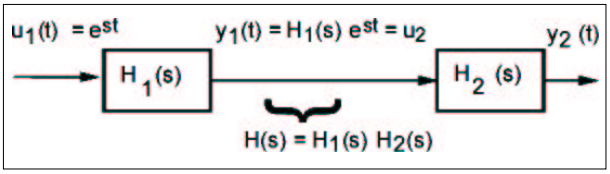

Figure 3.14: Cascade connection of two systems.

3.2 Closed-loop Systems

Figure 3.13 shows a simple control system. $y(t)$ is the plant output and represents the controlled variable, $u(t)$ is the input (control signal) applied to the plant by the controller (manipulated variable) and $r(t)$ is the reference signal.

The control systems have a closed-loop structure (the control signal is a function of the difference between the reference and the measured value of the controlled variable) and contains at least two dynamic systems (the plant and the controller).

We shall examine in this section the computation of the closed-loop transfer function, the steady-state error with respect to the reference signal and stability of the closed-loop systems.

3.2.1 Cascaded Systems

Figure 3.14 represents the cascade connection of two linear systems characterized by the transfer functions $H_1(s)$ and $H_2(s)$.

If the input to $H_1(s)$ is $u_1(t) = e^{st}$ the following relations are found:

$$u_2(t) = y_1(t) = H_1(s)e^{st} \tag{3.28}$$

$$y_2(t) = H_2(s)u_2(t) = H_2(s)H_1(s)e^{st} = H(s)e^{st} \tag{3.29}$$

and we can conclude that the transfer function of two cascaded systems is

$$H(s) = H_1(s)H_2(s) \tag{3.30}$$

or in the general case of n cascaded systems

$$H(s) = H_n(s)H_{n-1}(s)....H_2(s)H_1(s) \tag{3.31}$$

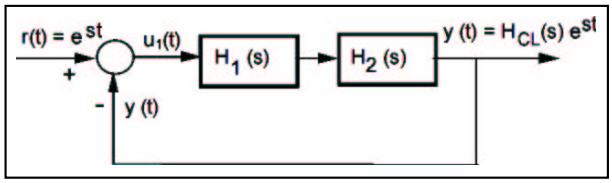

Figure 3.15: Closed-loop system.

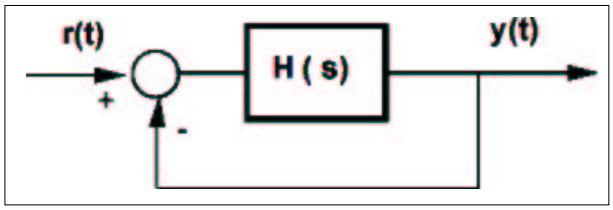

Figure 3.16: Closed-loop system.

3.2.2 Transfer Function of Closed-loop Systems

Consider the closed-loop system represented in Figure 3.15.

The output $y(t)$ of the closed-loop system in the case of an external reference $r(t) = e^{st}$ is written as

$$y(t) = H_{CL}(s)e^{st} = H_2(s)H_1(s)u_1(t) \tag{3.32}$$

But $u_1(t)$ is given by the relation

$$u_1(t) = r(t) - y(t) \tag{3.33}$$

Introducing this relation into Equation 3.32, one gets

$$[1 + H_2(s)H_1(s)]y(t) = H_2(s)H_1(s)r(t) \tag{3.34}$$

from which

$$H_{CL}(s) = \frac{H_2(s)H_1(s)}{1 + H_2(s)H_1(s)} \tag{3.35}$$

The stability of the closed-loop system will be determined by the real parts of the roots (poles) of the transfer function denominator $H_{CL}(s)$.

3.2.3 Steady-state Error

When carrying out the synthesis of a closed-loop system, our aim is to obtain an asymptotically stable system having a given response time, a specified overshoot and ensuring a zero steady-state error with respect to the reference signal. In Figure 3.16, it is desired that, in steady-state, $y(t)$ equals $r(t)$, i.e. the steady-state gain of the closed-loop system between $y(t)$ and $r(t)$ must be equal to 1.

In Figure 3.16 the global transfer function of the feed forward channel $H_{OL}(s)$ is of the form

$$H_{OL}(s) = \frac{b_0 + b_1 s + ... + b_m s^m}{a_0 + a_1 s + ... + a_n s^n} = \frac{B(s)}{A(s)} \tag{3.36}$$

and the transfer function in closed-loop is given by

$$H_{CL}(s) = \frac{H_{OL}(s)}{1 + H_{OL}} = \frac{B(s)}{A(s) + B(s)} \tag{3.37}$$

The steady-state corresponds to a zero frequency ($s = 0$). The steady-state gain is obtained by making $s = 0$ in the transfer function given by Equation 3.37.

$$y = H_{CL}(0)r = \frac{B(0)}{A(0) + B(0)}r = \frac{b_0}{a_0 + b_0}r \tag{3.38}$$

in which y and r represent the stationary values of the output and the reference. To obtain a unitary steady-state gain ($H_{CL}(0) = 1$), it is necessary that

$$\frac{b_0}{a_0 + b_0} = 1 \Rightarrow a_0 = 0 \tag{3.39}$$

This implies that the denominator of the transfer function $H(s)$ should be of the following form:

$$A(s) = s(a_1 s + a_2 s + ... + a_{n-1}s^{n-1}) = sA'(s) \tag{3.40}$$

and, respectively:

$$H_{OL}(s) = \frac{1}{s}.\frac{B(s)}{A'(s)} \tag{3.41}$$

Thus to obtain a zero steady-state error in closed-loop when the reference is a step, the transfer function of the feed forward channel must contain an integrator.

This concept can be generalized for the case of time varying references as indicated below with the internal model principle: to obtain a zero steady-state error, $H_{OL}(s)$ must contain the internal model of the reference $r(t)$.

The internal model of the reference is the transfer function of the filter that generates $r(t)$ from the Dirac pulse. E.g., step $=(1/s)$. Dirac , ramp $=(1/s^2)$. Dirac).

Therefore, for a ramp reference, $H_{OL}(s)$ must contain a double integrator in order to obtain a zero steady-state error [26].

3.3 PI and PID Controllers

The PI (proportional + integral) and PID (proportional + integral + derivative) controllers are widely used for the control of continuous-time systems.

An extremely rich literature has been dedicated to design methods and parameters adjustment of these controllers. Also note that there are several structures for PI and PID controllers (with different transfer function and tuning parameters).

Synthesis methods for PI and PID controllers have been developed and implemented [26]. These methods can be divided into two categories: a) methods using frequency and time characteristics of the plant (non-parametric model) and b) methods using the plant transfer function (parametric model) [27].

3.3.1 PI Controller

In general PI controllers have as input the difference between the reference and the measured output and as output the control signal delivered to the actuator (see Figure 3.15). A typical transfer function of a PI controller is

$$H_R(s) = K\left[1 + \frac{1}{T_i s}\right] = \frac{K(T_i s + 1)}{T_i s}$$

in which K is called the proportional gain and the integral action of the PI controller. There also exist, however also PI controllers with independent actions, i.e.

$$H_R(s) = K_P + \frac{1}{T_i s}$$

In certain situations the proportional action may operate only on the measured output as we will later [27, 28].

3.3.2 PID Controller

The transfer function of a typical PID controller is

$$H_{PID}(s) = K\left(1 + \frac{1}{T_i s} + \frac{T_d s}{1 + \frac{T_d s}{N}}\right) \tag{3.42}$$

in which K specifies the proportional gain, T_i characterizes the integral action, T_d characterizes the derivative action and $1 + (T_d/N)s$ introduces a filtering effect on the derivative action (low-pass filter) [28, 29].

By summing up the three terms, the transfer function given by Equation 3.43 can also be rewritten as

$$H_{PID}(s) = \frac{K\left[1 + s\left(T_i + \frac{T_d}{N}\right) + s^2\left(T_i T_d + \frac{T_i T_d}{N}\right)\right]}{T_i s\left(1 + \frac{T_d}{N} s\right)} \tag{3.43}$$

Several structures for PID controllers exist. In addition there are situations when the proportional and derivative actions act only on the measured output.

Chapter 4

Computer Control Systems

4.1 Introduction to Computer Control

The first approach for introducing a digital computer or a microprocessor into a control loop is indicated in Figure 4.1; the measured error between the reference and the output of the plant is converted into digital form by an analog-to-digital converter (ADC), at sampling instants k defined by synchronization clock. The computer interprets the converted signal $y(k)$ as a sequence of numbers, which it processes using a control algorithm and generates a new sequence of numbers $u(k)$ representing the control. By mains of a digital-to-analog converter (DAC), this sequence is converted into an analog signal, which is maintained constant between the sampling instants by a zero order hold (ZOH). The cascade: ADC-computer-DAC should behave in the same way as an analog controller, which implies the use of a high sampling frequency but the algorithm implemented on the computer is very simple.

A second and much more interesting approach of a digital computer or microprocessor in a control loop is illustrated in Figure 4.2 which can be obtained from Figure 4.1 by moving the reference-output comparator after the analog-to-digital converter. the reference is now specified in a digital way as a sequence provided by a computer [30].

In Figure 4.2 the set DAC-plant-ADC is interpreted as a discretized system, whose control input is the sequence $u(k)$ generated by the computer, the output being the sequence $y(k)$ resulting from the A/D conversion of the system output $y(t)$. This discretized system is characterized by a discreet-time model, which describes the relation between the sequence of numbers $u(k)$ and the sequence of numbers $y(k)$. This model is related to the continues-time model of the plant.

This approach offers several advantages among these advantages here we recall the following :

1. The sampling frequency is chosen in accordance with the bandwidth of the continuous time system (it will be much lower than for the first approach).

2. Possibility of a direct design of the control algorithms tailored to the discretized plant models.

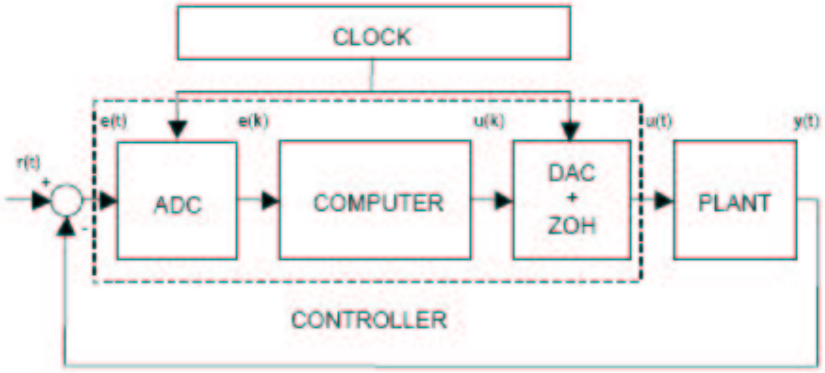

Figure 4.1: Digital realization of an analog type controller.

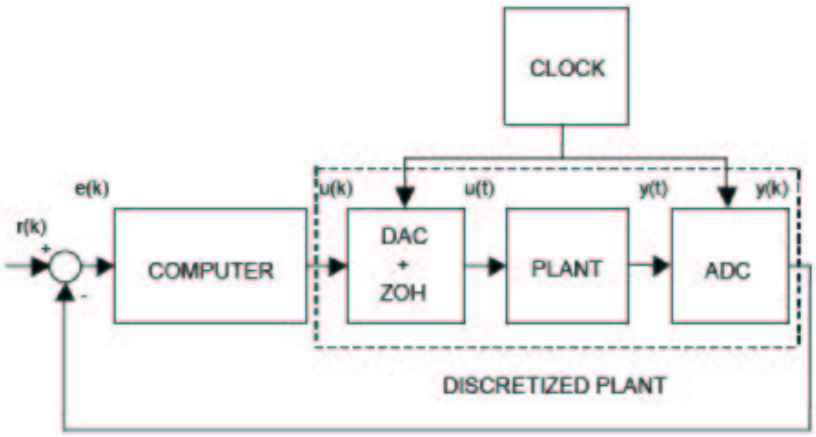

Figure 4.2: Digital control system

.

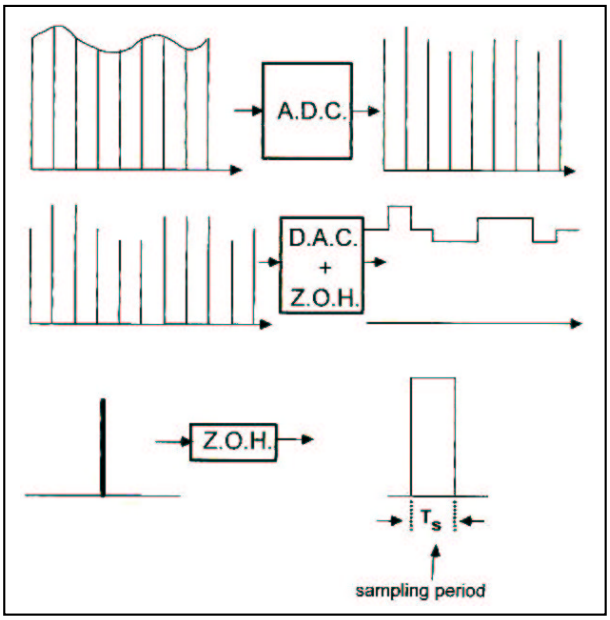

Figure 4.3: Operation of the analog-to-digital converter (ADC), the digital-to-analog converter (DAC) and zero-order hold (ZOH).

3. Efficient use of the computer since the increase of the sampling period permits the computation power to be used in order to implement algorithms which are more performant but more complex than a PID controller, and which require a longer computation time.

The changing over to new language (discreet-time dynamic models) makes possible to use various high performing control strategies which can not be implemented by analog controllers.

The operating details of the ADC, the DAC and ZOH are illustrated in Figure 4.3.

The analog-to-digital converter implements two functions:

1. Analog signal sampling: this operation consists in the replacement of the continuous signal with a sequence of values equally spaced in the time domain (the temporal distance between two values is the sampling period), as these values correspond to the continuous signal amplitude at sampling instants.

2. Quantization: this is the operation by means of which the amplitude of a signal is represented with a discrete set of different values (quantized values of the signal), generally coded with a binary sequence.

The general use of high-resolution A/D converters (where the samples are coded with 12 bits or more) allows one to consider the quantification effects as negligible, and this assumption will hold in the following.

The digital-analog converter (DAC) converts at the sampling instants a discrete signal, digitally coded, in a continuous signal.

The zero-order hold (ZOH) keeps constant this continuous signal between two sampling instants (sampling period), in order to provide a continuous-time signal [31].

4.2 Discretization and Overview of Sampled-data Systems

4.2.1 Discretization and Choice of Sampling Frequency

Figure 4.4 illustrates the discretization of a sinusoid of frequency f_0 for several sampling frequencies f_s.

It can be noted that, for a sampling frequency $f_s = 8\ f_0$, the continuous nature of the analog signal is unaltered in the sampled signal.

For the sampling frequency $f_s = 2\ f_0$, if the sampling is carried out at instants $2\pi f_0 t$, other than multiples of π , a periodic sampled signal is still obtained.

However if the sampling is carried out at the instants where $2\pi f_0 t = n\pi$, the corresponding sampled sequence is identically zero.

If the sampling frequency is decreased under the limit of $f_s = 2f_0$, a periodic sampled signal still appears, but its frequency differs from that of the continuous signal ($f = f_s - f_0$).

In order to reconstruct a continuous signal from the sampled sequence, the sampling frequency must verify the condition (Nyquist's theorem):

$$f_s > 2f_{max} \tag{4.1}$$

in which f_{max} is the maximum frequency to be transmitted. The frequency $f_s = 2f_{max}$ is a theoretical limit; in practice. a higher sampling frequency must be chosen.

The existence of a maximum limit for the frequency that may be converted without distortion, for a given sampling frequency, is also understandable when it is observed that the sampling of a continuous-time signal is a "magnitude modulation" of a "carrier" frequency f_s. The modulation effect may be observed in the replication of the spectrum of the modulating signal (in our case the continuous signal) around the sampling frequency and its multiples.

The spectrum of the sampled signal. If the maximum frequency of the continuous signal (f_{max}) is less than $(1/2)f_s$ is represented in the upper part of Figure 4.5.

The spectrum of the sampled signal, if $f_{max} > (1/2)f_s$, is represented in the lower part of Figure 4.5. The phenomenon of overlapping (aliasing) can be observed.

This corresponds to the appearance of distortions. The frequency $(1/2)f_s$, which defines the maximum frequency (f_{max}) admitted for a sampling with no distortions, is known as "Nyquist frequency" (or Shannon frequency).

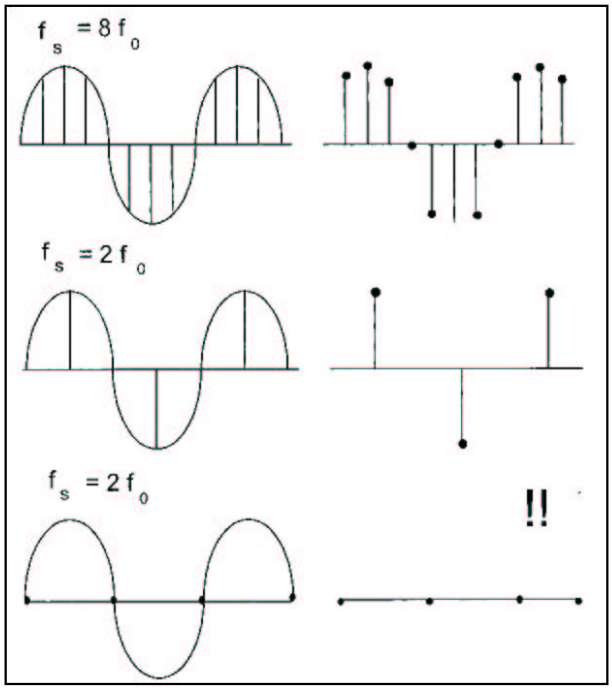

Figure 4.4: sinusoidal signal discretization.

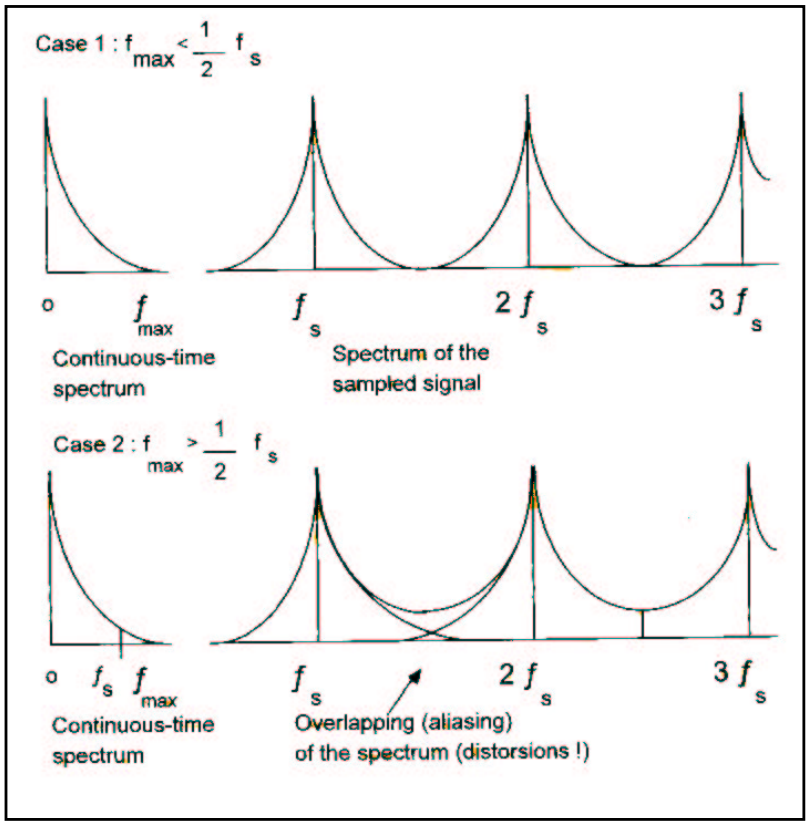

Figure 4.5: spectrum of sampled signal.

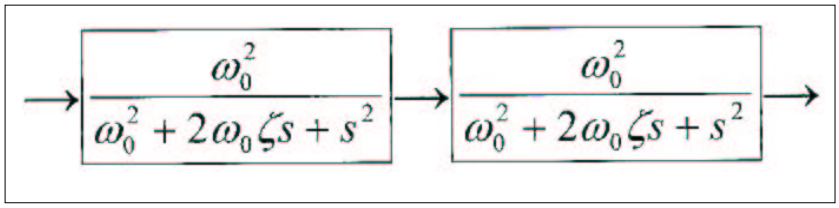

Figure 4.6: Anti-aliasing filter.

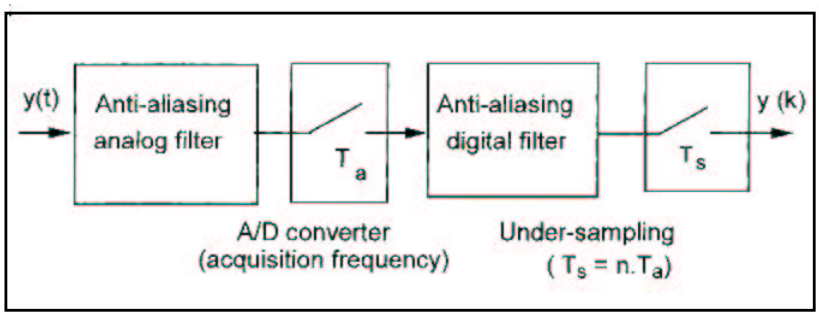

Figure 4.7: Anti-aliasing filtering with under-sampling.

For a given sampling frequency, in order to avoid the folding (aliasing) of the spectrum and thus of the distortions, the analog signals must be filtered prior to sampling to ensure that:

$$f_{max} < \frac{1}{2} f_s \tag{4.2}$$

The filters used are known as "anti-aliasing filters". A good anti-aliasing filter must have a minimum of two cascaded second-order cells ($f_{max} << (1/2)f_s$) . An example of an anti-aliasing filter of this type is given in Figure 4.6. These filters must introduce a large attenuation at frequencies higher than , but their bandwidth must be higher than $(1/2)f$ the required bandwidth of the closed loop system (generally higher than open loop system bandwidth). Circuits of this type (or more complex) are currently available.

In the case of very low frequency sampling, first a sampling at a higher frequency is carried out (integer multiple of the desired frequency), using an appropriate analog anti-aliasing filter. The sampled signal thus obtained is passed through a digital anti-aliasing filter followed by a frequency divider (decimation) thereby giving a sampled signal having the required frequency. This procedure is shown in Figure 4.7. It is also employed every time the frequency of data acquisition is higher than the sampling frequency chosen for the loop that must be controlled (the sampling frequency should be an integer divider of the acquisition frequency) [32].

4.2.2 Choice of the Sampling Frequency for Control Systems

The sampling frequency for digital control systems is chosen according to the desired bandwidth of the closed loop system. Note that no matter how the desired

performances are specified, these can always be related to the closed loop system bandwidth.

Example: Let us consider the performances imposed in section 3.1.6 on the response (maximum overshoot 5%, rise time 2.27 s). The transfer function to be determined corresponds to the desired closed loop system transfer function. From the diagrams given in Figure 3.11 we have deduced that the closed loop transfer function must be a normalized second-order transfer function with $\zeta = 0.7$ and ω_0 =1 rad/s. By immediately using the diagrams given in Figure 3.12 it can be observed that the bandwidth of the closed loop system is approximately equal to

$$f_B^{CL} = \frac{1}{2\pi} Hz$$

The rule used to choose the sampling frequency in control systems is the following:

$$f_s = (6 \; to \; 25) f_B^{CL} \tag{4.3}$$

where:

f_s: sampling frequency, f_B^{CL}: closed loop system bandwidth

Rule of Equation 4.3 is equally used in open loop, when it is desired to choose the sampling frequency in order to identify the discrete-time model of a plant. In this case f_B^{CL} is replaced by an estimation of the bandwidth of the plant.

For information purposes, Table 4.1 gives the sampling periods ($T_s = 1/f_s$) used for the digital control of different types of plants.

The rule for choosing the sampling frequency given in Equation 4.3 can be connected to the transfer function parameters.

First- order system

$$H(s) = \frac{1}{1 + sT_0}$$

In this case the system bandwidth is

$$f_B = f_0 = \frac{1}{T_0}$$

(an attenuation greater than 3 dB is introduced for frequencies higher than $w_0 = 1/T_0 = f_0$).

By applying the rule of Equation 4.3 the condition for choosing the sampling period is obtained ($T_s = \frac{1}{f_s}$):

$$\frac{T_0}{4} < T_s < T_0 \tag{4.4}$$

This corresponds to the existence of two to nine samples on the rise time of a step response.

Second- order system

$$H(s) = \frac{\omega_0^2}{\omega_0^2 + 2\zeta\omega_0 s + s^2}$$

Table 4.1: Choice of the sampling period for digital control systems

Type of variable (or plant)	Sampling period (s)
Flow rate	1 - 3
Level	5 -10
Pressure	1 - 5
Temperature	10 - 180
Distillation	10 - 180
Servo-mechanisms	0.001 - 0.05
Catalytic reactors	10 - 45
Cement plants	20 - 45
Dryers	20 - 45

The bandwidth of the second-order system depends on ω_0 and on ζ (see Figure 3.12).
For example:

$$\zeta = 0.7 \Rightarrow f_B = \frac{\omega_0}{2\pi}$$

$$\zeta = 1 \Rightarrow f_B = \frac{0.6\omega_0}{2\pi}$$

By applying the rule of Equation 4.3. the following relations are obtained between the natural frequency ω_0 and the sampling period T_s :

$$0.25 \leq \omega_0 T_s \leq 1; \quad \zeta = 0.7 \tag{4.5}$$

$$0.4 \leq \omega_0 T_s \leq 1.75; \quad \zeta = 1 \tag{4.6}$$

The lower values correspond to the choice of a high sampling frequency and the upper values to the choice of a low sampling frequency. For simplicity's sake. given that in closed loop the behavior frequently chosen as the desired behavior is that of a second order having a damping factor ζ between 0.7 and 1, the following rule can be used (approximation of Equations 4.5 and 4.6) [33]:

$$0.25 \leq \omega_0 T_s \leq 1.5; \quad 0.7 \leq \zeta \leq 1 \tag{4.7}$$

4.3 Discrete-time Models

4.3.1 Time Domain

Figure 4.8 illustrates the response of a continuous-time system to a step input, a response that can be simulated by a first order system (an integrator with a feedback gain indicated in the figure).

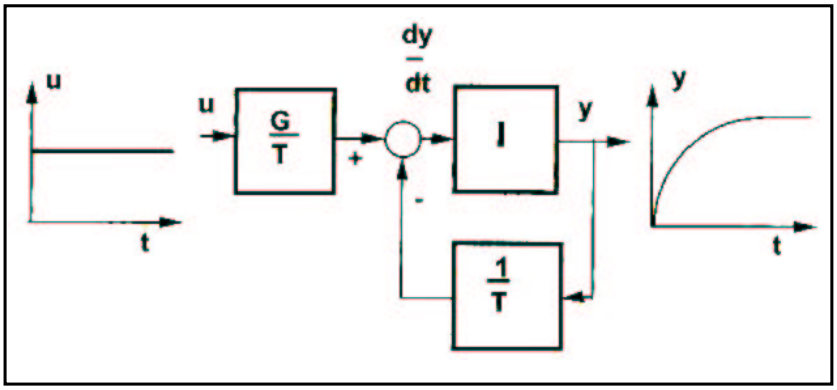

Figure 4.8: Continuous-time model.

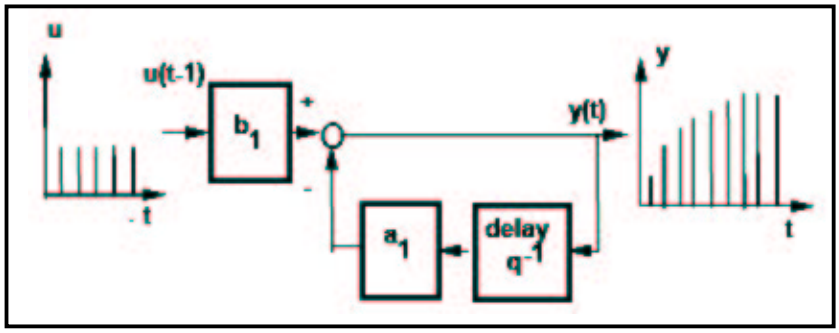

Figure 4.9: Discrete-time model.

The corresponding model is described by the differential equation

$$\frac{dy}{dt} = -\frac{1}{T}y(t) + \frac{G}{T}u(t) \tag{4.8}$$

or by the transfer function

$$H(s) = \frac{G}{1+sT} \tag{4.9}$$

where T is the time constant of the system and G is the gain.

If the input $u(t)$ and the output $y(t)$ are sampled with a specified sampling period, the representations of $u(t)$ and $y(t)$ are obtained as number sequences in which t (or k) is now the normalized discrete-time (real time divided by the sampling period, $t = t/T_s$). The relation between the input sequence $u(t)$ and the output sequence $y(t)$ can be simulated by the scheme given in Figure 4.9 by using a delay (backward shift) operator (symbolized by $q^{-1}y(t-1) = q^{-1}y(t)$), instead of an integrator. This relation is described in the time domain by the algorithm (known as recursive equation or difference equation)

$$y(t) = -a_1 y(t-1) + b_1 u(t-1) \tag{4.10}$$

Let us now examine in greater detail the discrete-time model given by Equation 4.10 for a zero initial condition ($y(0) = 0$) and a discrete-time unit step input:

$$u(t) = \begin{cases} 0 & t < 1 \\ 1 & t \geq 0 \end{cases}$$

Table 4.2: Step response of a first-order discrete-time model $a_1 = -0.5, b_1 = 0.5$

T	0	1	2	3	4	5
y_t	0	0.5	0.75	0.875	0.937	0.969

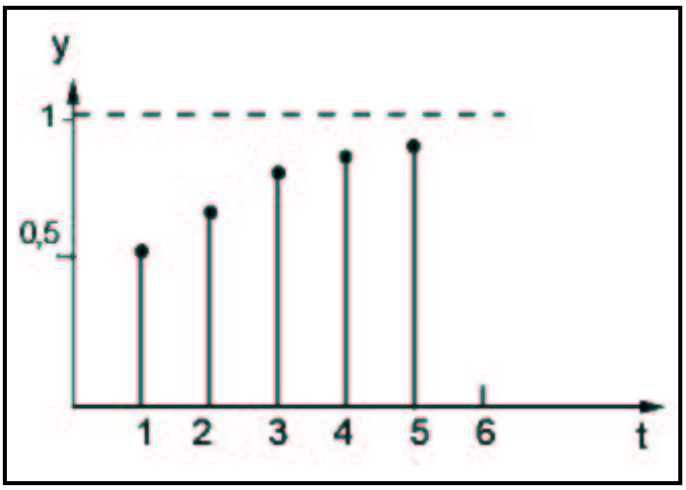

Figure 4.10: Step response of a first order discrete time mode($a_1 = -0.5, b_1 = 0.5$).

The response is directly computed by recursively using Equation 4.10 from $t = 0$ (in the case of discrete-time models there are no problem with the integration of the differential equations like in continuous time). We shall examine two cases.

case 1

$$a_1 = -0.5; \quad b_1 = 0.5$$

The output values for different instants are given in Table 4.2 and the corresponding sequence is represented in Figure 4.10.

It is observed that the response obtained resembles the step response of a continuous-time first order system which has been sampled. An equivalent time constant for the continuous-time system can even be determined (rise time from 0 to 90%:t_r=2.2T). From Table 4.2, one then obtains

$\frac{3T_s}{2.2} < T < \frac{4T_s}{2.2}$

case 2

$$a_1 = 0.5; \quad b_1 = 1.5$$

Output values for different instants are given in Table 4.3 and the corresponding sequence is represented in Figure 4.11.
An oscillatory damped response is observed with a period equal to two sampling periods. This type of phenomenon cannot result from the discretization of a continuous-time first order system, since this latter is always a-periodic. It may thus be concluded that the first order discrete-time model corresponds to the discretization of a first order continuous-time system only if a_1 is negative.

Table 4.3: response of a first-order discrete-time model $a_1 = 0.5, b_1 = 1.5$

T	0	1	2	3	4	5
y_t	0	1.5	0.75	1.125	0.937	1.062

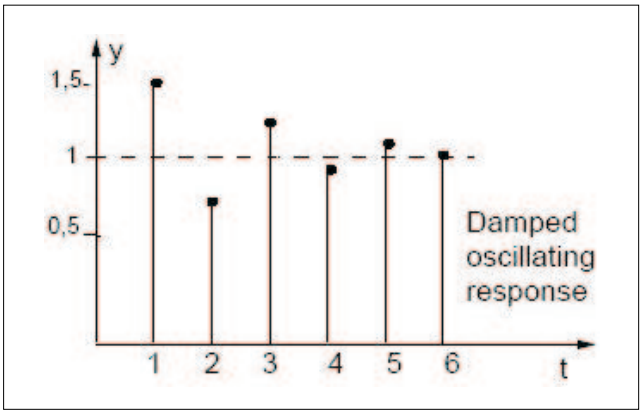

Figure 4.11: Step response of a first order discrete time model ($a_1 = 0.5, b_1 = 1.5$).

We now go back to the method used to describe discrete-time models. The delay operator q^{-1} is used to obtain a more compact writing of the recursive (difference) equations which describe discrete-time models in the time domain (it has the same function as the operator $p = d/dt$ for continuous-time systems). The following relations hold:

$$q^{-1}y(t) = y(t-1) \tag{4.11}$$

$$q^{-d}y(t) = y(t-d)$$

By using the operator q^{-1} , Equation 4.10 is rewritten as

$$(1 + a_1 q^{-1})y(t) = b_1 q^{-1} u(t) \tag{4.12}$$

Discrete-time models may also be obtained by the discretization of the differential equations describing continuous-time models. This operation is used for the simulation of continuous-time models on a digital computer.

Let us consider Equation 4.8 and approximate the derivative by

$$\frac{dy}{dt} = \frac{y(t+T_s) - y(t)}{T_s} \tag{4.13}$$

Equation 4.5 will be rewritten as

$$\frac{y(t+T_s) - y(t)}{T_s} + \frac{1}{T}y(t) = \frac{G}{T}u(t) \tag{4.14}$$

By multiplying both sides of Equation 4.14 by T_s , and with the introduction of the normalized time ($t = t/T_s$) , it follows that

$$y(t+1) + \left(\frac{T_s}{T} - 1\right) y(t) = \frac{G}{T} T_s u(t) \tag{4.15}$$

which can be further rewritten as:

$$(1 + a_1 q^{-1}) y(t+1) = b_1 u(t) \tag{4.16}$$

where

$$a_1 = \frac{T_s}{T} - 1 (< 0); \quad b_1 = \frac{G}{T} T_s$$

Shifting Equation 4.16 by one step. Equation 4.10 is obtained. We point out that in order to represent a first-order continuous model with Equation 4.16, the condition $a_1 < 0$ must be verified. As a consequence, the sampling period T_s, must be smaller than time constant $T (T_s < T)$. This result corresponds to the upper bound in Equation 4.4 introduced for sampling period selection of a first-order system as a function of the desired closed loop bandwidth.

If Equation 4.13 is the approximation of the "derivative", the digital integrator equation can be directly deduced. Thus, if normalized time is used. Equation 4.13 is written as

$$\frac{d}{dt} y = py \approx y(t) - y(t-1) = (1 - q^{-1}) y(t) \tag{4.17}$$

Where $(1 - q^{-1})$ is now equivalent to p. As the integration is the opposite differentiation, one obtains:

$$s(t) = \int y dt = \frac{1}{p} y \approx \frac{1}{1 - q^{-1}} y(t) \tag{4.18}$$

Multiplying both sides of Equation 4.18 by $(1 - q^{-1})$, it follows that

$$s(t)(1 - q^{-1}) = y(t) \tag{4.19}$$

which we can rewrite as

$$s(t) = s(t-1) + 1y(t) \tag{4.20}$$

corresponding to the approximation of the integration operation by mean of the rectangular rule, as illustrated in Figure 4.12 (if continuous-time is used, Equation 4.20 is written as
$s(t) = s(t - T_s) + T_s y(t))$ [34].

4.3.2 Frequency Domain

The study of continuous-time models in the frequency domain has been carried out considering a periodic input of the complex exponential type

$$e^{jwt} = cos(\omega t) + j sin(\omega t)$$

or

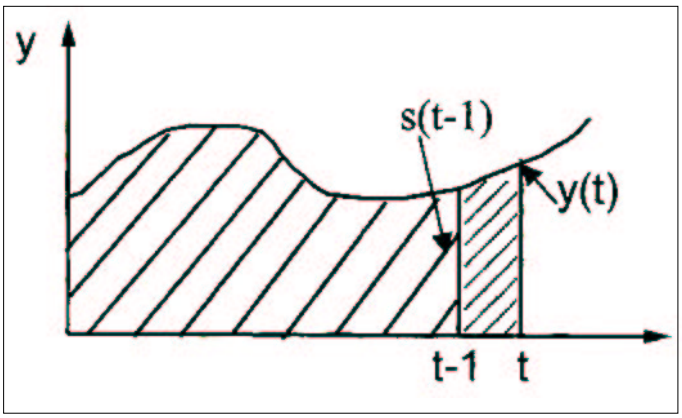

Figure 4.12: Numerical integration.

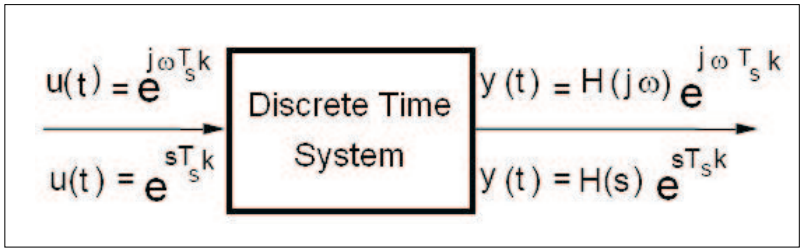

Figure 4.13: frequency response of a discrete-time system.

$$e^{st} \quad with \quad s = \sigma + j\omega$$

For the study of discrete-time models in the frequency domain we shall consider complex (sampled) exponentials, i.e. sequences resulting from complex continuous-time exponentials evaluated at the sampling instants $t = kT_s$.

These sequences will thus be written as

$$e^{j\omega T_s k}; \quad e^{sT_s k}; \quad k = 1, 2, 3...$$

Since the discrete-time models being considered are linear, if a signal of a certain frequency is applied to the input, a signal of the same frequency, but amplified or attenuated according to the frequency, will be found at the output. This is summarized in Figure 4.13. in which $H(s)$ is the "transfer function" of the system that expresses the dependence of the gain and the phase-deviation on the complex frequency $s(s = \sigma + j\omega)$.
If the input of the system is in the form $e^{sT_s k}$, the output will be

$$y(t) = H(s)e^{sT_s k} \tag{4.21}$$

and respectively

$$y(t-1) = H(s)e^{sT_s(k-1)} = e^{-sT_s}H(s)e^{sT_s k} = e^{-sT_s}y(t) \tag{4.22}$$

It is thus observed that shifting backward by one step is equivalent to multiplying by e^{-sT_s}.

Let now determine the transfer function related to the recursive Equation 4.10.

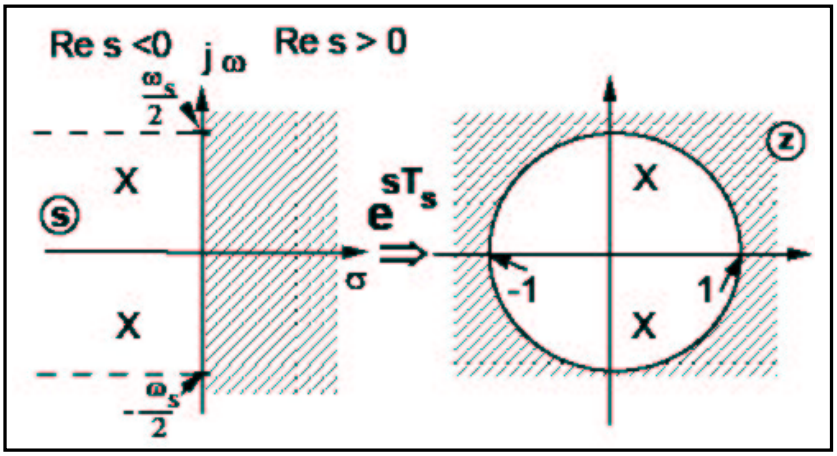

Figure 4.14: Effect of the transformation $z = e^{sT_s}$.

In this case $u(t) = e^{sT_s k}$ and the output will be in the form of Equation 4.21. By also using Equation 4.22 one obtains:

$$(1 + a_1 e^{-sT_s}) H(s) e^{sT_s k} = b_1 e^{-sT_s} e^{sT_s k} \tag{4.23}$$

from which results

$$H(s) = \frac{b_1 e^{-sT_s}}{1 + a_1 e^{-sT_s}} \tag{4.24}$$

We consider now the following change of variable:

$$z = e^{sT_s} \tag{4.25}$$

which corresponds to the transformation of the left half-plane of the s-plane into the interior of the unit circle centered at the origin in the z-plane, as illustrated by Figure 4.14.

With the transformation given by Equation 4.25 the transfer function given in Equation 4.24 becomes

$$H(z^{-1}) = \frac{b_1 z^{-1}}{1 + a_1 z^{-1}} \tag{4.26}$$

Note that the transfer function in z^{-1} can be directly obtained from the recursive Equation 4.10 by using the delay operator q^{-1} (see Equation 4.12), and afterwards by formally computing the ratio $y(t)/u(t)$ and replacing q^{-1} with z^{-1} , This procedure can obviously be applied to all models described by linear difference equations with constant coefficients. regardless of their complexity. We also remark that the transfer functions of discrete-time models are often written in terms of q^{-1} . It is of course understood that the meaning of q^{-1} varies according to the context (delay operator or complex variable). When q^{-1} is considered as a delay operator, the expression $H(q^{-1})$ is named ."transfer operator".

It must be observed that the representation by transfer operators can also be used for models described by linear difference equations with time varying coefficients as well. In contrast, the interpretation of q^{-1} as a complex variable z^{-1} is only possible for linear difference equations with constant coefficients.

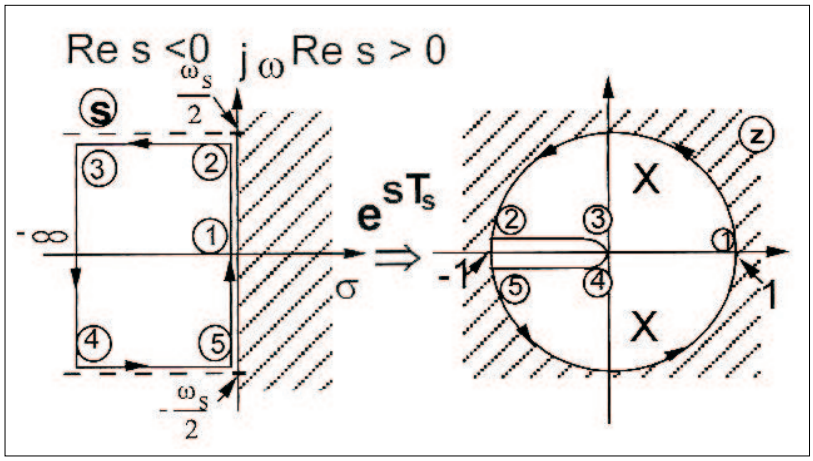

Figure 4.15: Effects of the transformation e^{sT_s} on the points located in the "primary strip" in s-plane.

Properties of the Transformation $z = e^{sT_s}$
The transformation of Equation 4.25 is not bijective because several points in the s-plane are transformed at the same point in the z-plane. Nevertheless we are interested in the s-plane being delimited between the two horizontal lines crossing the points $[0, +j\omega_s/2]$ and $[0, -j\omega_s/2]$ where $\omega_s = 2\pi f_s = 2\pi/T_s$. This region is called "primary strip".

The complementary bands are outside the frequency domain of interest if the conditions of the Nyquist's theorem (Section 4.2.1) have been satisfied.

Figure 4.15 gives a detailed image of the effects of the transformation $z = e^{sT_s}$ for the points that are inside the "primary strip". Attention must be focused on an important aspect for continuous second-order systems in the form:

$$\frac{\omega_0^2}{\omega_0^2 + 2\zeta\omega_0 s + s^2} (\zeta < 1)$$

for which the resonant damped frequency is equal to half the sampling frequency:

$$\omega_0 \sqrt{1-\zeta^2} = \frac{\omega_s}{2}$$

The image of their conjugates poles

$$s_{1,2} = -\zeta\omega_0 \pm j\frac{\omega_s}{2}$$

through the transformation $z = e^{sT_s}$ corresponds to a single point placed on the real axis in the z- plane and with negative abscissa.
One gets:

$$z_{1,2} = e^{s_{1,2}T_s} = e^{-\zeta\omega_0 T_s} e^{\pm j\frac{\omega_s}{2}T_s} = e^{-\zeta\omega_0 T_s} e^{\pm j\pi} = -e^{-\zeta\omega_0 T_s} = -e^{-\frac{\zeta}{\sqrt{1-\zeta^2}}\pi}$$

Since:

$$\omega_0 = \frac{\omega_s}{2\sqrt{1-\zeta^2}}$$

This is the reason why discrete-time models in the form of Equation 4.10 such as

$$(1 + a_1 q^{-1}) y(t) = b_1 q^{-1} u(t)$$

give oscillating step responses for $a_1 > 0$ (damped if $\mid a_1 \mid < 1$) with period $2T_s$(see Section 4.3.1). These first-order discrete-time models have the same poles as the discrete-time models derived from second-order continuous-time systems having a damped resonant frequency equal to $\omega_s/2$ [35].

4.3.3 General Forms of Linear Discrete-time Models

A linear discrete-time model is generally described as

$$y(t) = -\sum_{i=1}^{n_A} a_i y(t-i) + \sum_{i=1}^{n_B} b_i u(t-d-i) \tag{4.27}$$

in which d corresponds to a pure time delay which is an integer multiple of the sampling period.

Let us introduce the following notations:

$$1 + \sum_{i=1}^{n_A} a_i q^{-i} = A(q^{-1}) = 1 + q^{-1} A^*(q^{-1}) \tag{4.28}$$

$$A^*(q^{-1}) = a_1 + a_2 q^{-1} + \cdots + a_{n_A} q^{-n_A+1} \tag{4.29}$$

$$\sum_{i=1}^{n_B} b_i q^{-i} = B(q^{-1}) = q^{-1} B^*(q^{-1}) \tag{4.30}$$

$$B^*(q^{-1}) = b_1 + b_2 q^{-1} + \cdots + b_{n_B} q^{-n_B+1} \tag{4.31}$$

By using the delay operator q^{-1} in Equation 4.27 and taking into account the notations of Equations 4.28 to 4.31, the Equation 4.27 describing the discrete-time system is written as

$$A(q^{-1}) y(t) = q^{-d} B(q^{-1}) u(t) \tag{4.32}$$

or in the predictive form (by multiplying both sides by q^d)

$$A(q^{-1}) y(t+d) = B(q^{-1}) u(t) \tag{4.33}$$

Equation 4.32 can also be written in a compact form using the *pulse transfer operator*

$$y(t) = H(q^{-1}) u(t) \tag{4.34}$$

where the pulse transfer operator is given by

$$H(q^{-1}) = \frac{q^{-d} B(q^{-1})}{A(q^{-1})} \tag{4.35}$$

The pulse transfer function characterizing the system described by Equation 4.27 is obtained from the pulse transfer operator given in Equation 4.35 by replacing q^{-1} with z^{-1}

$$h(z^{-1}) = \frac{z^{-d}B(z^{-1})}{A(z^{-1})} \tag{4.36}$$

Pulse Transfer Function Order

To evaluate the order of a discrete time model represented by the pulse transfer function in the form of Equation 4.36, the representation in terms of positive power of z is needed. If d is the system pure time delay expressed as number of samples, n_A the degree of the polynomial $A(z^{-1})$ and n_B the degree of the polynomial $B(z^{-1})$, one must multiply both numerator and denominator of $H(z^{-1})$ by z^n in order to obtain a proper pulse transfer function $H(z)$ on the positive powers of z, where

$n = max(n_A, n_B + d)$

n represents the discrete-time system order (the higher power of a term in z in the pulse transfer function denominator).

Example 1:

$$H(z^{-1}) = \frac{z^{-3}(b_1 z^{-1} + b_2 z^{-2})}{1 + a_1 z^{-1}}$$

$n = max(1, 5) = 5$

$$H(z) = \frac{b_1 z + b_2}{z^5 + a_1 z^4}$$

Example 2:

$$H(z^{-1}) = \frac{b_1 z^{-1} + b_2 z^{-2}}{1 + a_1 z^{-1} + a_2 z^{-2}}$$

$n = max(2, 2) = 2$

$$H(z) = \frac{b_1 z + b_2}{z^2 + a_1 z + a_2}$$

One notes that the order n of an irreducible pulse transfer function also corresponds to the number of states for a minimal state space system representation associated to the transfer function [36].

4.3.4 Stability of Discrete-time Systems

The stability of discrete-time systems can be studied either from the recursive (differences) equation describing the discrete-time system in the time domain, or from the interpretation of difference equations solutions as sums of discretized exponentials. We shall use examples to illustrate both these approaches.

Let us assume that the recursive equation is

$$y(t) = -a_1 y(t-1); \quad y(0) = y_0 \tag{4.37}$$

which is obtained from Equation 4.10 when the input $u(t)$ is identically zero. The free response of the system is written as

$$y(1) = -a_1 y_0; \quad y(2) = (-a_1)^2 y_0; \quad y(t) = (-a_1)^t y_0 \tag{4.38}$$

The asymptotic stability of the system implies

$$\lim_{t \to \text{inf}} y(t) = 0 \tag{4.39}$$

The condition of asymptotic stability thus results from Equation 4.38. It is necessary and sufficient that

$$|a_1| < 1 \tag{4.40}$$

On the other hand, it is known that the solution of the recursive (difference) equations is of the form (for a first-order system):

$$y(t) = ke^{sT_0^{st}} = kz^t \tag{4.41}$$

By introducing this solution into Equation 4.37, and taking into account Equation 4.22, one obtains

$$(1 + a_1 e^{-sT_s})ke^{sT_s t} = (1 + a_1 z^{-1})kz^t = 0 \tag{4.42}$$

from which it follows that

$$z = e^{sT_s} = e^{(\sigma + j\omega)T_s} = e^{\sigma T_s} e^{j\omega T_s} = -a_1 \tag{4.43}$$

For this solution to be asymptotically stable, it is necessary that which implies that $e^{\sigma T_s} < 1$ and respectively $|z| < 1 (or |a_1| < 1)$.

However, the term $1 + a_1 z^{-1}$ is nothing more than the denominator of the pulse transfer function related to the system described by Equation 4.10 (see Equation 4.26).

The result obtained can be generalized. For a discrete-time system to be asymptotically stable, all the roots of the transfer function denominator must be inside the unit circle (see Figure 4.14):

$$1 + a_1 z^{-1} + \cdots + a_n z^{-n} = 0 \Rightarrow |z| < 1 \tag{4.44}$$

In contrast, if one or several roots of the transfer function denominator are in the region defined by $|z| > 1$ (outside the unit circle), this implies that $Re\ s > 0$ and thus the discrete-time system will be unstable.

As for the continuous-time case, some stability criteria are available (Jury criterion, Routh-Hurwitz criterion applied after the change of variable $w = (z+1)/(z-1)$ for establishing the existence of unstable roots for a polynomial in the variable z with no explicit calculation of the roots.

A helpful tool to test z-polynomial stability is derived from a necessary condition for the stability of a z^{-1}-polynomial. This condition states: the evaluations of the polynomial $A(z^{-1})$ given by Equation 4.44 in $z = 1$, $(A(1))$ and in $z = -1$, $(A(-1))$ must be positive (the coefficient of $A(q^{-1})$ corresponding to z^0 is supposed to be positive).

Example:

$$A(z^{-1}) = 1 - 0.5z^{-1}; \qquad (stable\ system)$$
$$A(1) = 1 - 0.5 = 0.5 > 0; \quad A(-1) = 1 + 0.5 = 1.5 > 0$$
$$A(z^{-1}) = 1 - 0.5z^{-1}; \qquad (unstable\ system)$$
$$A(1) = -0.5 < 0; \quad A(-1) = 2.5 > 0$$

4.3.5 Steady-state Gain

In the case of continuous-time systems [33]. the steady-state gain is obtained by making $s = 0$ (zero frequency) in the transfer function. In the discrete case, $s = 0$ corresponds to

$$s = 0 \Rightarrow z = e^{sT} = 1 \tag{4.45}$$

and thus the steady-state gain $G(0)$ is obtained by making $z = 1$ in the pulse transfer function. Therefore for the first-order system one obtains:

$$G(0) = \left(\frac{b_1 z^{-1}}{1 + a_1 z^{-1}} \right)_{z=1} = \frac{b_1}{1 + a_1}$$

Generally speaking, the steady-state gain is given by the formula

$$G(0) = H(1) = H(z^{-1})|_{z=1} = \left(\frac{z^{-d} B(z^{-1})}{A(z^{-1})} \right)_{z=1} = \frac{\sum_{i=1}^{n_b} b_i}{1 + \sum_{i=1}^{n_A} a_i} \tag{4.46}$$

In other words, the steady-state gain is obtained as the ratio between the sum of the numerator coefficients and the sum of the denominator coefficients. This formula is quite different from the continuous-time systems, where the steady-state gain appears as a common factor of the numerator (if the denominator begins with 1).

The steady-state gain may also be obtained from the recursive equation describing the discrete-time models, the steady-state being characterized by $u(t) = constant$ and

$y(t) = y(t-1) = y(t-2)$.....

From Equation 4.10, it follows that

$$(1 + a_1) y(t) = b_1 u(t)$$

and respectively

$$y(t) = \frac{b_1}{1 + a_1} u(t) = G(0) u(t)$$

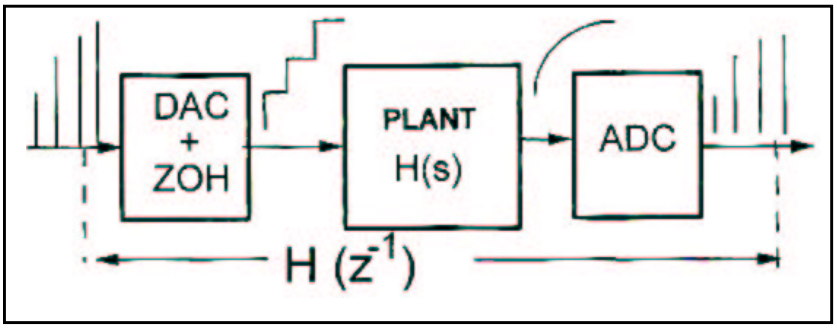

Figure 4.16: Control system using an analog-to-digital converter followed by a zero-order hold.

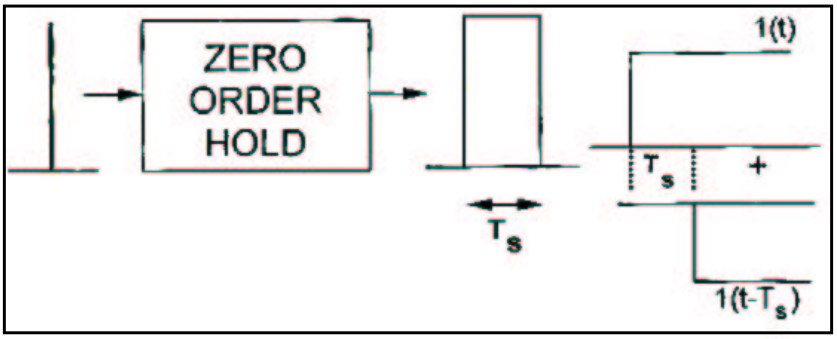

Figure 4.17: Operation of the zero-order hold.

4.3.6 Models for Sampled-data Systems with Hold

Up to this point we have been concerned with sampled-data systems models corresponding to the discretization of inputs and outputs of a continuous-time system. However, in a computer controlled system, the control applied to the plant is not continuous. It is constant between the sampling instants (effect of the zero-order hold) and varies discontinuously at the sampling instants, as is illustrated in Figure 4.16.

It is important to be able to relate the model of the discretized system, which gives the relation between the control sequence (produced by the digital controller) and the output sequence (obtained after the analog-to-digital converter), to the transfer function $H(s)$ of the continuous-time system. The zero-order hold, whose operation is reviewed in Figure 4.17 introduces a transfer function in cascade with $H(s)$ [37].

The hold converts a Dirac pulse given by the digital-to-analog converter at the sampling instant into a rectangular pulse of duration T_s, which can be interpreted as the difference between a step and the same step shifted by T_s. As the step is the integral of the Dirac pulse, it follows that the zero-order hold transfer function is

$$H_{ZOH}(s) = \frac{1 - e^{-sT_s}}{s} \tag{4.47}$$

Equation 4.47 allows one to consider the zero-order hold as a filter having a frequency response given by

$$H_{ZOH}(j\omega) = \frac{1 - e^{-j\omega T_s}}{j\omega} = T_s \frac{sin(\omega T_s/2)}{\omega T_s/2} e^{-j\omega \frac{T_s}{2}}$$

From the study of this response in the frequency region $0 \leq f \leq f_s/2 (0 \leq \omega \leq \omega_s/2)$, one can conclude:

1. The ZOH gain at the zero frequency is equal to: $G_{ZOH}(0) = T_s$.
2. The ZOH introduces an attenuation at high frequencies. For $f = f_s/2$ one gets $G(f_s/2) = \frac{2}{n} T_s = 0.637 T_s (-3.92\ dB)$.
3. The ZOH introduces a phase lag which grows with the frequency. This phase lag is between 0 (for $f = 0$) and $-\pi/2$(for $f = f_s/2$) and should be added to the phase lag due to $H(s)$.

The global continuous-time transfer function will be

$$H'(s) = \frac{1 - e^{-sT_s}}{s} H(s) \tag{4.48}$$

to which a pulse transfer function is associated. Tables which give the discrete-time equivalent of systems with a zero-order hold are available. Some typical situations are summarized in Table 4.4 [38].

Table 4.4: Pulse transfer functions for continuous-time systems with zero-order hold

$H(s)$	$H(z^{-1})$
$\frac{1}{s}$	$\frac{T_s z^{-1}}{1-z^{-1}}$
$\frac{G}{1+sT}$	$\frac{b1 z^{-1}}{1+a_1 z^{-1}}; b1 = G(1-e^{-T_s/T}); a_1 = -e^{-T_s/T}$
$\frac{Ge^{-sL}}{1+sT}; L < T_s$	$\frac{b_1 z^{-1}+b_2 z^{-2}}{1+a_1 z^{-1}}; b1 = G(1-e^{(L-T_s)/T});$ $b2 = Ge^{-T_s/T}(e^{L/T}-1); a_1 = -e^{-T_s/T}$
$\frac{\omega_0^2}{\omega_0^2+2\zeta\omega_0 s+s^2}$ $\omega = \omega_0\sqrt{1-\zeta^2}$ $\zeta < 1$	$\frac{b_1 z^{-1}+b_2 z^{-2}}{1+a_1 z^{-1}+a_2 z^{-2}}$ $b_1 = 1-\alpha(\beta+\frac{\zeta\omega_0}{\omega}\partial); b_2 = \alpha^2+\alpha(\frac{\zeta\omega_0}{\omega}\partial-\beta)$ $a_1 = -2\alpha\beta; a_2 = \alpha^2$ $\alpha = e^{-\zeta\omega_0 T_s}; \beta = cos(\omega T_s); \partial = sin(\omega T_s)$

Chapter 5

Setup, Modeling and Parameters Identification of a Magnetic Levitation Model

5.1 Introduction

Modelling and simulation are very important approaches for designing control systems. Therefore, laboratory set-ups, which model real processes, and mathematical models have a significant role [39, 40, 41]. The CE152 is a laboratory magnetic levitation made by Humusoft [42]. It is used for studying system dynamics and control engineering principles from the theoretical point of view and enables a wide range of practical experiments in the fields of modelling, simulation and control. The goal of modelling and identification is to prepare a basis for the students' laboratory assignments, such as designing a multivariable controller that ensures satisfactory control in the whole operating range. There are two well known modelling approaches: theoretical and experimental. Usually, both approaches have to be combined, and used in modeling of the laboratory magnetic levitation.

A dynamic model of the magnetic levitation for the magnetic force experienced by the levitated object is a substantial part of the researches on the magnetic levitation systems. It has been focused on the development of precise magnetic force models which led to the proposition of several force models over the past years. Most of the models are generally assuming a squared relationship between the electric current in the coil and the magnetic force. Peterson et al in [43] proposed a static magnetic force model assuming that the force is proportional to the magnetic flux squared. Due to the linear relationship between the magnetic flux and electrical current in the coil, this assumption leads to a second order relationship between the magnetic force and the current. The authors in [44, 45] assumed that the magnetic force is directly proportional to the squared current in the coil and inversely proportional to the squared gap distance between the electromagnet and the object. Lin et al [46] assumed that the magnetic force is linearly proportional to the current and inversely proportional to the forth power of distance. Magnetic Levitation System CE152 shown in Figure 5.1 has the dynamical properties which can be described by the motion equation that is based on the balance of all forces, i.e. gravity force, acceleration force and the magnetic force, the last force is assumed proportional to

Figure 5.1: Model of the magnetic levitation system.

the square of the coil current and inversely proportional to the square gap distance between the electromagnetic and the object [47].

5.2 The Laboratory Magnetic Levitation Set-Up

The CE152 Magnetic Levitation Model is designed for the theoretical study and practical investigation of basic and advanced control engineering principles. This can include system dynamics modelling, identification, analysis and various controllers design by classical and modern methods.

A system configuration for the CE152 follows from Figure 5.2 as shown below where the system is connected to IBM PC compatible computer. The scheme shows, that the model interface can be considered at two different levels:

- Physical level - input and output voltage to the coil power amplifier and from the ball position sensor.
- Logical level - voltage converted by the data acquisition card and scaled to 1 machine unit [MU].

The core part of the model is a steel ball hanging in the magnetic field of the coil. The position of the ball is measured with a magnetic position sensor. The current for the coil is amplified by an external amplifier and therefore is directly proportional to the input voltage. The model is connected to the PC via universal data acquisition card, like the HUMUSOFT MF614. Note that all the experiments used in this thesis are done in Matlab-Simulink environment using Real Time Toolbox [48].

Later it will be shown that the Magnetic Levitation Model can be approximated by a single input single output nonlinear dynamic system of order 2 or 3 depending on the modeling precision [49].

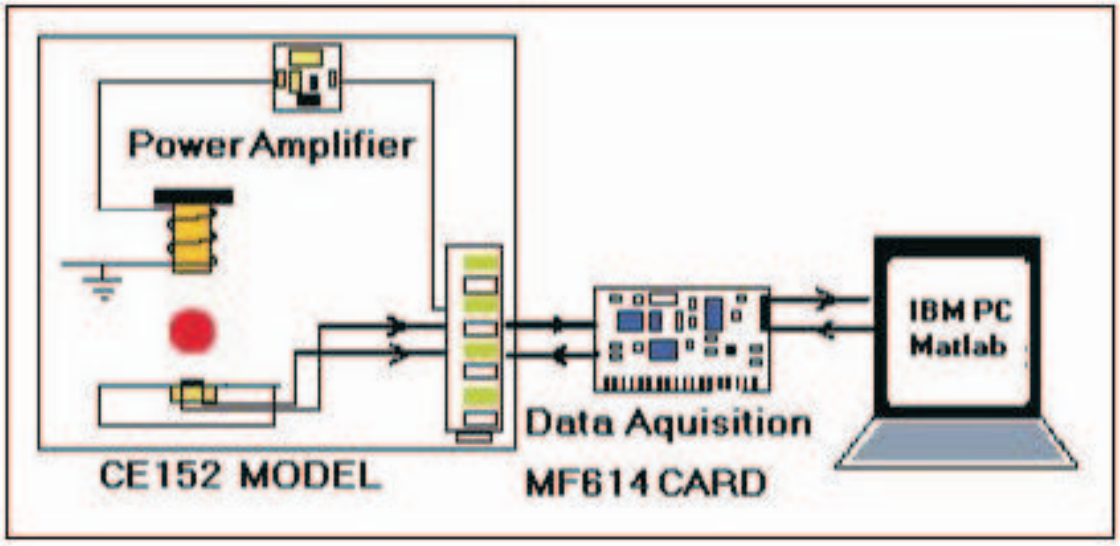

Figure 5.2: Interface of the magnetic levitation model CE152 to PC.

5.3 Theoretical Modelling

When modelling a system it is important to find a balance between simplicity and complexity of the model, according to its purpose and operating conditions [50]. The model has to be clear, concise and flexible, yet it must consider all the relevant sub-processes in the system. Modelling of dynamic systems is a cyclic process, therefore usually many iterations are needed before a satisfactory model is obtained [51]. Sometimes validation of a particular sub-system gives unsatisfactory results. Hence, another approach has to be considered and some of the previously neglected properties have to be taken into account [52]. In the following section, modelling procedure will be described.

5.3.1 Model Structure

The overall model shown in Figure 5.3 consists from the following blocks:

- D/A converter
- The power amplifier
- The ball and coil subsystem
- The position sensor
- A/D converter

Note: the above blocks arrangement is according to the signal flow from left to right, see Figure 5.3, but we will fellow other arrangement in modelling the different subsystem, firstly the Power Amplifier, then Ball and Coil Subsystem, then D/A Converter, then Position Sensor and lastly A/D Converter.

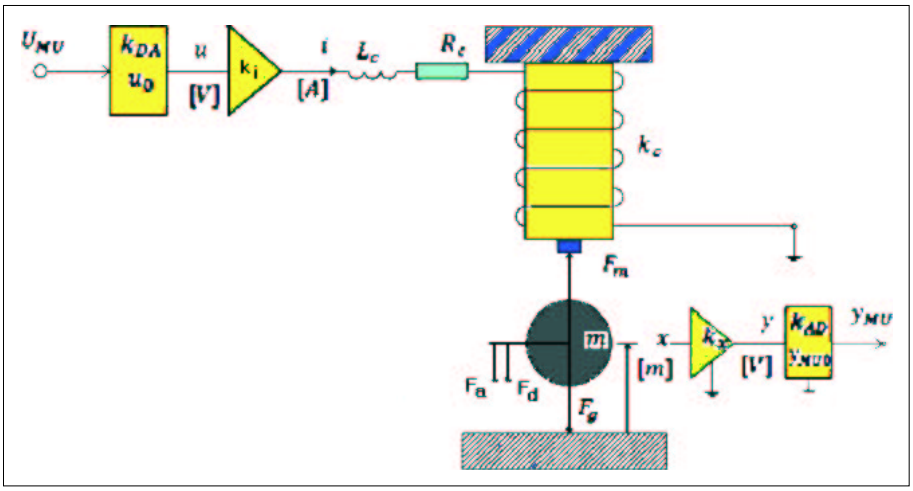

Figure 5.3: Scheme of the Magnetic Levitation Model.

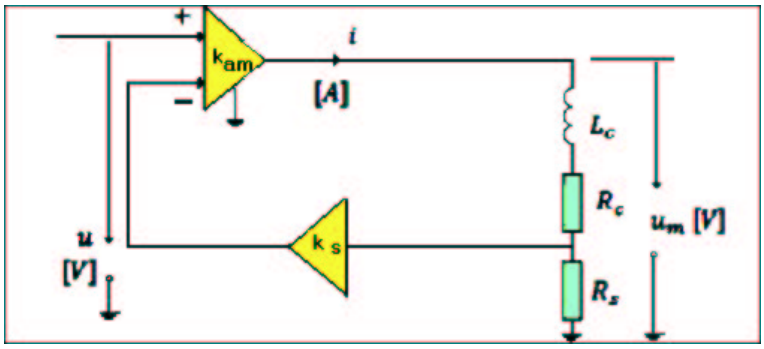

Figure 5.4: The Power Amplifier Internal Structure.

The Power Amplifier

The power amplifier is designed as a source of constant current with the feedback current stabilization. The power amplifier internal structure is shown in Figure 5.4. By applying **K**irchhoff's **V**oltage **L**aw **(KVL)** at the circuit in Figure 5.4 we get the following:

$$u_m = (R_C + R_s)i + L_C \frac{di}{dt} \tag{5.1}$$

$$u_m = k_{am}(u - k_s R_s i) \tag{5.2}$$

By solving Equation 5.1 and Equation 5.2, then taking the Laplace transform, we have the transfer function of amplifier output current $I(s)$ to amplifier input voltage $U(s)$. Thus, the amplifier and coil subsystem can be modelled with the transfer function of 1st order as in Equation 5.3, and the power amplifier block is shown in Figure 5.5,

$$\frac{I(s)}{U(s)} = k_i \frac{1}{T_a s + 1} \tag{5.3}$$

where:

$$k_i = \frac{k_{am}}{(R_c + R_s) + k_{am} K_s R_s} \tag{5.4}$$

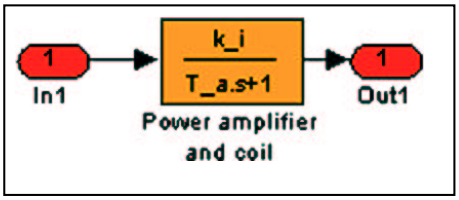

Figure 5.5: Power Amplifier and Coil Model.

$$T_a = \frac{L_c}{(R_c + R_s) + k_{am} K_s R_s} \tag{5.5}$$

k_i is called coil and amplifier gain and T_a is called coil and amplifier time constant.

Note: because T_a is very small, as we will show later in section 5.2, so Equation 5.3 becomes:

$$i = k_i u \tag{5.6}$$

Ball and Coil Subsystem

This subsystem can be modelled using Lagrange's Equations, The Lagrangian for the magnetic levitation is given by Equation 5.7,

$$\pounds(x, \dot{x}) = T - V = \frac{1}{2} m\dot{x}^2 - mgx \tag{5.7}$$

where T, V is the kinetic and the potential energy of the ball respectively. Without any non-conservative external forces, Lagrange's equation for the system is given by Equation 5.8,

$$\frac{d}{dt}\frac{\partial \pounds}{\partial \dot{x}} - \frac{\partial \pounds}{\partial x} = \frac{d}{dt}(m\dot{x}) + mg = 0 \tag{5.8}$$

To include the force F_d due to air damping and the input force (electromagnetic F_m), we simply append them as follows,

$$\frac{d}{dt}\frac{\partial \pounds}{\partial \dot{x}} - \frac{\partial \pounds}{\partial x} = F_d + F_m \tag{5.9}$$

$$F_m = k_c \frac{i^2}{(x - x_0)^2} \qquad is \quad given \quad in \ [44,\ 45] \tag{5.10}$$

$$\Downarrow$$

$$\frac{d}{dt}(m_k \dot{x}) + m_k g = -k_{FV}\dot{x} + k_c \frac{i^2}{(x - x_0)^2}$$

$$m_k \ddot{x} + m_k g = -k_{FV}\dot{x} + k_c \frac{i^2}{(x - x_0)^2} \tag{5.11}$$

where:

m_k	=	Ball Mass	[kg]
F_g	=	Gravity Force	[N]
F_c	=	Acceleration Force	[N]
F_d	=	Damping Force	[N]
x	=	Distance	[m]
x_0	=	Coil Offset	[m]
i	=	Coil Current	[A]
g	=	Gravity Constant	$[m/s^2]$
k_c	=	Aggregated Coil constant	[N/A]
t	=	Time	[s]
k_{FV}	=	Damping Constant	$[N.s/m]$

Rearranging Equation 5.11, the dynamic differential equation of motion becomes;

$$m_k\ddot{x} + k_{FV}\dot{x} = \frac{i^2 k_c}{(x - x_0)^2} - m_k g \tag{5.12}$$

Note that in some cases the damping force F_d is very small, for example in case of a low varying tracking signal like a sinusoidal with a very small amplitude and low frequency, but its large in case of a tracking signal like a square function with a high frequency, so in the modeling we will consider two cases, the first one with damping force which is given in Equation 5.12, and the second one without damping force which is given in Equation 5.13.

$$m_k\ddot{x} = \frac{i^2 k_c}{(x - x_0)^2} - m_k g \tag{5.13}$$

If we substitute $i = k_i u$ (Equation 5.13), we get

$$m_k\ddot{x} = \frac{(k_i u)^2 k_c}{(x - x_0)^2} - m_k g \tag{5.14}$$

or

$$m_k\ddot{x} = \frac{u^2 k_f}{(x - x_0)^2} - m_k g \tag{5.15}$$

where:

$k_f = k_i^2 k_c$

k_f is called aggregated coil constant [N/V]

Both Equation 5.12 and Equation 5.13 can be represented in a Simulink model as shown in Figure 5.6 and Figure 5.7 respectively.

D/A Converter

D/A converter can be represented as a Simulink block as shown in Figure 5.8 and described by a linear function as in Equation 5.16.

$$u = k_{DA} u_{MU} + u_0 \tag{5.16}$$

where:

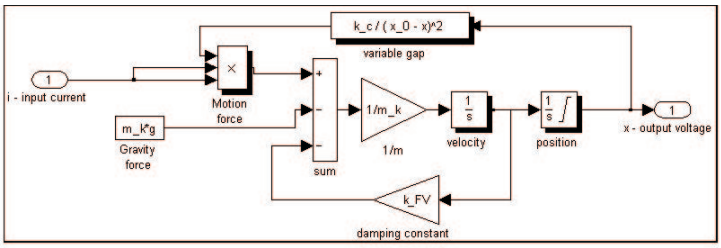

Figure 5.6: The Ball and Coil Subsystem Model (damping force included).

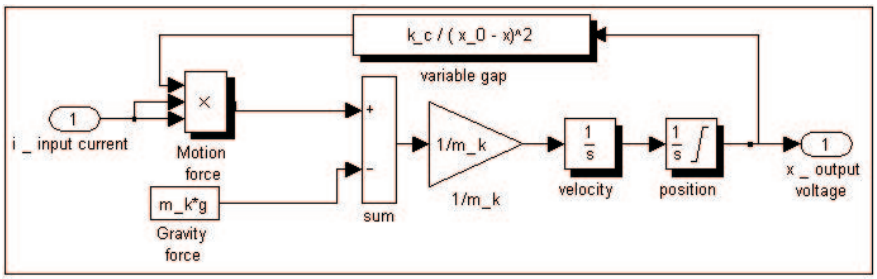

Figure 5.7: The Ball and Coil Subsystem Model (damping force excluded).

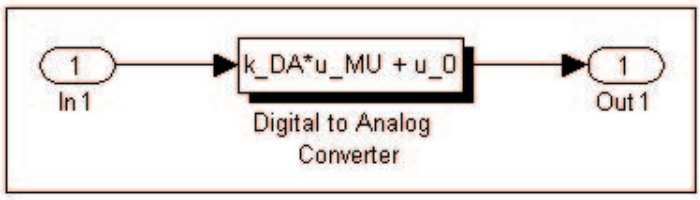

Figure 5.8: Digital to Analog Converter model.

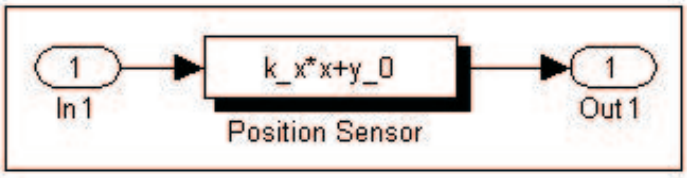

Figure 5.9: Position Sensor Model.

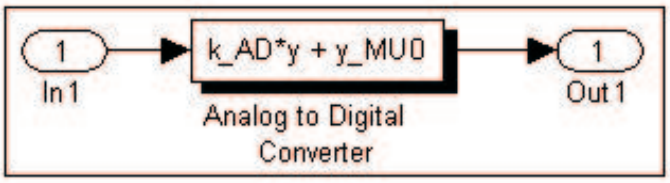

Figure 5.10: Analog to Digital Model.

u	=	Model Output Voltage	[V]
u_{MU}	=	D/A Converter Input	[MU]
k_{DA}	=	D/A Converter Gain	[V/MU]
u_0	=	D/A Converter Offset	[V]

Position Sensor

An inductive position sensor is used to measure the ball position. The sensor can be described with a linear function in Equation 5.17 and a Simulink block as shown in Figure 5.9.

$$y = k_x x + y_0 \tag{5.17}$$

where:

k_x	=	Position Sensor Gain	[V/m]
y_0	=	Position Sensor Offset	[m]
x	=	Ball Position	[m]
y	=	Model Output Voltage	[V]

A/D Converter

A/D converter can be represented by a Simulink block it is shown in Figure 5.10 and described by a linear function in Equation 5.18.

$$y_{MU} = k_{AD} y + y_{MU0} \tag{5.18}$$

where:

y_{MU}	=	A/D Converter Output	[V]
k_{AD}	=	A/D Converter Gain	[MU/V]
y_{MU0}	=	Converter Offset	[MU]
y	=	Model Output Voltage	[V]

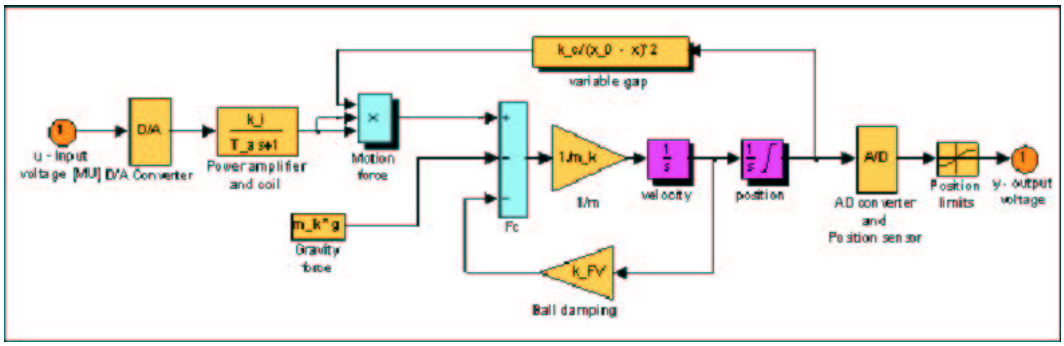

Figure 5.11: The Whole System Model.

Table 5.1: Data at input channel of DAQ.

i	$y[V]$	y_{MU}
1	5	1
2	-5	-1
3	0	0

5.3.2 The Whole System – Simulink Model

Using Equations 5.1- 5.18, a Simulink block diagram of the whole system is developed and arranged in Figure 5.11;

5.4 Measurements and Identification of the Parameters

Once the theoretical model of the laboratory magnetic levitation set-up is obtained, then a thirteen (13) parameters have to be determined: k_c, k_f, x_0, m_k, y_{MU0}, k_{AD}, u_0, k_{DA}, k_x, y_0, k_{FV}, T_a and k_i, there are two possible approaches:

- Direct measurements of the accessible physical quantities;
- Identification, i.e. experimental estimation of the parameters by means of measuring inputs and outputs [39].

5.4.1 Parameters of A/D and D/A Converters

In order to identify the A/D converter parameters, a simple experiment is implemented, we apply a different voltage values at the input of the A/D channel and read the corresponding values at the computer side, and fill in Table 5.1.

In order to identify of D/A converter parameters, a simple experiment is implemented, we assign a different values in Machine Unit (MU) and measure the output voltage at the outside of DAQ, and fill in Table 5.2.

Table 5.2: Data at output channel of DAQ.

i	u_{MU}	$u[V]$
1	1	5
2	-1	-5
3	0	0

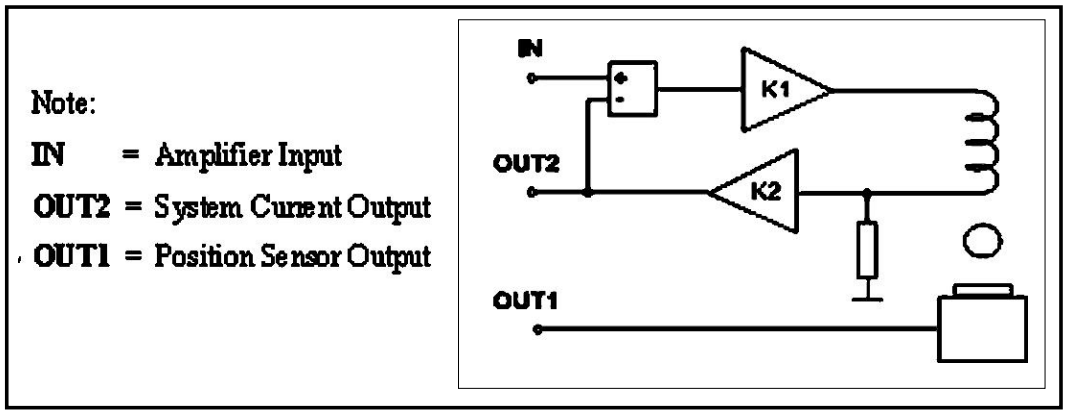

Figure 5.12: The base diagram of the model.

Based on the measurement in Table 5.1 and Table 5.2, the following parameter values are obtained:

$$\begin{array}{lcll} k_{DA} & = & 5 & [\text{V/MU}] \\ u_0 & = & 0 & [\text{V}] \\ k_{AD} & = & 0.2 & [\text{MU/V}] \\ y_{MU0} & = & 0 & [\text{MU}] \end{array}$$

Note: we used Data Acquisition card from Humusoft MF614, and during the experiments above, the DAQ is software selected at 5 volts.

5.4.2 The Power Amplifier

In case the typical values of the discrete electronic components of the power amplifier are available, we can use them to identify the power amplifier transfer function parameters T_a and k_i by directly substituting in Equation 5.4 and Equation 5.5. Otherwise, use experimental identification method, applying input signal like a square function at the input of the block (IN) and record the output signal of the block (OUT2), see the base unit diagram of the apparatus Figure 5.12.

Both Figure 5.13 and Figure 5.14 show the Experiment results, where k_i and T_a can be determined,

$$\begin{array}{lcll} k_i & = & 0.3 & [\text{A/V}] \\ T_a & = & 3 \times 10^{-3} & [\text{s}]. \end{array}$$

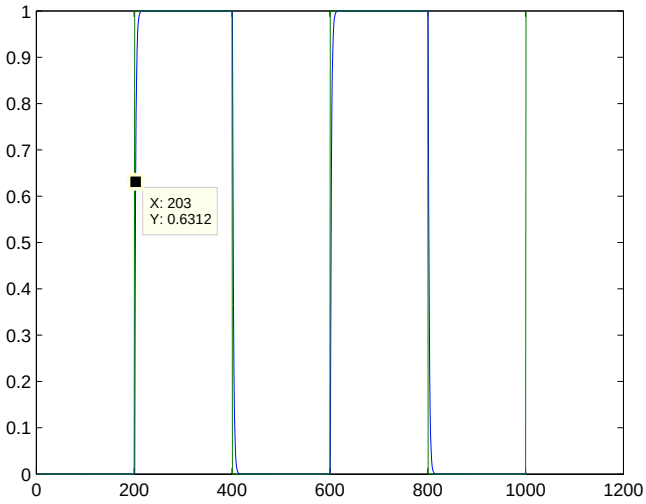

Figure 5.13: The step response of the Power Amplifier block.

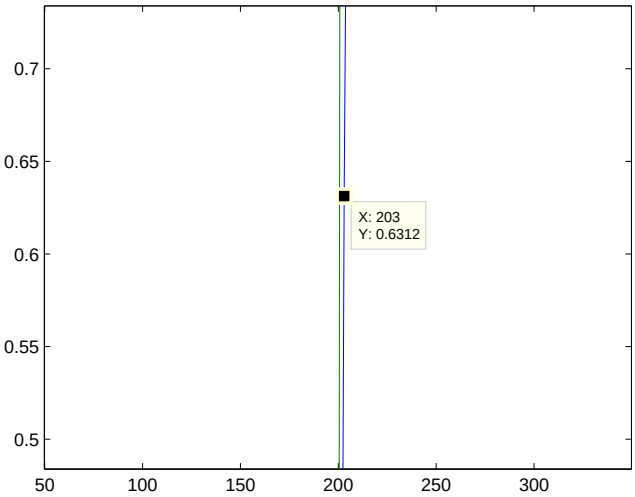

Figure 5.14: Magnified response of the Power Amplifier block.

Table 5.3: Data for position sensor calibration.

i	y_{MU}	y_i	x_i
1	0.0025	0.0125	0
2	0.774	3.87	6.3×10^{-3}

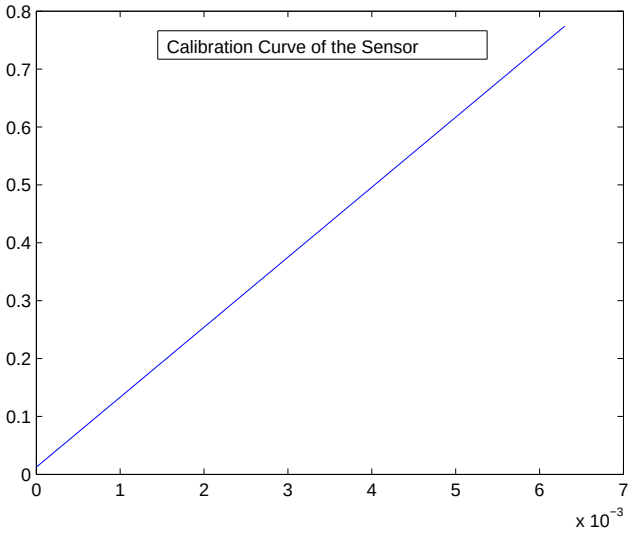

Figure 5.15: Calibration Curve of The Position Sensor.

5.4.3 The Position Sensor

The position sensor can be calibrated by simple ball position measurements as shown in Table 5.3, note that $k_{AD} = 5$ for measurements in the table. Note that the first measurement position is at the bottom travelling point, and the second measurement point is at the top travelling point

The position sensor parameters can be calculated as follows,

$k_x = (y_2 - y_1)/(x_2 - x_1)$

$y_0 = y_1 = 0.0125$

$k_x = 612.3016\ [V/m]$

Note:The calibration curve of the position sensor is plotted in Figure 5.15.

5.4.4 Ball and Coil Subsystem

Ball Mass

The mass of the ball is measured by using a precision balance and it's approximated numerical value is:

$m_k = 8.4 \times 10^{-3}$ [kg].

Coil Constant

The coil constant parameters k_f and x_0 are estimated by means of interpolation technique, two interpolation techniques are used to calculate the coil constant parameters, firstly we used the **Two Point** interpolation method, then the **L**inear **Q**uadratic (**LQ**) Optimal method, then we compared between them to choose the best one according to the least square error or the minimum cost function.

- **Two Points Interpolation Method**

  In Figure 5.19, we processed the data using **Two Point** interpolation method, the sample data was 4 points of the system input voltage versus the ball position,where the ball was nearly at balance against its weight at every point. By plotting u versus x, and interpolate the data we can obtain a *two point* model calibration graph as shown in Figure 5.19.

  By equating the magmatic force at the number of different points, at points $x2$ and $x3$ for example, we ca find x_0 using the equation below:

  $$x_0 = \frac{\frac{x_3}{u_3} - \frac{x_2}{u_2}}{\frac{1}{u_3} - \frac{1}{u_2}}$$

  by substituting with numerical values, we get $x_0 = 0.0095\ [m]$.

  To find k_f, we equate the magnetic force to the weight of the ball at equilibrium point at specific point,

  $$m_k g = \frac{u^2 k_f}{(x - x_0)^2}$$

  Then:

  $$k_f = m_k g \frac{(x_2 - x_0)^2}{u_2^2}$$

  By substituting with numerical values, we get $k_f = 0.71214 \times 10^{-6}$, and $k_c = k_f / k_i^2 = 7.9126 \times 10^{-6}$.

- **LQ Optimal Method**

  If the input data is many points, We processed the data using *Optimal Linear Quadratic* method to fit the parameters in an optimal way, this criterion of optimally is a *minimization of the sum of squared errors* of estimated equilibrium force [53], see Equation 5.19, the sample data is obtained with closed loop control(here I used a controller designed by the manufacture) with a low and slowly varying sinusoidal tracking signal, the sample data was a large number of data points of the system input voltage $u(k)$ versus the ball position $x(k)$, these sampled two signals $x(k)$ and $u(k)$ are shown in Figure 5.17 and Figure 5.18 respectively,

```
%%%%%%%%%%%%%%%%%%%%%%%%%%%%%%%%%%%%%%%%%%%%%%%%%%%%%%%%%%%%%%%%%%%%%%%%%%%%
%   C o i l   c o n s t a n t
%   L Q   o p t i m a l   c a l i b r a t i o n
load statchar.mat
k_DA = 5;
%%%%%%%%%%%%%%%%%%%%%%%%%%%%%%%%%%%%%%%%%%%%%%%%%%%%%%%%%%%%%%%%%%%%%%%%%%%%
%   convert measured data to SI
Ttt = Tr * ( 1:length(z) )';          % time
Yt = (z(:,1) - y_MUO)/k_AD ;          % actual position sesnor signal
[V]
Wt = (z(:,3) - y_MUO)/k_AD ;          % desired position sensor signal
[V]
Ut = z(:,4) ;        % system input [V]
Xt = (Yt - y_0) / k_x;            % actual position [m]
%%%%%%%%%%%%%%%%%%%%%%%%%%%%%%%%%%%%%%%%%%%%%%%%%%%%%%%%%%%%%%%%%%%%%%%%%%%%
%   referential results to be plotted
tmp = Ut.^2 * k_f ./ (Xt - x_0).^2;
tmpy  = [0 x4];
tmpu  = -sqrt(mk * g / k_f ) * ( tmpy - x_0 );
%%%%%%%%%%%%%%%%%%%%%%%%%%%%%%%%%%%%%%%%%%%%%%%%%%%%%%%%%%%%%%%%%%%%%%%%%%%%
%   Run minimisation procedure
x = [x_0 k_f];                % initial guess
P1 = Ut;                      % parameters
P2 = Xt;
P3 = mk * g;
                    % simplex optimisation
[x,fval,exitflag] = fminsearch('norm(P1.^2 * x(2) ./ (P2 - x(1)).^2 -
P3)',x,[],P1,P2,P3)

k_f = x(2)               % aggregated coil constant [N/V]
```

Figure 5.16: Matlab Code of The LQ Optimal Calibration.

$$J = \sum_i \left(\frac{u_i^2 k_f}{(x - x_0)^2} - m_k g\right)^2 \tag{5.19}$$

using the minimization procedure of the least square error to calculate the constant x_0 and after that calculating the constant k_f.

Figure 5.16 shows part of matlab code for the LQ Optimal Calibration method by the least square interpolation, and the result of the coil constant parameters are:

x_0	=	0.0083	[m]
k_f	=	0.609×10^{-6}	[N/V]
k_c	=	6.9×10^{-6}	[N/A]

- **Comparison of the Two Interpolation Methods**

To compare between the two methods, one should calculate the error by plotting the magnetic force f_m in time domain in each method, and then you can compare, different plots in Figure 5.19 show clearly the difference between the two techniques.

It's clear that the error generated by LQ method is smaller than that by Two Point method, so the results of the second method (LQ) will be considered.

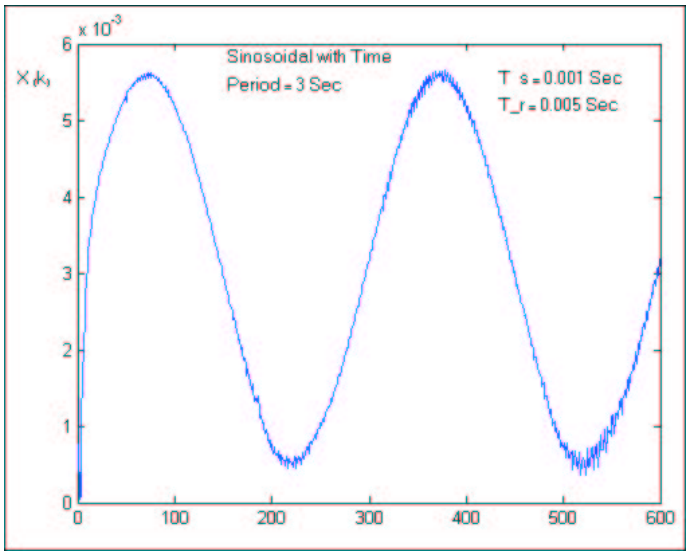

Figure 5.17: Plot of Data Sample of Actual Position $x(k)$.

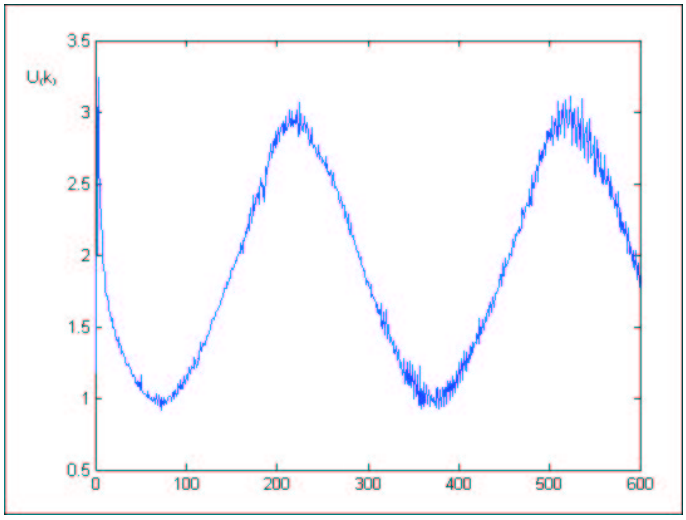

Figure 5.18: Plot of Data Sample of Input Voltage $u(k)$.

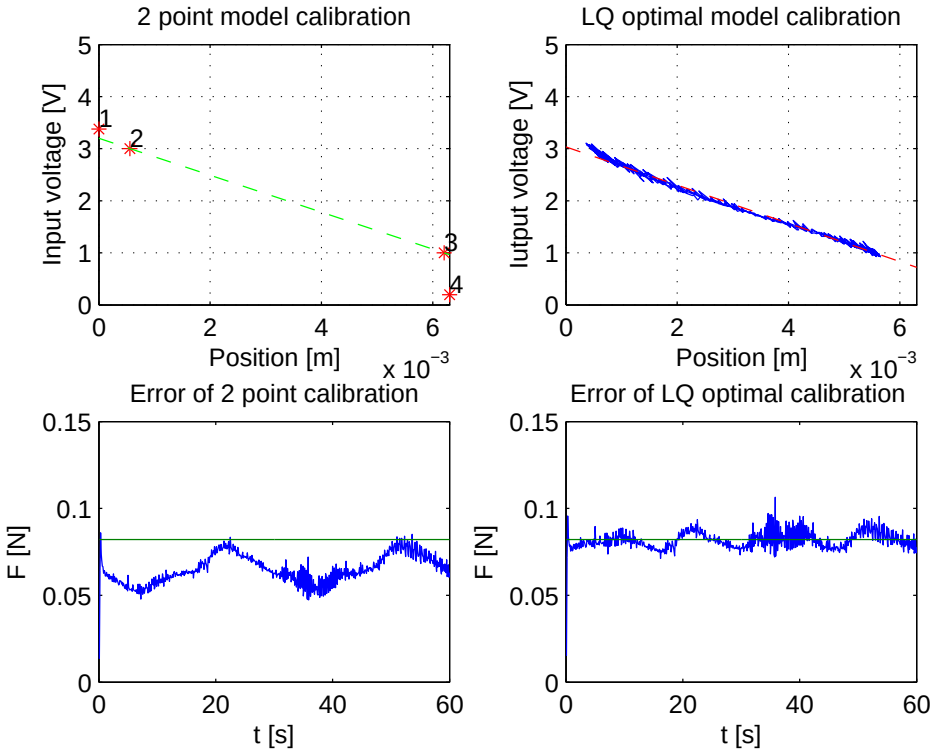

Figure 5.19: Plots For Comparison Between Two Interpolation Methods.

Damping Constant

For more accurate and exact model, the ball damping constant k_{FV} should be estimated using offline model adaptation, by comparing the real response y_{real} with the model response y_{mod} using *Parameter Estimation Toolbox* through optimization algorithm like Simplex Search [54]. In this technique the Simulink model is tuned until the Simulink model matched the real time model to a Least Square Error Cost Function (LSECF) equals 1.75, after many iterations the following satisffactory result is obtained.

$k_{FV} = 0.03$

Note: In Figure 5.20, a group of plots are included to show the process of estimation and to justify the result.

A summery of model CE152 parameters are listed in table 5.4

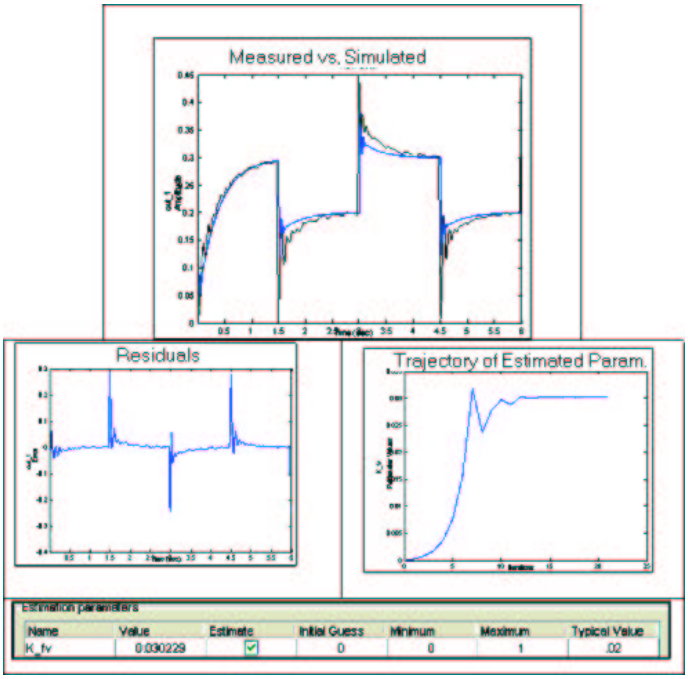

Figure 5.20: Group of plots generated during estimation of the damping constant.

Table 5.4: Parameters for magnetic levitation model CE152.

m_k	Ball Mass [kg]	8.4×10^{-3}
x_0	Coil Offset [m]	0.0083
g	Accelaration of Gravity$[m/s^2]$	9.81
k_c	Aggregated Coil constant [N/A]	6.9×10^{-6}
k_F	Damping Constant [N/V]	0.0609×10^{-6}
k_{FV}	Damping Constant [N.s/m]	0.03
k_i	Power Amplifier Gain [A/V]	0.3
T_a	Power Amplifier Time Constant [s]	3×10^{-3}
k_{DA}	D/A Converter Gain [V/MU]	0.2
u_0	D/A Converter Offset [V]	0
k_{AD}	A/D Converter Gain [V/MU]	0.2
u_{MU0}	A/D Converter Offset [V]	0
k_x	Position Sensor Gain [V/m]	612.3
y_0	Position Sensor Offset [m]	0.0

Chapter 6

Control of Magnetic Levitation Model

6.1 Control

PID controllers are widely used in industrial practice more than 60 years. The development went from pneumatic through analogue to digital controllers, but the control algorithm is in fact the same. The PID controller is a standard and proved solution for the most of industrial control applications. In spite of this fact, there is not some standard and generally accepted method for PID controller design and tuning based on known process model.

The selection of the three coefficients of PID controllers is basically a search problem in a three-dimensional space. Points in the search space correspond to different selection of a PID controller's three parameters. By choosing different points of the parameter space, we can produce, for example, different step responses. A PID controller can be determined by moving in this search space on a trial-and-error basis.

The main problem in the selection of the three coefficients is that these coefficients do not readily translate into the desired performance and robustness characteristic that the control system designer has in mind. Several rules and methods have been proposed to solve this problem. In this thesis we will consider the root locus as a design method for PID controller.

6.1.1 Model Linearization

Normally there are two approaches to linearize the nonlinear system [55], numerical and analytical linearization, analytical linearization is used here.

The standard form of state space model is:

$$\begin{aligned} \dot{\boldsymbol{x}} &= \boldsymbol{A}\boldsymbol{x} + \boldsymbol{B}\boldsymbol{u} \\ \boldsymbol{y} &= \boldsymbol{C}\boldsymbol{x} + \boldsymbol{D}\boldsymbol{u} \end{aligned} \tag{6.1}$$

where:

$\boldsymbol{u}$ - system input $[u_{MU}]$,

$\boldsymbol{x}$ - system state $[x\ v\ i]$,
$\boldsymbol{y}$ - system output $[y_{MU}]$,
$\boldsymbol{A}$, $\boldsymbol{B}$, $\boldsymbol{C}$, $\boldsymbol{D}$ - linear model matrices.

The components of system state x were chosen as ball position, ball velocity and coil current. System state is measured in metric units to make the space state description more general. To simplify the controller design the system input u and the output y are scaled to machine units.

Analytical linearization

The state equations of the magnetic levitation are described as follows:

$$\begin{aligned}\dot{x} &= v \\ \dot{v} &= -\frac{k_{FV}}{m_k}v - g + \frac{k_c i^2}{m_k(x_0-x)^2} \\ \dot{i} &= \frac{k_i k_{DA} u_m}{T_a} - \frac{i}{T_a}\end{aligned}$$

$$y_m = k_x k_{AD} x \tag{6.2}$$

where x is the ball position, i is the coil current, u_m is the model input voltage and y_m is the A/D converter output. The objective of the control is to keep the displacement y_m of the ferric ball under the influence of magnetic force following a desired trajectory y_d as closely as possible. In order to apply the PID controller for the magnetic levitation system which is a system with high nonlinearities, we firstly have to linearize Equation 6.2. According to the equilibrium point $[x_{00},\ v_{00},\ i_{00}\ ]$, we obtain the linearization state equations in Equation 6.3 and Equation 6.4,

$$\begin{aligned}\dot{x}_\delta &= v_\delta \\ \dot{v}_\delta &= \frac{2i_{00}^2 k_c}{(x_0-x_{00})^3 m_k} x_\delta - \frac{k_{FV}}{m_k} v_\delta + \frac{2i_{00}k_c}{(x_0-x_{00})^2 m_k} i_\delta \\ \dot{i}_\delta &= \frac{k_i k_{DA} u_\delta}{T_a} - \frac{i_\delta}{T_a}\end{aligned}$$

$$y_m = k_x k_{AD} x_\delta \tag{6.3}$$

Which can be represented in a state space representations as shown below (as $\boldsymbol{A}$, $\boldsymbol{B}$, $\boldsymbol{C}$ and $\boldsymbol{D}$ matrices represent the actual state system matrices),

$$\mathbf{A} = \begin{bmatrix} 0 & 1 & 0 \\ \frac{-2i_{00}^2 k_c}{(x_{00}-x_0)^3 m_k} & -\frac{k_{FV}}{m_k} & \frac{2i_{00}k_c}{(x_{00}-x)^2 m_k} \\ 0 & 0 & -\frac{1}{T_a} \end{bmatrix}$$

$$\mathbf{B} = \begin{bmatrix} 0 \\ 0 \\ \frac{k_i k_{DA}}{T_a} \end{bmatrix}$$

$$\mathbf{C} = \begin{bmatrix} k_x k_{AD} & 0 & 0 \end{bmatrix}$$

$$\mathbf{D} = \begin{bmatrix} 0 \end{bmatrix} \tag{6.4}$$

The numerical values for the state matrices at the equilibrium point [0.0032 0.0 0.5612] are;

$$\mathbf{A} = \begin{bmatrix} 0 & 1 & 0 \\ 3834.4 & -2.4 & 35.2 \\ 0 & 0 & -333.3 \end{bmatrix},$$

$$\mathbf{B} = \begin{bmatrix} 0 \\ 0 \\ 500 \end{bmatrix},$$

$$\mathbf{C} = \begin{bmatrix} 122.4 & 0 & 0 \end{bmatrix},$$

$$\mathbf{D} = \begin{bmatrix} 0 \end{bmatrix}. \tag{6.5}$$

6.1.2 Continuous Time Controller Design

Before we can design a controller to stabilize the system, the poles and zeroes of $H(s)$ should be located. The system transfer function $H(s)$ of the actual position to the desired position (Equation 6.6) is obtained from the space state representation in Equation 6.5

$$H(s) = \frac{y(s)}{w(s)} = \frac{2154240}{(s^3 + 335.7s^2 - 3034.48s - 1278005.52)}$$

$$H(s) = \frac{y(s)}{w(s)} = \frac{2.154487 \times 10^6}{(s - 60.73)(s + 63.12)(s + 333.3)} \tag{6.6}$$

Analog PID Controller

To design a standard **PID** controller for the system with $H(s)$ in Equation 6.6, we should guess the two zeros of the **PID** controller, see Equation 6.7.

$$\begin{aligned} H_c(s) = & \\ & = K_p + \frac{K_i}{s} + K_d s \\ & = \frac{K_p s + K_i + K_d s^2}{s} \\ & = \frac{K_d s^2 + K_p s + K_i}{s} \\ & = K_p \frac{(K_d/K_p)s^2 + s + (K_i/K_p)}{s} \\ & = K \frac{K'_d s^2 + s + K'_i}{s} \\ & = K \frac{(T_{z1}s + 1)(T_{z2}s + 1)}{s} \end{aligned} \tag{6.7}$$

where:

$K = K_p$, $K'_d = K_d/K_p$; $K'_i = K_i/K_p$; and T_{z1}, T_{z2} = time constants corresponding with controller zeros.

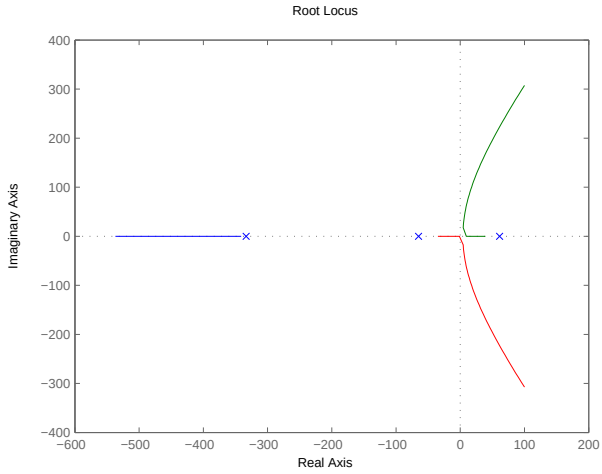

Figure 6.1: A root locus of open loop system $H(s)$.

Design and Tuning PID Controller

Investigating the root locus of the open loop of the magnetic levitation system $H(s)$ (Figure 6.1, we can guess the two zeros of the PID controller, after a number of trials, we get a satisfactory trajectory which assign the two zeros at -200 and -1.5, then the PID controller has Equation 6.8.

$$H_c(s) = \frac{(s+200)(s+1.5)}{s} \tag{6.8}$$

$$H_c(s) = \frac{s^2 + 201.5s + 300}{s} \tag{6.9}$$

Normalizing K_p which is the factor of s term in Equation 6.9,

$$H_c(s) = \frac{0.005s^2 + s + 1.4888}{s} \tag{6.10}$$

Then we can write $H_c(s)H(s)$

$$= \frac{(0.005s^2 + s + 1.4888)}{s} \frac{2.4591 \times 10^8}{(s-67)(s+70)(s+53452)} \tag{6.11}$$

Now plot the root locus of the open loop of $H_c(s)H(s)$ and tune controller gain K, that to move the unstable pole as far to the left as possible, also taking on account a trade−off between minimum overshoot, reasonable control action, and fast transient response. For every K possible on the root locus trajectory, we tried a number of step response until we have a good system performance, see Figure 6.2 as one of the trial to PID tuning, satisfactory performance is met after many trial like the result in Figure 6.3, the K value was 2. Thus the PID controller parameters are:

$K_p = 2, \quad K_d = K_p K_d' = 0.005 \times 2 = 0.01, \text{ and } K_i = K_p K_i' = 2 \times 1.4888 = 2.97.$

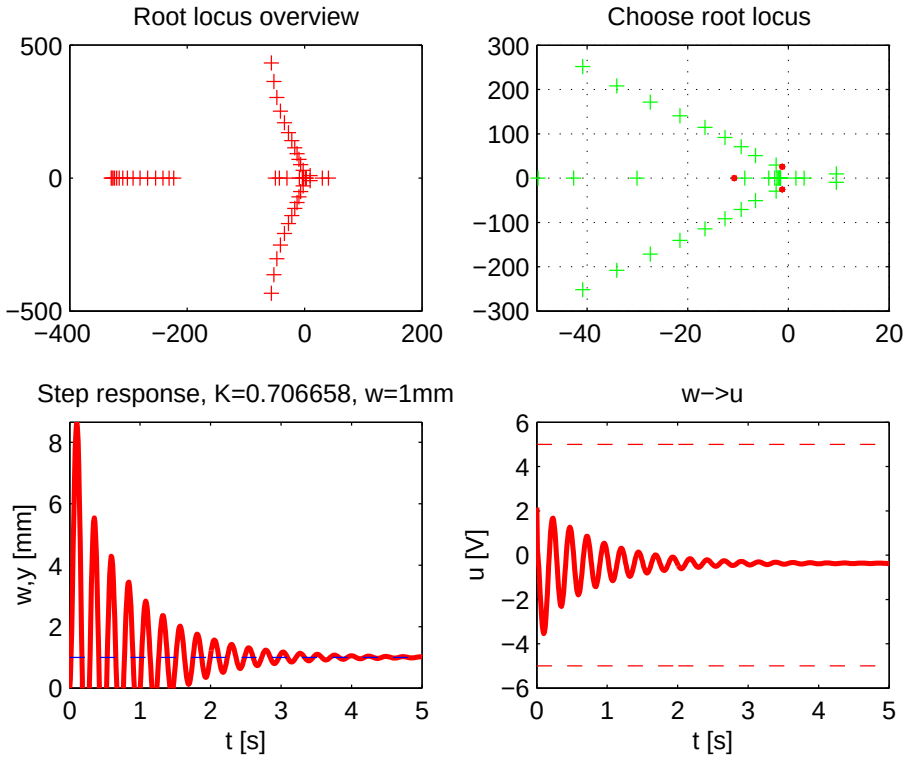

Figure 6.2: Root Locus of PID Tuning(one of the trials).

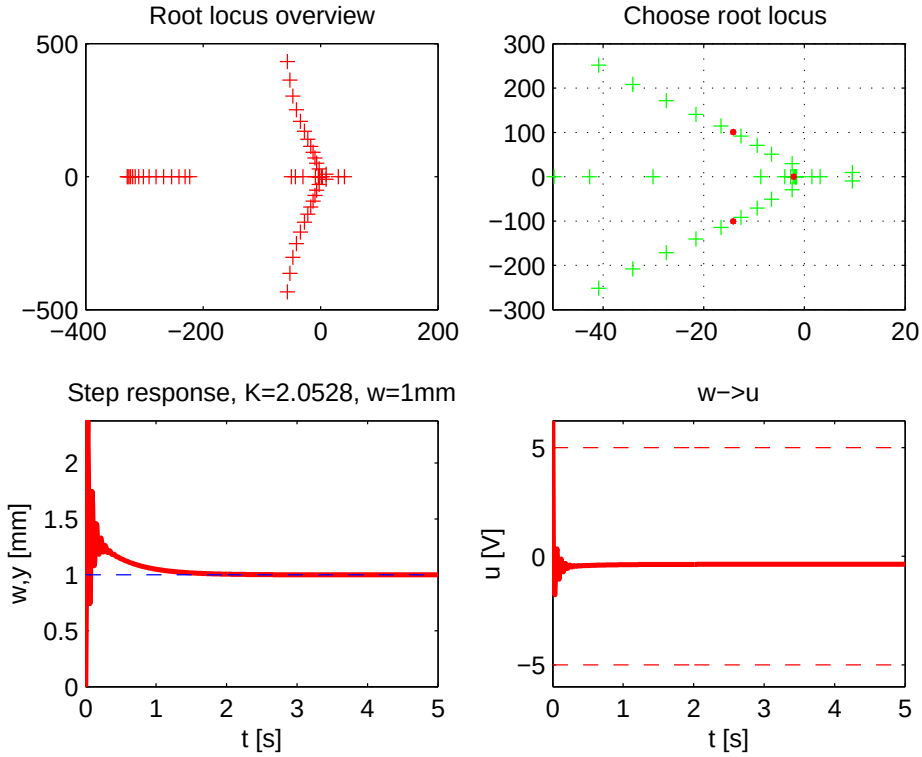

Figure 6.3: Root Locus of PID Tuning(satisfactory trial).

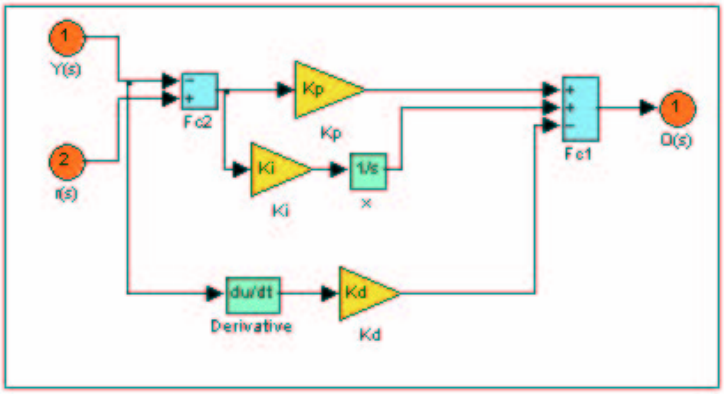

Figure 6.4: Modified analog PID (PI-D) controller.

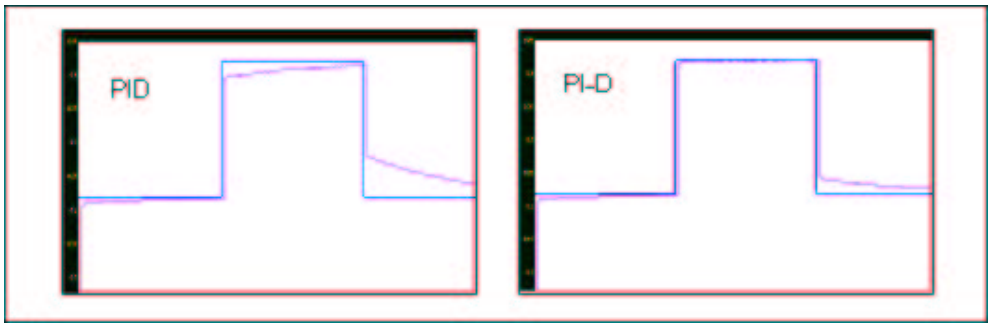

Figure 6.5: Simulation of PID controller versus PI-D(simulation done under the same condition).

Modified PID Controller

The modified PID controller with the transfer function in Equation 6.12 and a Simulink block in Figure 6.4, the modification of the standard one is that the derivative term processes only the output of the system and not the error signal. By simulation it has be seen that introducing the modification makes the responses more smooth as shown in Figure 6.5, while keeping on the stability of the controller, and also need no further tuning to the standard PID parameters.

$$O_c(s) = (K_p + \frac{K_i}{s})E(s) - K_d s Y(s) \tag{6.12}$$

6.1.3 Computer Control Design

Figure 6.6 illustrates the different blocks of the computer or digital control system, the figure also shows that the controller is embedded in the computer as a software, this software is working in Matlab-Simulink environment.

Discrete PID Controller

The standard analog PID controller can be discretized using ZOH method by the substitution:

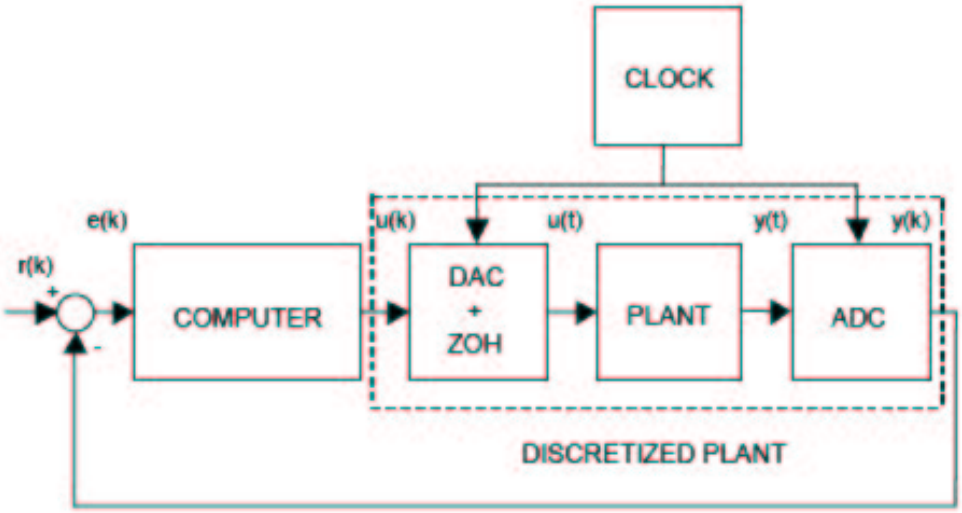

Figure 6.6: Digital Control System.

$$s = \frac{z-1}{zT_s} \tag{6.13}$$

where:

T_s = sampling period [s]

This will give the Z transform of the standard PID as follow:

$$H_c(z) = K_p + K_i\frac{zT_s}{(z-1)} + K_d\frac{z-1}{T_s z} \tag{6.14}$$

$$= \frac{K_p z(z-1) + K_i T_s z^2 + K_d/T_s(z-1)^2}{z(z-1)} \tag{6.15}$$

Discrete Modified PID (PI-D)Controller

This standard discrete PID controller can be modified as discrete PI-D (Equation 6.16), and has a Simulink model as shown in Figure 6.7.

$$O_c(z) = (K_p + k_i\frac{zT_s}{(z-1)})E(z) - K_d\frac{(z-1)}{zT_s}Y(z) \tag{6.16}$$

Sampling Rate Selection

Selection of sampling rates is an important issue. For economical reasons, sampling rates are kept as low as possible: A lower rate means that there is more time available for control algorithm execution, which can thereby be carried out on slower computers. Digitizing well behaved analog control systems can heavily affect system response. If sampling frequencies is too low, the systems may even become unstable. According to the Nyquist criterion [37], the sampling frequency should at least be twice as high as the bandwidth of the error signal. This bandwidth is bounded by the system bandwidth, hence $\omega_s \geq 2\omega_B$. However, in order to guarantee satisfactory response, a factor of 10 to 20 may be required.

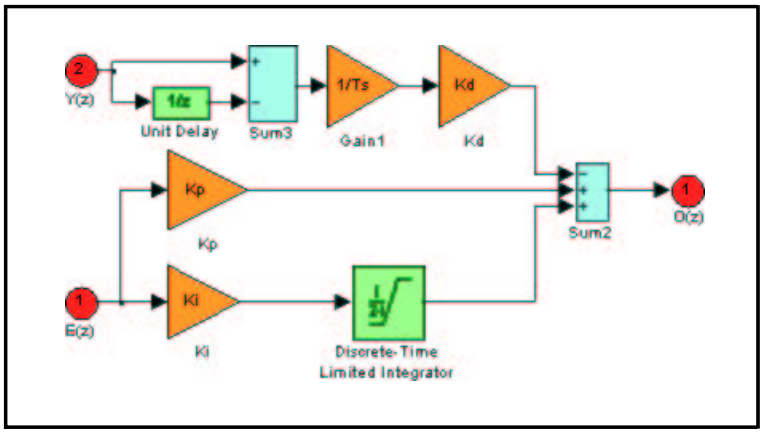

Figure 6.7: Discrete PI-D controller.

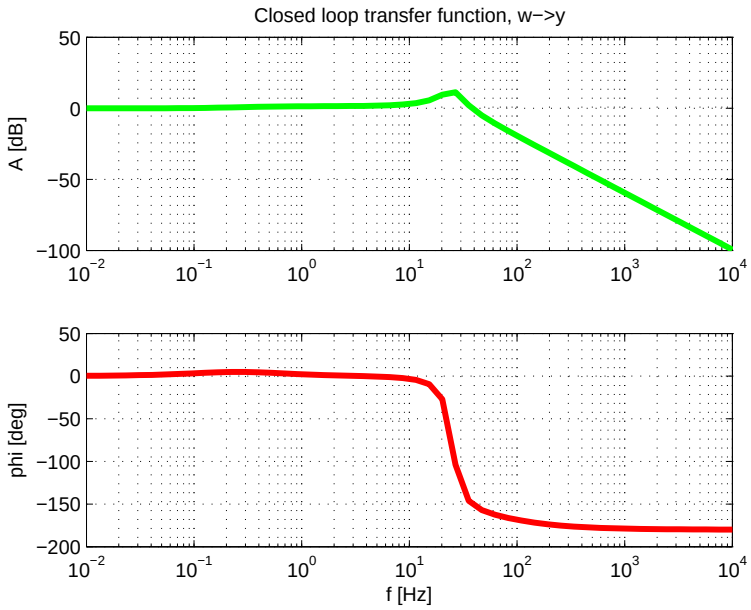

Figure 6.8: Closed loop transfer function with tuned PID, desired position to actual position.

In our case, ω_B can be determined from frequency response of the desired position to the actual position Figure 6.8,

$$\omega_s = 20\,\omega_B$$

or,

$$f_s = 20 f_B$$

When $f_B \approx 50Hz$, then the sampling frequancy $f_s = 1000Hz$

The modified discrete PID controller (PI-D) is tested on the Simulink model of the magnetic levitation, moreover it has been tested on the real time model, this the controller was able to stabilize both of the Simulink model and real time model, and has good tracking performance.

Note: The parameters of Discrete PI-D were: $K_p = 2$, $K_i = 2.97$, $K_d = 0.01$

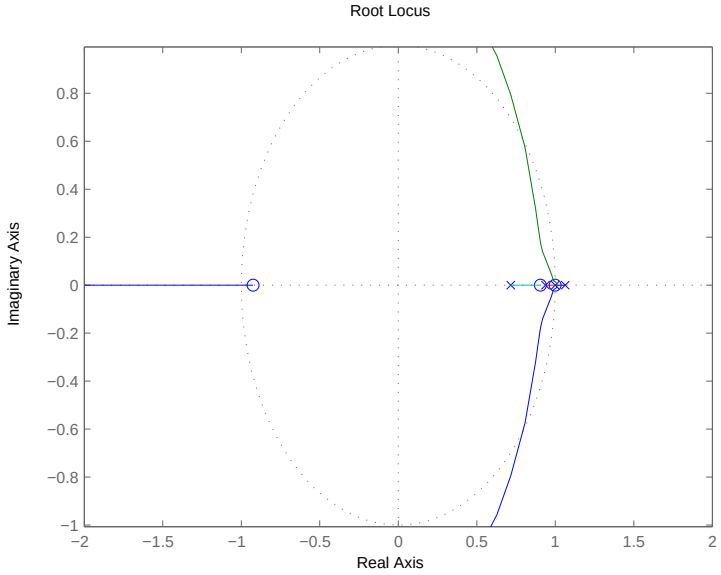

Figure 6.9: root locus of the compensated discretized system.

6.2 Digital Control Using Discrete PID Controller

Discretizing the plant $H(s)$ an Equation 6.6 using ZOH, we have Equation 6.17.

$$H(z) = \frac{0.0003309z^2 + 0.00122z + 0.0002798}{z^3 - 2.718z^2 + 2.432z - 0.7148}. \tag{6.17}$$

Now discretizing $H(s)H_c(s)(H_c(s)$ after normalizing the term of s Equation 6.10), we have Equation 6.18

$$H(z)H_c(z) = \frac{0.004992z^3 - 0.004886z^2 - 0.004276z + 0.004171}{z^4 - 3.717z^3 + 5.147z^2 - 3.144z + 0.714}. \tag{6.18}$$

We can find K_p by plotting the root locus in Figure 6.9 and picking $K_p = 2$ which gives the best response, the step response of the compensated system is in Figure 6.10.

6.3 Model Validation

Due to instability, the ball position dynamics can not be validated in an open loop experiment. Therefore, a closed loop experiment is used to validate the model as shown in Figure 6.11 below.

Therefore, a digital controller PI-D has to be provided, which will enable the tracking of a position reference w_{ref} as a square signal with time period 3s (green line). The comparison between the real response of the position w_{real} of magnetic levitation model (red line) and of the model (blue line) as shown in Figure 6.12 shows that the real system response is subject to significant external disturbances.

Also Figure 6.13 shows the input signal u provided by the controller in case of the real system is the green line and in case of the model is the blue line. From the

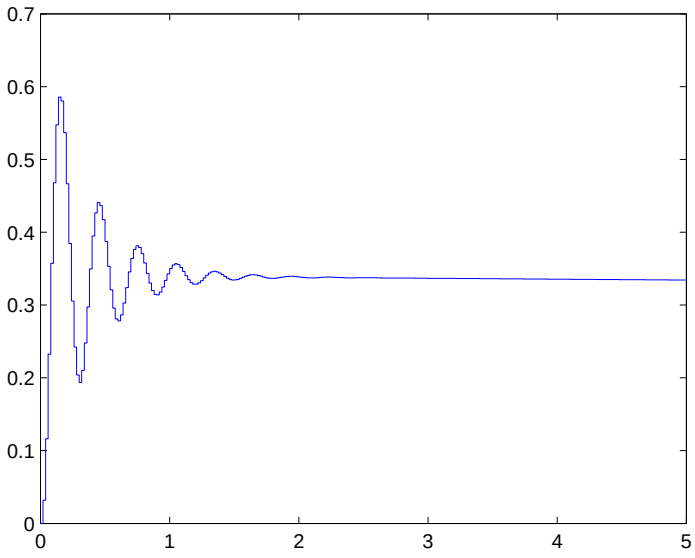

Figure 6.10: Step response of the compensated discretized system.

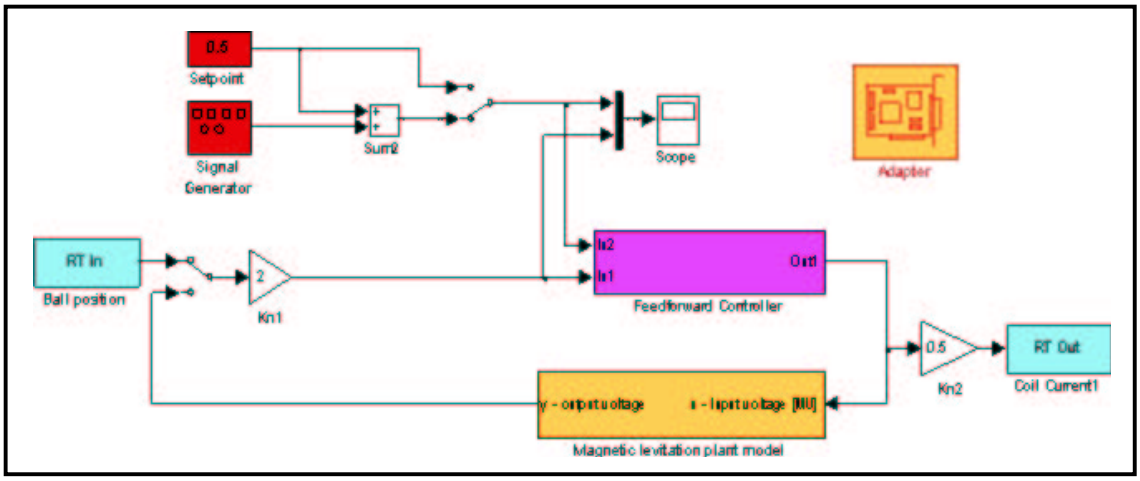

Figure 6.11: Closed loop control, A validation Diagram.

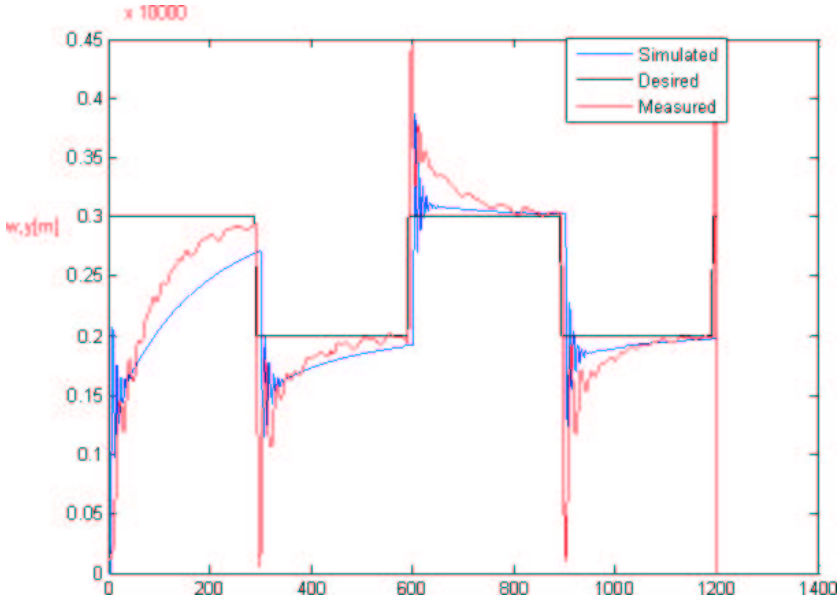

Figure 6.12: Simulation of closed loop PID control - Desired, measured and simulated position.

comparison we can see that the signals are quite similar in all the recorded period except from (600-900), which occur due to some noise.

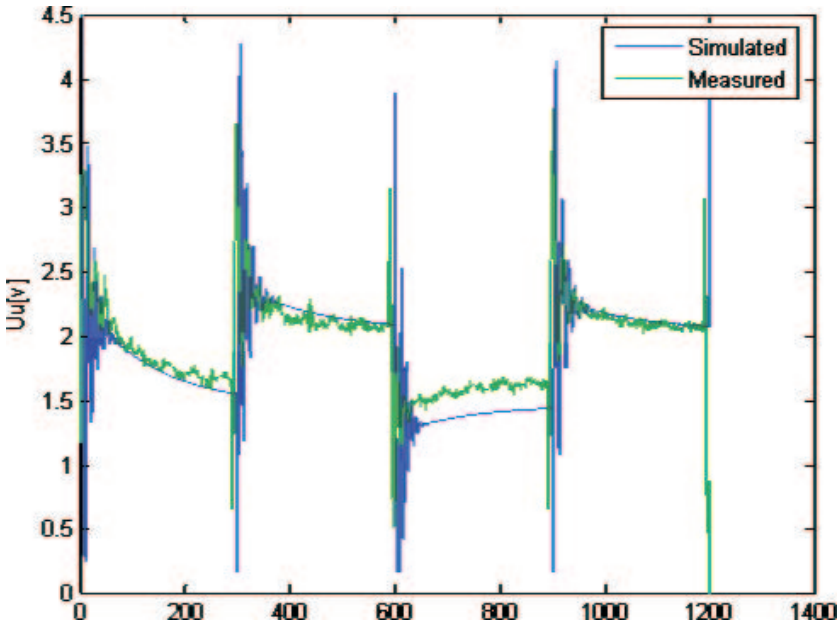

Figure 6.13: Simulation of closed loop PID control - measured and simulated controller output.

Chapter 7

Building a Laboratory Magnetic Levitation System Model

7.1 Introduction

The idea of building a laboratory magnetic levitation system comes after working on the ready made model CE 152 from HUMUSOFT, After searching the price of the apparatus we found it cost a lot of money, we searched the design of different models, then we tried to design a model and, we tried different designes, until we succeeded to build a nice shape one. Our model could be used in visual demonstrations of control principles and electronics designs.

The model has been stabilized by a proportional to derivative (PD) controller and a simple electromagnetic design for a given sphere have been implemented in this educational model and the performance of the system is investigated [56].

7.2 Magnetic Levitation System

In this section a general description of the magnetic levitation system considered in this work is presented. A general scheme of the levitator considered in this work is shown in Figure 7.1, where it is possible to identify the main components of the system. Figure 7.1 shows the principle of a magnetic levitation system using a controlled electromagnet. The position of the steel ball is sensed by an optical transducer comprising a light source and a photocell; the quantity of light falling on the photocell varies with the position of the ball, so the voltage output is a measure of the ball position. The photocell output is compared with a reference voltage which corresponds to the desired position of the ball; the difference represents a position error. This error voltage is passed to a DC amplifier which controls the current in the electromagnet, so that any displacement of the ball from its desired position causes a corrective change in the magnet current. Feedback control systems of this kind require additional circuitry to prevent instability; this is the function of the compensation block in Figure 7.1.

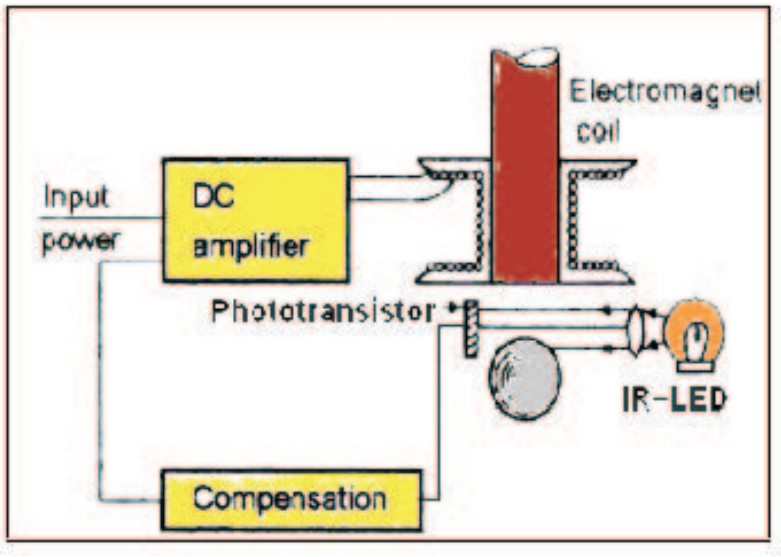

Figure 7.1: General Scheme of Magnetic Levitation System.

7.2.1 Position Measurement Subsystem

One of the main components of the levitator is the position measurement subsystem. This substantial part of the prototype was designed by means of an infrared emitter-detector formed by a couple of standard infrared LED (IRED) as emitter and a phototransistor as a detector. The main advantages of this arrangement are low cost, easy implementation and free maintenance properties. In Figure 7.1 one can see the physical location of the transmitter and captor. This device is able to detect changes in the position of the levitating object on the z axis but it is insensitive to any movement on the plane x-y. The emitter and captor are firmly fixed to the structure of the levitation device, and the emission of the infrared signal is constant. The object in levitation (sphere) is placed directly between the emitter and the detector see Figure 7.1. In this way, the intensity variation of the infrared signal collected by the detector depends exclusively on the position of the levitated object on the vertical axis. As a result, it is possible to obtain a relation of the voltage generated between terminals of the captor, as a function of the vertical position of the sphere, with an appropriate precision.

7.2.2 Magnetic Induction Subsystem

The intensity of the magnetic force produced by the inductor depends on the electric current that circulates the iron core. It is important to mention that a nucleus with type I laminations has been selected for the construction of the induction system and a wire of 0.6 mm of diameter and a bout 1200 turns was used. Figure 7.2 is an image of the laboratory magnetic levitation system, shows the construction of the full system and you can see also the shape of the core (cylindrical with 20 mm in

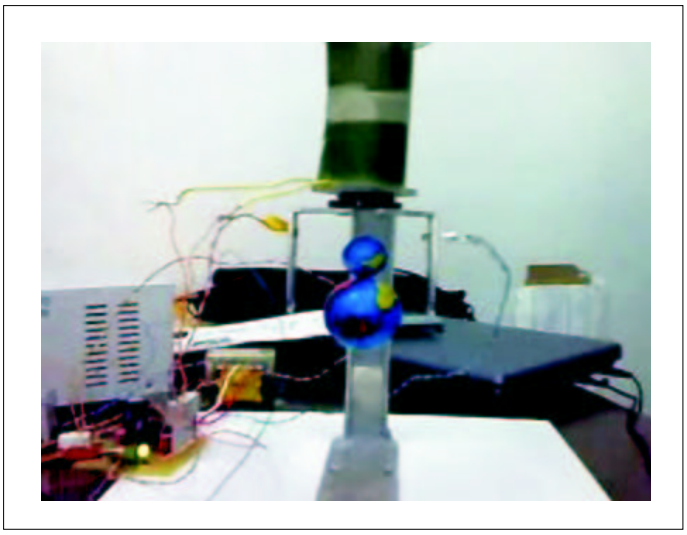

Figure 7.2: Prototype of laboratory magnetic levitation system.

diameter and 100 mm in length).

7.3 System Modelling

To have the students understand the control theory of the system, general model should be constructed.

The system model can be divided into three blocks, and the whole block diagram is in Figure 7.3.

- The linear power amplifier (the power transistor circuit).
- The ball and coil subsystem.
- The position sensor (IRED and phototransistor).

7.3.1 The Linear Power Amplifier

This block has to be modeled as current amplifier by

$$i = k_i u$$

or in Laplace form as:

$$\frac{I(s)}{U(s)} = k_i \tag{7.1}$$

Where:
k_i = Amplifier Gain $[A/V]$
i = Amplifier Output Current $[A]$
u = Amplifier Input Voltage $[V]$

7.3.2 The Ball and Coil Subsystem

The motion equation is based on the balance of all forces acting on the ball, i.e. gravity force F_g, electromagnetic force f_m, and the acceleration force F_a,

$$F_a = f_m - F_g$$

$$F_g = Mg$$

$$F_a = M\frac{d^2x}{dt^2} \tag{7.2}$$

Where:

M = Ball Mass $[kg]$

x = Ball Position $[m]$

g = Gravity Constant $[m.s^{-2}]$

Below is the derivation of the magnetic force and the transfer function of the block [57]. The inductance of the coil varies with the position of the ball. When the ball is in contact with the magnet the coils inductance is $L_0 + L_1$. When the ball is removed the inductance of the coil is L_1. The varying inductance between these two extremes is given by

$$L(x) = L_1 + L_0 e^{-\frac{x}{a}} \tag{7.3}$$

The magnetic co energy of the system is a function of coil current i and separation x

$$W'(i,x) = \frac{1}{2}L(x)i^2 \tag{7.4}$$

The force of magnetic origin acting on the ball is given by [57]

$$f_m = \frac{\partial W'}{\partial x} = -\frac{L_0}{2a}i^2 e^{-\frac{x}{a}} \tag{7.5}$$

where a is a constant depends on the diameter of the iron core and the mass of the ball.

When the ball is in its equilibrium position, the gravitational force is equal to the magnetic force acting on the ball. At $x = d$ and $i = I$

$$L_d \cong \frac{L_0}{N^2}e^{-\frac{d}{a}} \tag{7.6}$$

$$Mg = \frac{L_0}{2a}e^{-\frac{d}{a}}I^2 = \frac{N^2 L_d}{2a}I^2 \tag{7.7}$$

Where:

N = The number of turns in the coil

L_d = The incremental inductance at $x = d$ due to a single turn coil.

Rearranging Equation 7.7 we can get an equation for I.

$$I = \sqrt{2Mg\frac{a}{N^2 L_d}} \tag{7.8}$$

The force of magnetic origin acting on the ball is given by Equation 7.5

$$f_m = f(i,x) = -\frac{1}{2a} L_0 e^{-\frac{x}{a}} i^2 \tag{7.9}$$

Consider a perturbation about the equilibrium point at $x = d$, $i = I$

$$x = d + x'$$

$$i = I + i'$$

$$f_m = F_m + f' \tag{7.10}$$

By Taylor's series expansion

$$f(i,x) = f(I,d) = x' \frac{\partial f}{\partial x} \mid_{I,d} + i' \frac{\partial f}{\partial i} \mid_{I,d} \tag{7.11}$$

This now becomes

$$f' = \frac{1}{2a^2} L_0 e^{-\frac{d}{a}} I^2 x' - \frac{I}{a} L_0 e^{-\frac{d}{a}} I i' \tag{7.12}$$

The mechanical force is

$$f_m = Mg + M\frac{d^2x'}{dt^2} \tag{7.13}$$

At equilibrium $Mg = f(I,d)$ and the incremental equation of motion becomes

$$M\frac{d^2x'}{dt^2} - \frac{N^2 L_d I^2}{2a^2} x' + \frac{N^2 L_d I}{a} i' = 0 \tag{7.14}$$

This gives us the differential equation that describes the system. By getting the Laplace transform of this equation, the transfer function can be derived.

$$\frac{X(s)}{I(s)} = \frac{\frac{N^2 L_d I}{a}}{Ms^2 - \frac{N^2 L_d I^2}{2a^2}} \tag{7.15}$$

Using Equation 7.8 gives

$$\frac{X(s)}{I(s)} = \frac{-\frac{2g}{I}}{s^2 - w_n^2} \tag{7.16}$$

Where $w_n^2 = \sqrt{\frac{g}{a}}$. This is the plant transfer function, It relates the coil current and the balls position.

7.3.3 The Position Sensor

The optical position sensor block is used to measure the ball position x, this block can be approximated with a linear function:

$$v_x = G_s x$$

or in Laplace form as:

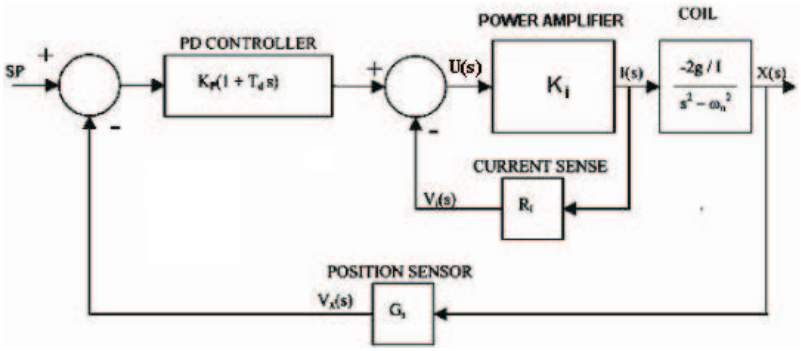

Figure 7.3: Block diagram on the compensated system.

$$\frac{V_x(s)}{X(s)} = G_s \tag{7.17}$$

Where:

v_x = The Sensor Output Voltage $[V]$

G_s = The Gain Of The Sensor $[V/m]$

7.4 Control of the Magnetic Levitation System

The system is actually nonlinear and instable, it has been linearized in section 3, and the transfer function is shown as instable with a pole in right half plan, ω_n, so a suitable controller should be designed to stabilize the system, in other words to pull the pole in the right half plan to the left half plane, the PD controller is a good choice to stabilize the system.

7.4.1 The PD Controller

The output of light sensor detector circuit is subtracted from position reference voltage by a difference amplifier to generate an error signal v_e and then fed to PD controller as shown in Figure 7.3, the Laplace form of PD controller is Equation 7.18.

$$v_{PD} = K_P(v_e + T_d\frac{dv_e}{dt})$$

$$V_{PD}(s) = K_P(1 + T_d s)V_e(s) \tag{7.18}$$

Where:

v_{PD} = PD Controller Output $[V]$.

v_e = The Error Input Voltage Of The Controller $[V]$.

K_P = PD Controller Proportional Constant.

T_d = Differential Time Constant $[s]$.

7.4.2 The Electronic Circuit of Magnetic Levitation System

Figure 7.4 shows a practical implementation of the whole electronic circuit of the system. The optical position transducer is formed from the infra-red LED **D1** and the phototransistor **Q1**. The position of the steel ball controls the amount of light falling on the phototransistor, and thus varies the emitter current, which in turn varies the voltage drop in the emitter load resistor RV1. This resistor is made variable to compensate for different phototransistor sensitivities, so that the circuit can be set up to give a standard output voltage [58].

The output of the position transducer is compared with an adjustable position reference voltage from **RV2**; the difference is an error signal, which appears at the output of op-amp **U1**. This error signal is used to control the current in the magnet coil. There is an external input to the error amplifier, which allows you to investigate the dynamic behaviour of the system.

Current in the magnet coil is supplied by the magnet driver - a feedback circuit based on the power transistor **Q2**. Note that **Q2** is actually two transistors connected as a Darlington pair, which behaves as a single transistor with a high current gain - typically several thousand. Current feedback is applied via resistor **R13**, which senses the current in the coil; the effect is to make the magnet current proportional to the voltage at the input of the circuit.

A critical part of the system is the compensator circuit, based on op-amp **U2**, which links the error amplifier to the magnet driver. This is effectively a combination of an inverting amplifier and a differentiator; its action can be explained as follows. If the capacitors **C1** and **C2** were omitted, the magnet current would be proportional to the ball displacement. Since the force of attraction depends on the current, the system would have a spring-like action: for small displacements, the restoring force would be proportional to the displacement, so the ball would tend to oscillate like a mass on a spring. In itself this behaviour would be a nuisance, but not damaging. The problem is the inductance of the magnet coil, which introduces a phase lag, or time delay, between a change in the ball position and a corrective change in the magnet current. This lag has the effect of making the system unstable, so that any oscillation tends to grow in amplitude until the magnet loses control of the ball. To damp this oscillation of the ball, the capacitor **C1** adds a control term proportional to the rate of change of displacement, in other words velocity. This derivative term counteracts the effect of inductance. It causes a change in the magnet current proportional to the velocity, but in a direction which opposes the motion; thus the velocity will be reduced, and the amplitude of the oscillation will keep decreasing until the ball ceases to move [59].

The additional capacitor **C2** in the circuit limits the gain at high frequencies; this does not affect the control action, but it prevents a high-frequency oscillation which can occur in this kind of circuit. Resistor **R9** compensates for the base-emitter drop in the Darlington transistor **Q2**.

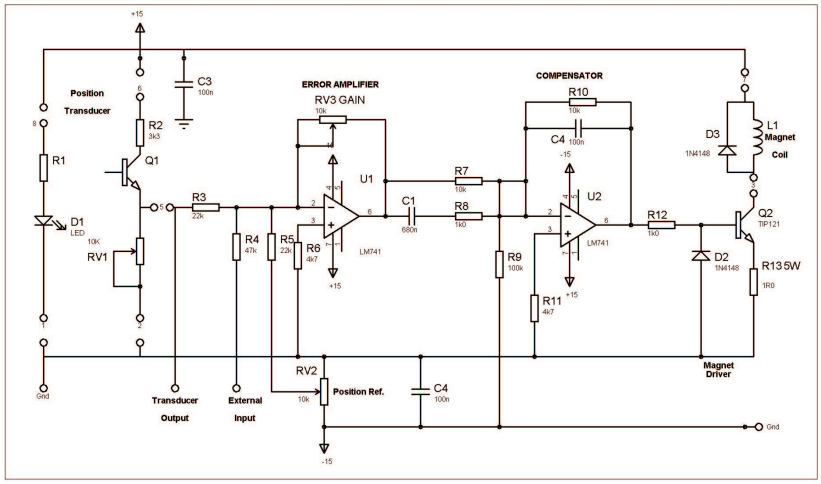

Figure 7.4: Levitation Controller Circuit.

7.5 Circuit Construction and Testing

7.5.1 Components and Facilities

You will need the following components:

- Circuit board.
- Power transistor TIP 121, heat sink, nut and bolt.
- Terminal pins (6).
- Potentiometers $10k\Omega(3)$.
- IC Socket (2).
- 741 Op Amps (2).
- IN4148 Diode.
- Resistors: 1Ω, $1k\Omega(2)$, $4.7k\Omega(2)$, $10k\Omega(2)$, $22k\Omega(2)$, $47k\Omega$, $100k\Omega$, 220Ω.
- Capacitors: $22nF, 100nF(2), 680nF$.
- Phototransistor $BPX38$.
- IR Transmitter.

7.5.2 Preliminary Tests

Position transducer

Figure 7.5: Seven Different Position of the Potentiometer

Connect the digital multimeter to measure the voltage at the output of the position transducer with respect to Gnd, using the Pos o/p terminal pin on the board, and make the following checks.

1. When there is nothing in the path of the (invisible) infra-red light beam, the voltage should lie between 7 V and 10 V. If it is outside this range, adjust the potentiometer on the magnet terminal block (**RV1**) to give a value close to 8 V. If you cannot obtain a voltage in the range (7 - 10)V, make necessarily correction.

2. Interrupt the light beam, and see whether the transducer voltage falls below 1 V. If it does not, make necessarily correction.

Control circuit

The two potentiometers in the control circuit have a critical effect on the operation of the system. The position reference potentiometer will need to be set correctly, as described below. But the stability of the system is affected by the gain potentiometer, so it will be necessary to set this control to defined positions. Although there are no scale markings on the potentiometer, seven different positions are easily distinguished see Figure 7.5.

If you have used the standard layout for the board, the gain varies from zero in position 1 to maximum in position 7. If you have modified the layout, check whether you need to reverse the numbers. Proceed as follows to test the system.

1. Set the gain potentiometer **RV3** to the middle position 4.

2. Turn the position reference potentiometer **RV2**, and observe the current monitored by the power supply meter. With nothing in the path of the infra-red light beam, you should be able to vary the current smoothly between zero and a maximum of about 1.2 A.

3. Set the position reference potentiometer as follows: increase the setting until the current is at its maximum; and then reduce it slowly until the current just starts to decrease.

4. Try interrupting the infra-red light beam with your hand. You should be able to reduce the current smoothly to zero. If this does not happen, switch off and look for wiring faults.

5. If you cannot get the control circuit to behave as described, look for faulty components.

7.5.3 Levitating the Ball

If the previous tests were successful, the system is probably working and you can try levitating a ball as follows.

1. Start with the ball away from the magnet, so that there is nothing in the path of the light beam. Use the power-supply meter to monitor the current in the positive supply line.

2. Try raising the ball towards the magnet. You should find a balance point where the current falls to about 0.6A and the magnet force balances the weight of the ball. Gently release the ball; it will probably remain levitated.

3. If the levitation is unstable, remove the ball and reduce the gain by turning the gain potentiometer to position 3 (see section 3.3).

4. Re-adjust the position reference potentiometer as before, and try again.

5. If you still cannot get the ball to levitate, try making small adjustments to the position reference control. If necessary, use position 2 for the gain potentiometer; but it is more likely that there is a fault in the circuit

6. When you have got the ball levitated, you should be able to raise and lower its position by several millimeters by adjusting the position reference control.

7. This simple system is not very good at coping with sudden disturbances. You can easily verify this by thumping the table with your fist: it does not take a very large thump to make the ball drop.

7.6 Investigating the System

7.6.1 Sine-Wave Response

This test uses a laboratory function generator to supply an external input to the levitation system. And an oscilloscope to examine the response. The signal is applied to the Ext i/p terminal of the control circuit, it has the effect of altering the position reference.

1. Switch off the power supply. Connect the oscilloscope channel **II** to the output of the function generator.

2. Connect the signal lead of channel **I** to the output of the position transducer: this is the pin labeled Pos o/p on the control circuit board Figure 7.1. Leave the channel **I** earth (ground) Lead unconnected.

3. Select a sine-wave output from the function generator, and set the amplitude to zero. Select the frequency range $(1 - 10)\ Hz$, and set the frequency dial to 0.5 - this is below 1 on the dial.

4. Levitate the ball again, and slowly increase the signal amplitude until you have the largest value that works reliably. If the ball drops off. Reduce the amplitude and try again. You should be able to get the ball to move up and down by several millimeters with an amplitude setting between 5 and 10 V. If necessary, adjust the position reference and gain controls.

5. The scope display should show two horizontal lines moving up and down together at 0.5 Hz. Channel **II** effectively shows the change in the position reference resulting from the external input to the control circuit; channel **I** shows the resulting change in the ball position.

6. Reduce the signal amplitude by about a half. and increase the signal frequency to 5 Hz. Adjust the scope channel **I** and **II** settings and the time base setting to display one cycle of each waveform on the screen; you may need to adjust the trigger controls to get a stable display. Make sure that chopped mode is selected (DUAL and ADD pushbuttons both in).

You should see a sine-wave shape for the signal input on channel **II**, and a similar shape for the ball position on channel **I**. If the position waveform is very distorted, try adjusting the position reference control. Similarly you can investigate the triangle-wave response and the square-wave response.

7.6.2 Square-Wave Response

A square-wave input is a very severe test for the suspension system. This wave shape makes sudden changes in the demanded ball position, which require a corresponding increase or decrease in the coil current; but the inductance of the magnet coil prevents the current from changing suddenly. The result is a temporary loss of control, followed by an oscillation in the ball position as the system recovers. You can observe it as follows.

1. Reduce the amplitude to zero and select a square-wave output from the function generator. Leave the frequency set to 5 Hz.

2. With the ball suspended, slowly increase the signal amplitude to about 1 V. If the suspension becomes unstable, reduce the amplitude. The motion of the ball is too small to observe directly, but you can view the position signal on the scope.

3. Select AC coupling for scope channel **I**, so that you can increase the sensitivity sufficiently to observe the waveforms. Adjust the scope settings to get a clear display of both waveforms. You should now see a damped oscillation superimposed on the square-wave response. The sloping top and bottom of the response waveform is caused by the scope; you can confirm this by selecting AC coupling for channel **II**.

Chapter 8

Conclusions and Suggestions

As a result of this experimental research, a simple control approach was presented, which involves a modified PID controller (PI-D) applied on the linearized model. As modeling and identification of a laboratory magnetic levitation was dealt with, the CE 152 laboratory magnetic levitation made by Humusoft was presented as a single input a single output. The modeling of magnetic levitation was systematically tackled by disassembling the system into simpler subsystems, i.e. modeling of the sensors, power amplifier dynamics and ball and coil subsystem dynamics. Furthermore, the A/D and D/A models have been modeled separately. In addition, measurement and identification of all the parameters needed was illustrated. Finally, validation of the developed mathematical model was treated. The validation results with successful experiments suggest that the developed mathematical model adequately represents the laboratory magnetic levitation.

In the final conclusion of this thesis, an educational magnetic levitation model have been built and PD controller have been designed to stabilize the system.

The robustness of the PID controller is generally based on the system's model. Here we adopt several idealizing assumption to establish the system's model, and this may result in ignoring many nonlinear characteristics. Since the magnetic levitation system has many uncertainties, e.g. magnetic field distribution, variation of coil inductance, etc. We may consider these components to establish a more accurate model for further performance.

Finally, I suggest building a number of magnetic levitation apparatuses that could be used as a training media in schools and universities.

Bibliography

[1] Trumper D.L., Olson S.M., Subrahmanyan P.K., "Linearizing Control of Magnetic Suspension Systems", Control Systems Technology, IEEE Transactions, Vol. 5 Issue: 4, pp. 427- 438, July 1997.

[2] Cho D., Kato Y., Spilman D., "Sliding Mode and classical Controller in Magnetic Levitation Systems", IEEE Control Systems Magazine, Vol. 13, pp. 42-48, Feb. 1993.

[3] Fujita M., Namerikawa T., Matsumura F., Uchido K, "Synthesis of an Electromagnetic Suspension System", Decision and Control, Proceedings of the 31st IEEE Conference, Vol. 3, pp 2579- 2579, 1992.

[4] C.E. Lin, H.L Jou, Y.R. Sheu, "Exact Model Identification for Magnetic Suspension System via Magnetic Field Measurement", Institute of Aeronautics and Astronautics, National Cheng Kung University, Taiwan, China, 1992.

[5] Namerikawa T., Fujita M., "Modeling and robustness analysis of a magnetic suspension system considering structured uncertainties", Proceedings of the 36th IEEE Conference, Vo. 3, pp. 2559 - 2564, Dec. 1997.

[6] Sun L., Ohmori H., Sano A. "Direct closed-loop identification of magnetic suspension system", Proceedings of the 1999 IEEE International Conference, Vol.1, pp. 749 - 754, 1999.

[7] Velasco-Villa, M., Castro-Linares R., Corona-Ramirez L., "Modeling and passivity based control of a magnetic levitation system", Proceedings of the 2001 IEEE International Conference , Vol. 3, pp.64 - 69, 2001.

[8] H. Yu , T.C. Yang, D. Rigas and B.V. Jayawant,"Modeling and Control of Magnetic Suspension Systems", Proceeding of the 2002 International Conference on Control Applications, Scotland, UK, 2002.

[9] Galvao R.K.H., Yoneyama T., de Araujo F.M.U., Machado R.G., " A Simple Techniques for a Didactic Magnetic Levitation System", IEEE Transactions on Education, Vol. 46, No. 1, Feb. 2003.

[10] Watkins J.M., Piper G.E., " An Undergraduate Course in Active Magnetic Levitation: Bridging the Gap", Proceedings of the 35th Southeastern Symposium, pp. 313 - 316, USA, 16-18 March 2003.

[11] Anakwa W.K.N., Akyil N.K., Lopez J.A. "Control of a magnetic suspension system using TMS320C31-based dSPACE DS1102 and Simulink", IEEE International Conference, ICM'05, pp. 25-27, July. 2005 2005.

[12] Ji-Hyuck Yang, Tae-Shin Kim, Su-Yong Shim, Young-Sam Lee, Oh-Kyu Kwon, "Actuator and sensor modeling for magnetic levitation system", ICCAS 2007, International Conference, pp. 917 - 922, Oct. 2007.

[13] J.D. Kraus, Electromagnetics, McGraw Hill Companies, pp. 288, New York, 1992.

[14] B.V. Jayawant, Electromagnetic Levitation and Suspension Techniques, Edward Arnold Publishers, London, 1981.

[15] Yukikazu Iwasa, Case Studies in Superconducting Magnets: Design and Operational Issues, Plenum Press, New York, 1994.

[16] Francis Moon, Magneto-Solid Mechanics, Wiley and Sons, New York, 1984.

[17] E. Purcell, Electricity and Magnetism, McGraw-Hill Book Companies, New York, 1965.

[18] Francis Moon, Superconducting Levitation: Applications to Bearings and Magnetic Transportation, Wiley and Sons, New York, 1994.

[19] J.L. He, D.M. Rote, H.T. Coffey, "Study of Japanese Electrodynamic Suspension Maglev Systems", Argonne National Lab, Argonne, IL, 60439, April 1994.

[20] Michael Proise, "New York State Technical and Economic Maglev Evaluation", Grumman Space and Electronics Division, New York, June 1991.

[21] David Atherton, "Electrodynamic Suspension and Linear Synchronous Motor Propulsion for High Speed Guided Ground Transportation", Canadian Maglev Group, CIGGT Report No. 77-13, Sept. 1977.

[22] Ford Motor Co., "Conceptual Design and Analysis of The Tracked Magnetically Levitated Vehicle Technology Program Repulsion Scheme, Vol. 1 - Technical Studies", US DOT/FRA, Report PB247931, Feb. 1975.

[23] Franklin G., Powell J.D., Feedback Control of Dynamic Systems, Addison Wesley, Reading, Mass, 1986.

[24] Ogata K., Modern Control Engineering , 2nd ed., Prentice Hall, NJ, 1990.

[25] Kuo B.C., Automatic Control Systems, 6th ed., Prentice Hall, NJ, 1991.

[26] Shinskey F.G., Process Control Systems, McGraw-Hill, N.Y., 1979.

[27] Astrom K.J., Hagglund I., PID Controllers Theory, Design and Tuning, 2nd edition, ISA, Research Triangle Park, N.C., U.S.A, 1995.

[28] Voda A., Landau I.D., A method for the auto-calibration of PID controllers. Automatica, Vol.31. No. 1, pp. 45-53, 1995.

[29] Voda A., Landau I.D., The auto-calibration of PI controllers based on two frequency measurements. Int. J. of Adaptive Control and Signal Processing, Vol. 9, No. 5, pp. 395-422, 1995.

[30] Wirk G.S., Digital Computer Systems, MacMillan, London, 1991.

[31] Loan D. Landau, Gianluca Zito, Digital Control Systems - design, identification and implementation, Springer Verlag, London, 2006.

[32] Kuo B., Digital Control Systems, Holt Saunders, Tokyo, 1980.

[33] Ogata K., Discrete-Time Control Systems, Prentice Hall, N.J, 1987.

[34] Astrom K.J., Wittenmark B., Computer Controlled Systems - Theory and Design. 3rd edition, Prentice-Hall, Englewood Cliffs. N.J., 1997.

[35] Narendra K.S., Taylor J.H., Frequency Domain Criteria for Absolute Stability, academic Press, New York, 1973.

[36] Franklin G.F., Powell J.D., Workman M.L., Digital Control of Dynamic Systems, 3rd edition, Addison Wesley, Reading, Mass, 1998.

[37] Landau I.D., Robust digital control systems with time delay. Int. J. of Control, Vol. 62, no. 2, pp. 325-347, 1995.

[38] Phillips C.L., Nagle H.T., Digital Control Systems Analysis and Design, 3rd edition. Prenctice Hall, N.J., 1995.

[39] Alvarez-Sanchez E., Alvarez-Gallegos J., Castro-Linares R., "Modeling and controller design of a magnetic levitation system", 2nd International Conference on Electrical and Electronics Engineering, Vol. 5, pp. 330-334, Sep. 2005.

[40] Naumovic M.B., "Modeling of a didactic magnetic levitation system for control education", Telecommunications in Modern Satellite, Cable and Broadcasting Service, TELSIKS 2003, 6th International Conference, Vol. 2, pp. 783 - 786, Oct. 2003.

[41] Richard C. Dorf, Robert H. Bishop, Modern Control Systems, Addison Wesely, 2002.

[42] Humusoft, CE 152 magnetic levitation model: User's manual, Humusoft, Prague, 2002.

[43] Peterson K. S., Grizzle J. W., Stefanopoulou A. G., "Nonlinear control for magnetic levitation of automotive engine vales", IEEE Transaction on Control Systems Technology, Vol. 14, No. 2, pp.346-354, Mar. 2006.

[44] Fallaha C., Kanaan H., Saad M., "Real time implementation of a sliding mode regulator for current-controlled magnetic levitation system", Proceedings of the 2005 IEEE International Symposium on Intelligent Control, Vol. 1, pp. 696-701, Jun. 2005.

[45] Jalili-Kharaajoo M.,"Robust variable structure control applied to voltage controlled magnetic levitation systems", 2nd IEEE International Conference on Industrial Informatics, Vol. 1, pp. 335-338, Jun. 2004.

[46] Lin F. J., Teng L. T., Shieh P. H., "Intelligent adaptive backstepping control system for magnetic levitation apparatus", IEEE Transaction on Magnetics, Vol. 43, No. 5, pp. 2009-2018, May 2007.

[47] Onuki, T., Nakatsu, T., Wakao, S., Hori, M.,"Magnetic field analysis of nonlinear system considering both motion and voltage equations", IEEE Transactions on Magnetics, Vol. 33, Issue 2, Part: 2, pp. 2097 - 2100, March 1997.

[48] Humusoft, Real time toolbox for use with SIMULINK: User's manual, Humusoft, Prague, 2002.

[49] Hyun Chang Lee; Min-Hung Hsiao; Jen-Kuang Huang; Chung-Wen Chen, "Identification of stochastic system and controller via projection filters", American Control Conference, 1994 Vol. 1, pp. 127-131, July 1994.

[50] Galvao R.K.H., Yoneyama, T., de Araujo, F.M.U., Machado, R.G., "A simple technique for identifying a linearized model for a didactic magnetic levitation system", IEEE Transactions on Education, Vol. 46, Issue 1, pp. 22 - 25, Feb 2003.

[51] Loan D. Landau, Gianluca Zito, Digital Control Systems – design, identification and implementation, Springer Verlag, London, 2006.

[52] Sun, L., Ohmori, H., Sano, A. "Direct closed-loop identification of magnetic suspension system", Proceedings of the 1999 IEEE International Conference, Vol. 1, pp. 749 - 754, 1999.

[53] Anderson Brian.O., Moore Jone B., Optimal Control-Linear Quadratic Methods, Prentice-Hall International, USA, 1989.

[54] Lord William, Hwang Jackson H,"DC Servomotors: Modeling and Parameter Determination", IEEE Transactions on Vol. IA-13, Issue 3, pp. 234-243, May 1977.

[55] Gene F. Franklin, J. David Powell, Abbas Emami-Naeini, Feedback Control Of Dynamic Systems, 5th ed., New Jersy, Prentice Hall, 2006.

[56] Ali Khalid, Abdelati Muhammed, "Magnetic Levitation of Iron Sphere Using Analog PD Controller", AIP Conference Proceedings, the proceedings of the CISA'09 conference, Vol.1107, Tunisia, 23 - 25 March 2009.

[57] W. G. Hurley, M. Hynes, W. H. Wolfle, "PWM Control of Magnetic Suspension System," IEEE Transactions On Education, vol.47, No.2, May 2004.

[58] T.H.Wong, "Design of a Magnetic Levitation Control System-an undergraduate project," IEEE Transactions on Education, Vol.29, pp.196-200, November 1986.

[59] Thomas L. Floyd, Electronics Fundamentals: Circuits, Devices and Applications, Prentice Hall, 7th Ed., 2006.